Partially Rated Soft Open Points for Electricity Distribution Networks

Mohamed A. Abdelrahman

School of Engineering

Cardiff University

A thesis submitted for the degree of

Doctor of Philosophy

November 2021

Acknowledgement

I want to express my sincere gratitude to Prof. Nick Jenkins. His guidance and advice were essential to this work, and I truly appreciate his help on thesis revision.

I would like to thank my supervisors Prof. Jianzhong Wu and Dr Wenlong Ming, for their help, support and advice during my PhD study.

I would like to acknowledge Netwon-Mosharafa Fund for their financial support to my PhD study at Cardiff University.

I want to thank my colleagues in the CIREGS research group. I am very grateful for the help and suggestions from Dr Tibin Joseph, Rajesh Rajamony and Peng Yang, especially during experimental work. I want to thank Dr Karolina Rucinska for her valuable advice and encouragement.

I would like to thank my family for all their love and encouragement.

Declaration

This work has not been submitted in substance for any other degree or award at this or any other university or place of learning, nor is being submitted concurrently in candidature for any degree or other award.

Signed: Date:

STATEMENT 1

This thesis is being submitted partial fulfilment of the requirements for the degree of PhD

Signed: Date:

STATEMENT 2

This thesis is the result of my own independent work/investigation, except where otherwise stated, and the thesis has not been edited by a third part beyond what is permitted by Cardiff University's Policy on the Use of Third Party Editors by Research Degree Students. Other sources are acknowledged by explicit references. The views expressed are my own.

Signed: Date:

STATEMENT 3

I hereby give consent for my thesis, if accepted, to be available online in the University's Open Access repository and for inter-library load, and for the title and summary to be made available to outside organisations.

Signed: Date:

Abstract

The connection of multiple Distributed Generators (DGs) to medium voltage (MV) distribution networks requires careful control of the power flow in order to maintain the voltages and currents within limits. At present, the operation of distribution networks is passive. New devices are required to provide distribution network operators with the means of controlling the power flow and improving the utilisation of existing distribution networks.

In this thesis, various topologies of Soft Open Points (SOPs) to be used in MV distribution networks were examined. The following points were addressed:

1. The benefits of a multi-terminal back-to-back (B2B) SOP were quantified and compared with a two-terminal SOP and with no SOPs. An optimisation problem was solved to determine the setpoints of the SOPs to achieve multiple control objectives separately. The three-terminal B2B SOP enabled the distribution network to host more DGs and achieved lower energy losses than the two-terminal SOP. However, B2B SOPs have not been widely deployed in MV distribution networks as they are too expensive.

2. The operation of a Transformer-less Unified Power Flow Controller (UPFC) in distribution networks was investigated. It offered power flow control with the complete removal of interfacing transformers. However, its ability to control reactive power is limited by the converter's current ratings. A small-scale experimental setup was used to test the performance of the Transformer-less UPFC in response to control signals to step changes in active and reactive power.

3. The well-established conventional UPFC, that has been demonstrated in some transmission systems, was improved for use in MV distribution networks. The Improved UPFC provides similar performance to the conventional UPFC with no need for an interfacing series transformer. The series converter was protected against immediate overvoltage and overcurrent applied when faults occur on the distribution network using a fast-acting protection circuit.

Abstract

A model of a two-busbar distribution network was used for the investigation, supported by simulations and some experimental tests. The results showed that SOPs with a series connection can provide power flow control similar to that of B2B SOPs with lower rating converters and size.

iv

Contents

Contents

Contents

Contents

Contents

Contents

x

List of Figures

List of Tables

Abbreviations

AC	Alternative Current
AVC	Automatic Voltage Control
B2B	Back-to-Back
CB	Circuit Breaker
CMI	Cascaded Multilevel Inverter
DC	Direct Current
DERs	Distributed Energy Resources
DG	Distributed Generator
DNO	Distributed Network Operator
DPFC	Distributed Power Flow Controller
d-q	Direct- Quadrature
DVR	Dynamic Voltage Restorer
EV	Electric Vehicle
FACTs	Flexible AC Transmission Systems
FPL	Flexible Power Link
GAMS	General Algebraic Modelling System
GTO	Gate Turn-Off
IGBT	Insulated Gate Bipolar Transistor
LCT	Low Carbon Technology

LI	Load Index
MICP	Mixed Integer Conic Programming
MMC	Modular Multilevel Converter
MOV	Metal Oxide Varistor
MV	Medium Voltage
MVDC	Medium Voltage DC Link
NIA	Network Innovation Allowance
NIC	Network Innovation Competition
NOP	Normally Open Point
NPC	Neutral-Point Clamped
Ofgem	Office for Gas and Electricity Market
OLTC	On-load Tap Changer
PCC	Point of Common Coupling
PI	Proportional-Integral
PLL	Phase Locked Loop
POC	Point of Connection
PR	Proportional-Resonant
PV	Photovoltaic
SD	Switch Disconnector
SDPR	Semiconductor Device Power Rating

SOP	Soft Open Point
SPB	Soft Power Bridge
SPWM	Sinusoidal Pulse Width Modulation
SSSC	Static Series Synchronous Compensator
STATCOM	STATic synchronous COMpensator
TBS	Thyristor Bypass Switch
THD	Total Harmonic Distortion
TSO	Transmission System Operator
UPFC	Unified Power Flow Controller
VSC	Voltage Source Converter

Chapter 1 Introduction

This chapter introduces the background, motivation, and objectives of the thesis. In addition, it provides an outline for the thesis.

1.1 Background

Climate change is a real and rapidly growing risk that must be addressed. The main drive of climate change is the greenhouse gas emissions by human activities [1]. Since the industrial period between 1850 and 1900, greenhouse gas emissions are estimated to have increased Earth's global average temperature by about 1 degree Celsius, a number that is currently increasing by 0.2 degree Celsius per decade [2]. The implications of temperature rise are global warming, changes in precipitation patterns, more droughts and heatwaves, etc. [3].

The energy sector[*] that mainly includes electricity, heat generation, and transport, is the major contributor to climate change. Figure 1-1 shows the global greenhouse gas emissions by economic activities that lead to their production [4].
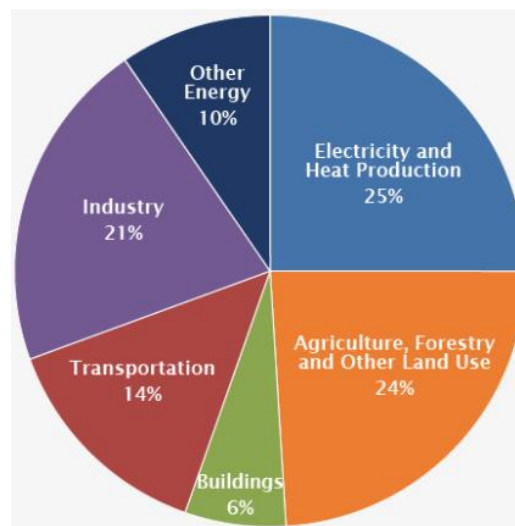
Figure 1-1 Global greenhouse gas emission by economic sector [4]

Coordinated actions across the world are required to limit global warming and reduce greenhouse gas emissions. The Paris Agreement on climate change is a legally binding international treaty that set out a global framework to limit global warming to well below 2 °C above pre-industrial levels and to pursue efforts to limit the temperature increase to 1.5 °C [5].

[*]Energy sector can be broadly defined as a system of interconnecting components that enables energy (e.g., electricity, gases and fuels) to be produced and supplied to end-users in homes, businesses and industry. It includes production, conversion, trading, transport, and delivery [6].

In order to reach the goals of the Paris Agreement, new plans are required to target cutting greenhouse gas emissions. This will need the use of more clean energy (i.e., decarbonise) and to use that energy more efficiently (i.e., optimise). It will also require shifting energy demand to electricity and away from the combustion of fossil fuels (i.e., electrify) [7].

1.1.1 Decarbonisation of the energy sector

Decarbonisation includes enabling more Low Carbon Technologies (LCTs) to reduce carbon dioxide emissions [8], besides, promoting the electrification of heat and transport [9].

Decarbonisation is driving electricity systems towards decentralisation. This is demonstrated by the growth in Distributed Energy Resources (DERs), which include wind generation, solar photovoltaics, fuel cells, distributed energy storage, electric vehicles (EVs), smart appliances and electric heat pumps [10]. Figure 1-2 shows the growth in renewable energy globally [11].
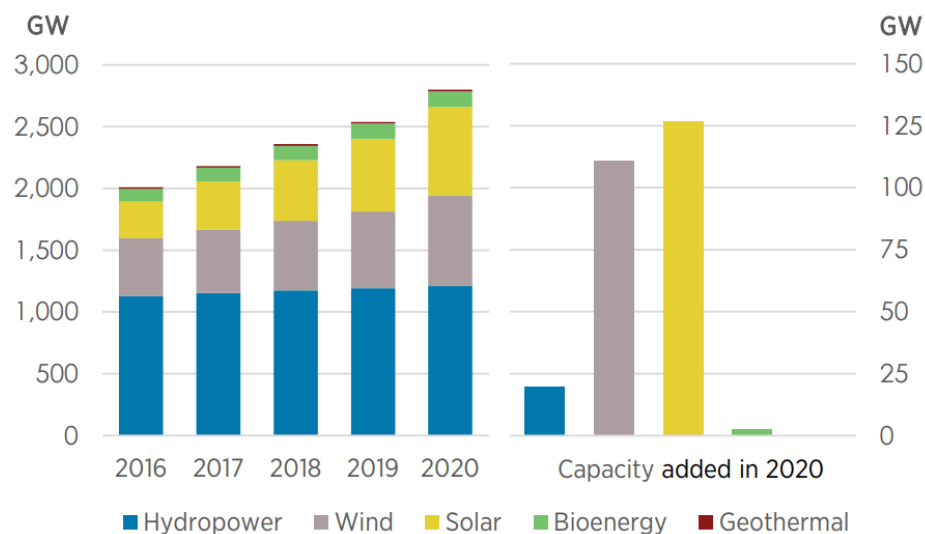
Figure 1-2 Global capacities of renewable resources [11]

The effects of DERs can be attributed to the uncertainty, variability of generation, and several technical problems (e.g., voltage, frequency and congestion) on electricity systems. Therefore, new tools and technologies are required to manage highly renewable electricity systems [12].

1.1.2 Operational challenges of highly renewable electricity systems

Network operators (i.e., distribution network operators (DNOs) and transmission system operators (TSOs)) need to maintain their primary role of delivering a secure and reliable supply of electricity to consumers. The increase in DERs has consequences on the operation of transmission and distribution networks.

In transmission networks, large generators are being replaced by Distributed Generators (DGs), causing operability challenges in terms of power system inertia, short circuit level, voltage and reactive power control and system restoration [13]. For example, a number of voltage excursions were reported in transmission networks during periods of low demand [14], [15].

Several technologies could be used to manage the operation of transmission networks, such as virtual synchronous machines, flywheel, pumped storage hydropower plants and Flexible AC Transmission Systems (FACTs) [13].

In distribution networks, the main challenges limiting more uptake of LCTs, that will often be connected to distribution networks, are voltage rise and network congestion [16]. Distribution networks should accommodate more LCTs at the lowest cost and maximum flexibility.

1.1.3 The UK's net-zero emissions target by 2050

In 2019, the UK became the first major economy to adopt an ambitious policy to bring all greenhouse gas emissions to net-zero by 2050 [17]. Achieving the UK's net-zero emissions target while keeping costs and disruption to a minimum requires innovative approaches to decarbonisation [18].

Figure 1-3 shows the proportion of UK energy supplied from low carbon sources from 2000 to 2019 [19].
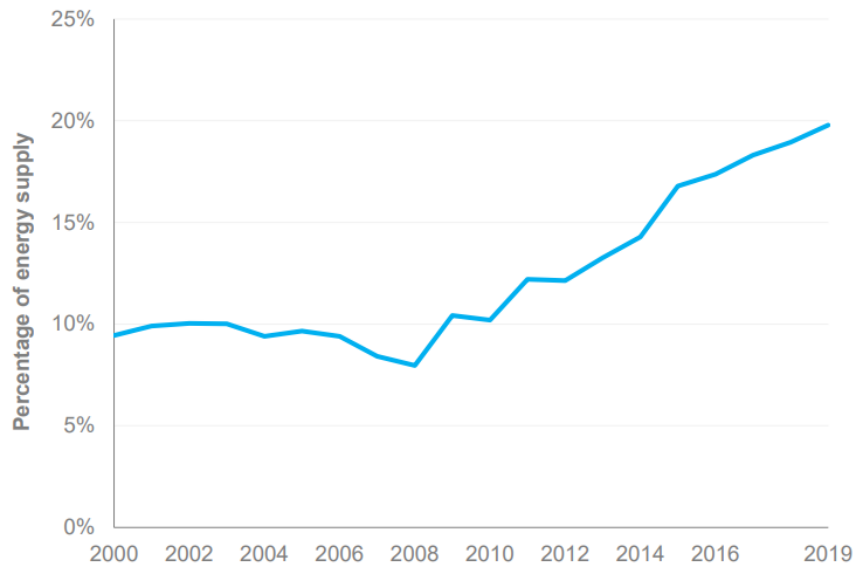
Figure 1-3 Percentage of energy supply from low carbon sources, 2000-2019 [19]

The growth in renewable generation has increased the supply of green electricity. Still, it has imposed operational challenges as renewable energy is intermittent, and the output does not necessarily coincide with the local demand. This was demonstrated by a record low demand and plenty of renewable generation during the Covid-19 lockdown led to a significant increase in balancing costs [20].

In the UK, the accumulated capacity of solar photovoltaics generation connected to the distribution networks has increased to 12.9 GW and wind generation to 5.7 GW [21]. In order to adapt the distribution networks in the UK to meet the operational challenges, the Office of Gas and Electricity Markets (Ofgem) in Great Britain has introduced innovation stimuli. The Network Innovation Competition (NIC) and Network Innovation Allowance (NIA) are available to the licensed network companies to support innovation and encourage competition on emerging technologies, products and services that supports decarbonisation [22], [23].

Several projects have trialled new innovative methods and tools to actively manage and optimise the operation of the distribution networks at different voltage levels and provide the required operational flexibility. This includes improving distribution networks' visibility, controllability, and automation to guarantee safe operation with significant levels of LCTs. A good example is the integration of power electronic devices such as Soft Open Points (SOPs) in medium voltage (MV) distribution networks.

5

1.2 Research motivation

The connection of multiple DGs to MV distribution networks requires new devices to actively control the power flow to maintain the voltages and currents within limits.

Power electronic devices (e.g., Voltage Source Converters (VSCs)) can be used to provide power flow control in MV distribution networks, similar to the well-established Flexible AC transmission Systems (FACTs) and MV motor drive systems.

There has been increasing activity in the engineering development of power electronic material (e.g., silicon carbide power electronics) and hardware design (e.g., new converter topologies) [24]. This is demonstrated by several projects that have been trialling new configurations and arrangements of power electronic converters in MV distribution networks [25], [26], [27], [28], [29], [30].

SOPs are power electronic devices installed in distribution networks to provide power flow control and voltage regulation. For example, SOPs can interconnect two or more substations that could not normally be interconnected, allowing the transfer of excess power generated by DGs to other load centres. This will avoid or delay reinforcement, release the latent capacity of distribution networks and support the growth of LCTs.

There are two types of SOPs: fully-rated back-to-back (B2B) SOPs and partially rated SOPs similar to the conventional Unified Power Flow Controller (UPFC).

This thesis investigated various topologies of SOPs to be used in MV distribution networks. The thesis quantified the benefits of a multi-terminal fully-rated B2B SOP and compared them to those of a two-terminal SOP and no SOPs. Despite the benefits of installing fully-rated B2B SOPs, they have not been widely deployed in MV distribution networks as they are too expensive. The cost and size of the fully-rated converters and the interfacing transformers account for the lack of applications of fully-rated B2B SOPs in MV distribution networks.

SOPs with a series connection were examined as an alternative solution to achieve the required power flow control using lower rating converters and size.

1.3 Objectives of the thesis

The objectives of the thesis are to:

- Investigate the benefits of multi-terminal fully-rated B2B SOPs in MV distribution networks.
- Investigate using a conventional UPFC to control power flow in MV distribution networks using partially rated converters.
- Investigate the performance of a Transformer-less UPFC in MV distribution networks.
- Test the performance of a Transformer-less UPFC using a small-scale experimental setup.
- Propose a power electronic topology with lower rating converters and size than fully-rated B2B VSCs.
- Examine the performance of the series converter during faults on the distribution network, then propose a protection circuit to bypass the series converter within a few milliseconds when faults occur on the distribution network.

1.4 Main contributions of the thesis

The main contributions of the thesis are described below.

- Quantify the benefits of installing a multi-terminal B2B SOP over a two-terminal B2B SOP in MV distribution networks. The multi-terminal B2B SOP offers more operational benefits than the two-terminal B2B SOP by controlling the power exchange among multiple circuits. The multi-terminal B2B SOP increased the headroom of voltage limits and reduced the energy losses of a distribution network more than the two-terminal SOP. Despite the benefits of installing B2B VSCs, they have not been widely deployed in MV distribution networks as they are expensive.

- SOPs with a series connection can provide power flow control similar to B2B fully-rated SOPs with lower rating converters and size. Several topologies were investigated, such as the conventional UPFC, the Transformer-less UPFC and the Improved UPFC.

- The Transformer-less UPFC can provide independent control of active and reactive power using series and shunt converters that are not connected to a common DC-link and with complete removal of the interfacing transformers. It can control active power using a small shunt current. However, it has limited capability to control reactive power as this requires a large shunt current. A small-scale experimental setup was used to demonstrate the performance of the Transformer-less UPFC in response to control signals to step changes of active and reactive power.

- An Improved UPFC was proposed to control power flow in distribution networks. The Improved UPFC has a similar performance to the conventional UPFC and does not require an interfacing series transformer. Hence it offers a smaller size and less cost. The performance of the series converter was investigated when AC faults occurred on the distribution network. A fast-acting protection circuit was proposed to protect the series converter against immediate overvoltage and overcurrent applied when faults occur on the distribution network.

1.5 List of publications

- **Journal paper**

[1] **Mohamed A. Abdelrahman**, Sheng Wang, Wenlong Ming, Jianzhong Wu, Nick Jenkins, "Transformer-less Unified Power Flow Controller in Medium Voltage Distribution Networks," (submitted to the IET Generation, Transmission & Distribution journal; under peer review process).

[2] **Mohamed A. Abdelrahman**, Peng Yang, Wenlong Ming, Jianzhong Wu, Nick Jenkins, "Modified Unified Power Flow Controller for Medium Voltage Distribution Networks," (submitted to the IET Generation, Transmission & Distribution journal; under peer review process).

- **Conference paper**

[1] **M. A. Abdelrahman**, C. Long, J. Wu, and N. Jenkins, "Optimal Operation of Multi-Terminal Soft Open Point to Increase Hosting Capacity of Distributed Generation in Medium Voltage Networks," International Universities Power Engineering Conference (UPEC), Glasgow, Sept. 2018., doi: 10.1109/UPEC.2018.8541861.

[2] S. Abeysinghe, **M. A. Abdelrahman**, C. Wickins, J. Wu, and N. Jenkins, "Use of Distributed Generation to Control Reactive Power at the Transmission Distribution Interface," ISGT Europe, Finland, pp. 1–5, Dec. 2021, doi: 10.1109/52324.2021.9640219.

9

1.6 Thesis outline

Figure 1-4 shows the structure of the thesis.

Literature Review   Technical Chapters
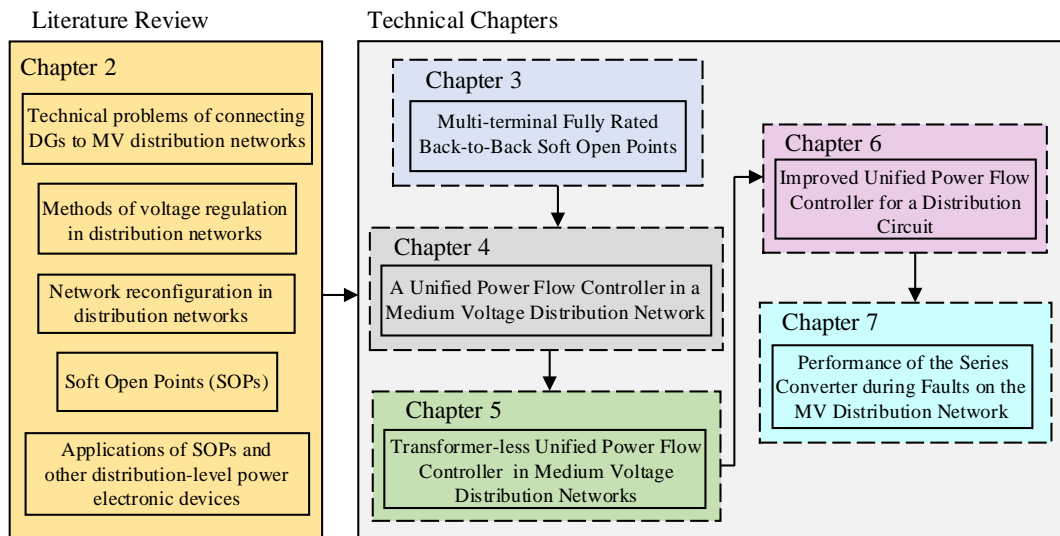
Figure 1-4 Structure of the thesis

The thesis is organised as follows:

Chapter 2 provides a literature review on the technical problems of connecting DGs to MV distribution networks and the methods used to address these challenges. It also reviews the principles of operation and the control strategies of fully-rated and partially rated SOPs.

Chapter 3 investigates the operational benefits of multi-terminal fully-rated B2B SOPs in MV distribution networks. An optimisation problem was formulated and solved to determine the setpoints of SOPs that achieve multiple objectives separately. The results showed that a three-terminal SOP reduced the energy losses and increased the headroom of voltage limits of a distribution network more than a two-terminal SOP.

Chapter 4 investigates the basic principles of power flow control using a UPFC connected to an MV distribution network with a low X/R ratio. The UPFC was controlled to operate in power flow control mode. The control scheme was implemented using decoupled dq voltage and current control loops. The results demonstrated the ability of the UPFC to control active and reactive power independently and regulate the voltage at the point of connection.

Chapter 5 investigates the use of a Transformer-less UPFC in MV distribution networks. The operating range of a Transformer-less UPFC and the required power ratings of the series and shunt converters were investigated. Simulation and small-scale experimental setup were used to validate the theoretical analysis. The results showed that a Transformer-less UPFC provided power flow control with complete removal of the interfacing transformers. However, its ability to control reactive power is limited by the converter's current ratings.

Chapter 6 proposes an improved topology of a UPFC suitable for MV distribution networks. The Improved UPFC provides similar performance to the UPFC with no need for an interfacing series transformer.

Chapter 7 investigates the performance of the series converter during faults on the MV distribution network and proposes a protection circuit for the series converter. The Improved UPFC topology was used to examine the challenges facing the series converter during external faults and test the performance of the proposed protection circuit.

Chapter 8 presents the thesis conclusions and the suggestions for future work.

Chapter 2 Literature Review

This chapter presents a literature review on technical problems of connecting Distributed Generators to medium voltage distribution networks and methods proposed to address these problems. It also reviews Soft Open Points and the state-of-the-art projects, along with the identified research gaps.

2.1 Technical problems of connecting Distributed Generators to medium voltage distribution networks

The increase in Distributed Generators (DGs), such as wind and solar photovoltaics (PVs), constitutes a significant challenge for distribution network operators (DNOs) to maintain their primary role of delivering a secure and reliable electricity supply to consumers.

Several technical problems must be addressed by DNOs when connecting DGs to distribution circuits, such as voltage rise, feeder congestion, power flow reversal and network fault level [31].

- **Voltage rise**

Voltage rise is the most serious problem of connecting large levels of DGs to MV distribution networks, especially during periods of low demand [32]. Figure 2-1 shows an equivalent circuit of a two-busbar distribution network with a DG at Busbar 2. The voltages at Busbar 1 and Busbar 2 are $\overline{V}_1$ and $\overline{V}_2$. The load has active and reactive power P_L and Q_L, and the feeder has impedance $Z_f = R + jX$, where R and X are the resistance and reactance of the feeder.
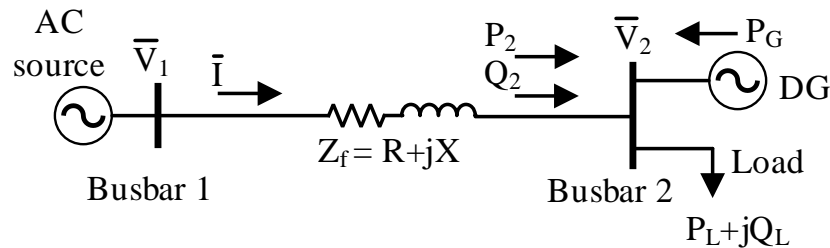
Figure 2-1 Equivalent circuit of a two-busbar distribution network

The DG operates at unity power factor and injects active power P_G. Note that the X/R ratio of a typical distribution network is usually smaller than that of a transmission network. Hence, the resistive component of the distribution feeder cannot be neglected.

Figure 2-2 shows a phasor diagram developed using the equivalent circuit in Figure 2-1.
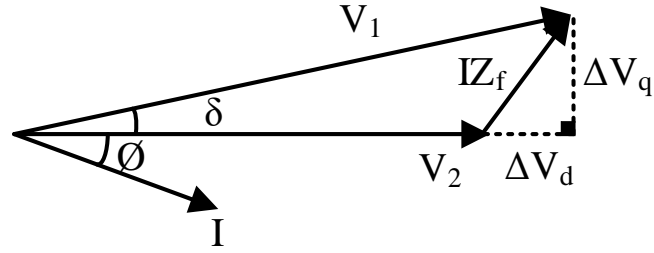
Figure 2-2 Phasor diagram of the two-busbar distribution network

The voltage difference between $\overline{V}_1$ and $\overline{V}_2$ is approximately obtained in terms of active and reactive power P_2 and Q_2 as in (2-1), where $P_2 = P_L - P_G$ and $Q_2 = Q_L$.

$$\Delta V_d = \left| \overline{V}_1 - \overline{V}_2 \right| \approx \frac{RP_2 + XQ_2}{\left| \overline{V}_2 \right|} \tag{2-1}$$

When $P_G = 0$, the power flows from Busbar 1 to Busbar 2 and $\left| \overline{V}_1 \right| > \left| \overline{V}_2 \right|$.

When $P_G > P_L$, the term RP_2 is negative. The power flow is reversed when $\left| RP_2 \right| > \left| XQ_2 \right|$ and a voltage rise occurs (i.e., $\left| \overline{V}_1 \right| < \left| \overline{V}_2 \right|$).

- **Feeder congestion**

Feeder congestion occurs when the power flow of a distribution feeder exceeds its rated power (i.e., violation of its current constraint) [33]. Switching actions (e.g., network reconfiguration) and other compensations devices (e.g., Soft Open Points (SOPs)) are used to manage feeder congestion [34]. This is achieved by transferring load from heavily loaded feeders to lightly loaded ones.

- **Reverse power flow**

Power flow reversal is likely to happen during low demand periods, and it is usually associated with voltage rise problems in distribution networks.

Certain types of on-load tap changers place constraints on the level of power flow reversal through transformers [35]. Hence, distribution networks might be constrained by the reverse power flow capability of tap-changers [36].

- **Network fault level**

Many DGs are interfaced to distribution networks using Voltage Source Converters (VSCs). The fault current of the DGs depends on the control strategy of the VSCs. Typically, current control schemes are used to control the VSCs [37], and they limit the fault current of DGs to 1-3 pu to protect the IGBTs from damage.

The integration of DGs in distribution networks increases the fault level of the existing distribution networks and affects the operation of protection relays. For example, the behaviour of DGs in grid-connected and island modes can alter the levels of fault current and affect the coordination of protective relays [38], [39].

2.2 Methods of voltage regulation in distribution networks

Several control strategies are discussed in literature to mitigate against voltage rise in distribution networks.

2.2.1 On-load tap changer (OLTC)

On-load ap-changers (OLTCs) are mechanical devices that are able to adjust the voltage magnitude by changing the position of the tap of the transformer under load [40]. They are usually used in distribution networks to control the voltage and maintain it within limits [41].

OLTCs are equipped with automatic voltage control (AVC) relays. An AVC relay monitors the secondary voltage of a distribution transformer and automatically make adjustment by signalling the OLTC [42].

The uncoordinated operation of OLTCs become less effective with the growing levels of DGs. In [43], [44], coordinated frameworks of OLTCs and other VAR compensators were discussed. The optimal setpoints were determined by solving optimisation problems considering real-time measurements [45]. It was shown that the coordinated voltage control maintained the voltage within permissible limits that was not achieved with independent control.

2.2.2 Volt/VAR control

Volt/VAR control is defined as the management of reactive power (i.e., supply or absorb VAR) to regulate the voltage and improve the performance of an AC network [46], [47].

A STATCOM and a Static Series Synchronous Compensator (SSSC) are equipment for providing controllable reactive power using switched power converters [48], [49]. Figure 2-3 shows schematic diagrams of a STATCOM and an SSSC.
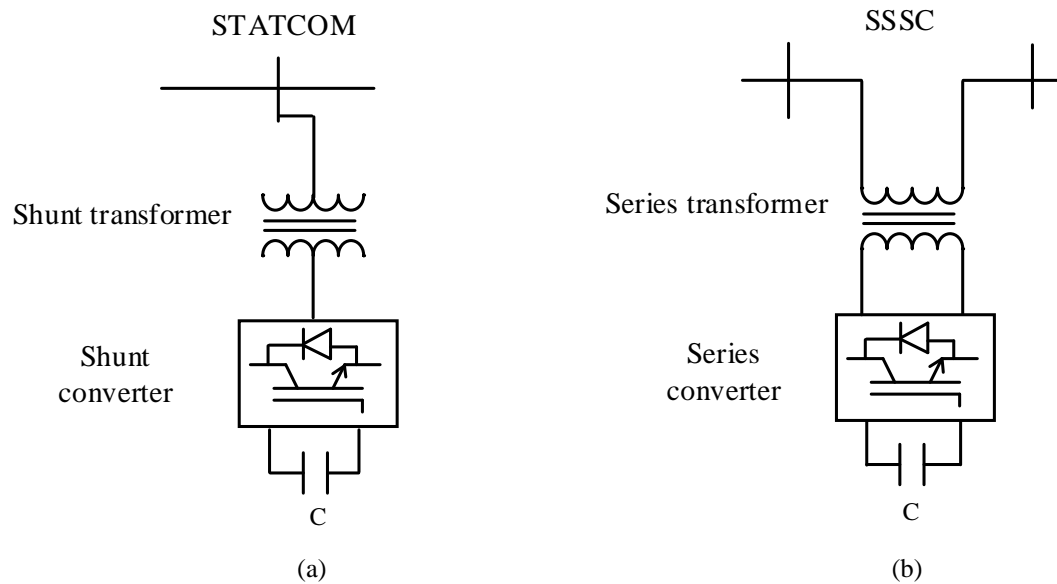
Figure 2-3 Schematic diagrams of (a) a STATCOM, and (b) an SSSC

Optimal placement and sizing of reactive power sources was discussed in [50], [51]. VAR allocation was formulated as an optimisation problem to improve voltage profiles and reduce power losses. The results showed a reduction in network power losses and improvements in network voltage. Practically, choosing the best site may not be feasible due to technical or economic restrictions [52].

In [53], [54], the power converters of PV plants and wind generators were used to provide reactive power management.

In [55], a PV solar farm was utilized as a STATCOM when no active power is generated at night. The solar farm inverter regulated the voltage at the point of common coupling (PCC) during low demand and plenty of wind farm generation.

In [56], a dynamic voltage restorer (DVR) with a storage element similar to an SSSC was proposed to mitigate against voltage sag. The DVR injects a controllable voltage phasor and can generate or absorb real and reactive power independently at its AC output terminals.

In [57], an SSSC was used to improve the voltage profile in an 11-kV distribution network. The SSSC was modelled as a series voltage that injects an AC voltage perpendicular to the line current. Results showed improvements in the transmitted active power.

A 6.6 kV, 1 MVA Transformer-less STATCOM was proposed in [58]. It was built using a cascaded configuration of H-bridge VSCs to eliminate the bulky line-

frequency interfacing transformer. A 200 V, 10 kVA prototype was used to test the voltage balance controller of the H-bridge VSCs.

In [59], a 6.6 kV hybrid Transformer-less STATCOM was proposed using Si and SiC devices and hybrid modulation. The hybrid Transformer-less STATCOM reduced the losses and overall volume compared with only Si and only SiC Transformer-less STATCOM.

2.2.3 Renewable energy curtailment

Renewable generation curtailment is the reduction in the output of DGs from what it could otherwise produce given available resources (e.g., wind or sunlight) [60]. Curtailment happens when DNOs command DGs to reduce output to keep the network within the operational limits (e.g., relieve voltage constraints).

Curtailment leads to revenue loss of DGs projects. Avoiding curtailment requires investing in network capacity (e.g., interconnection and storage) [61]. DNOs identified opportunities to offer cheaper and faster connections through actively managed non-firm connection instead of firm connection [62].

Non-firm connection or flexible connection to a distribution network is when network access is managed by DNOs, often through real-time control [63]. On the contrary, firm connection means that DGs' owners can access full generation capacity even during the outage of one distribution component. This connection scheme needs more than one circuit to the connection point of DGs, thus having a high cost and delivery time [64].

In [65], a DG curtailment method was discussed to manage voltage constraints in distribution networks. This method relies on using sensitivity factors of the Jacobian matrix to quantify the contribution of DGs P-Q injections to the voltage constraints.

The financial uncertainty of DGs non-firm connection was discussed in [66]. Three key points were addressed:

1. The order in which generators should be curtailed was defined, especially when more than one project contributes to the same constraint.
2. The estimated levels of curtailment were determined.
3. The financial risk of uncertainty was identified.

17

It was shown that DNOs should estimate the lost revenue from aggregated curtailment throughout the lifetime of a generation project. Then a trade-off between the lost revenue and shared reinforcement cost will identify the point at which developers would rather pay their shares of the reinforcement and have a firm connection than sustain the estimated curtailment cost [66].

2.3 Network reconfiguration in distribution networks

Network reconfiguration involves changing the distribution network structure by changing the states of tie-line and sectionalising switches [67].

During normal operation, network reconfiguration is used to alleviate feeder congestion and manage power flow in distribution networks. During faults, it is used for service restoration. The faulted area is isolated, and the non-faulted area is restored with minimum load shedding [68].

Network reconfiguration can be classified as static reconfiguration and dynamic reconfiguration.

2.3.1 Static reconfiguration

Static reconfiguration considers all switches (manually or remotely controlled) and looks for an improved fixed topology at the planning stage (e.g., yearly or seasonal).

In [69], a Metaheuristic Harmony Search algorithm was used to simultaneously reconfigure and identify the optimal locations for installing DGs in a distribution network. Network reconfiguration was conducted by generating all possible radial structures of a given network (without violating the constraints). Busbars were sorted according to the sensitivity of the change in active power losses to the change in DGs active power. Results showed that simultaneous network reconfiguration and DGs installation reduced power losses and improved voltage profile.

The operation of distribution networks with high DGs requires frequent reconfiguration to mitigate against the fluctuations of DGs output. This can be achieved by dynamically reconfigure the distribution networks.

2.3.2 Dynamic reconfiguration

Dynamic reconfiguration relies on a centralised control scheme that remotely controls switches to alleviate voltage constraints and manage network congestion in real-time.

In [70], mixed-integer conic programming (MICP) model was proposed for online hourly configuration. The multi-objective function minimises the weighted sum of the following three objectives: 1) DG active power curtailment, 2) line congestion, and 3) voltage deviation. The control variables are 1) the statuses of remotely controlled switches, 2) the active power curtailment factors of DGs and 3) the reactive power outputs of DGs. The load/generation scenarios were generated by the kmeans data clustering method to account for the stochastic behaviour of both load and DGs. Results showed a reduction in network power losses.

In [71], the general algebraic modelling system (GAMS) was used to analyse the worthiness of hourly reconfiguration in the presence of renewable energy, taking into account the switching cost. Results showed that the effectiveness of hourly reconfiguration in terms of loss reduction was greatly dependent on the DGs penetration level.

In [72], the benefits of online hourly based reconfiguration were presented considering the time-varying nature of loads. Hourly reconfiguration was compared with optimal fixed topologies obtained for maximum and average daily demand. Results showed a reduction in power losses when the network was reconfigured hourly. However, hourly reconfiguration is complex. It involves overvoltage transient problems and switching costs of frequent switching operations. These problems make daily fixed topology more efficient than hourly reconfiguration.

In [73], instead of hourly reconfiguration, the entire year was divided into four seasons. A probabilistic generation-load model that includes all possible operating conditions of DGs was generated and accommodated into power flow equations. The problem was solved based on genetic algorithm optimisation to determine the optimal seasonal configuration with different DG units. Results showed that a great reduction in annual losses was achieved.

19

2.4 Soft Open Points

SOPs are power electronic devices that consist of VSCs (two or more). They are installed in distribution networks in place of normally open points (NOP).

SOPs can be classified as; 1) fully-rated back-to-back (B2B) SOPs, and 2) partially rated SOPs. A fully-rated B2B SOP uses two or more VSCs connected B2B to a common DC-link and interfaced to AC networks using interfacing transformers. A partially rated SOP uses a series connection of VSC(s) similar to a Unified Power Flow Controller (UPFC) [74].

2.4.1 Role of Soft Open Points in medium voltage distribution networks

SOPs are installed to improve the controllability and automation of MV distribution networks. The key benefits of SOPs are summarised as follows:

- **Power flow management**

SOPs control active and reactive power independently and provide voltage regulation in MV distribution networks. They have several advantages such as fast response, frequent actions and continuous control. The setpoints of SOPs can be determined using several control strategies that adopt single-objective optimisation or multi-objective optimisation [75], [76], [77].

- **Power quality improvement**

SOPs can be used to improve power quality problems of distribution networks. For example, SOPs can provide instant reactive power support to tackle voltage problems (e.g., voltage fluctuation). In addition, they can adjust active power flow between feeders to mitigate against phase imbalance [78], [79].

- **Flexibility improvement**

SOPs provide distribution networks with the required operational flexibility to cope with the uncertainty of high levels of DGs [80], [81]. They can be considered energy hubs that realise mutual power support among multiple regions of distribution networks [82].

- **Fault isolation and quick supply restoration**

B2B SOPs enable the connection of AC networks without affecting the fault levels [83]. During fault conditions, B2B SOPs isolate the fault and limit the fault

propagation. They can also provide fast restoration to the isolated loads on one feeder through the other [84].

2.4.2 Fully rated Back-to-Back Soft Open Points

- **Principle of operation**

Figure 2-4 shows schematic diagrams of a two-terminal SOP in a distribution network. Figure 2-4(a) shows a basic configuration of an SOP installed in place of a normally open point. Figure 2-4(b) shows the circuit configuration of a two-terminal B2B SOP. VSC 1 and VSC 2 are interfaced to Feeder1 and Feeder 2 using line-frequency interfacing transformers Tr.1 and Tr.2.

(a)

(b)
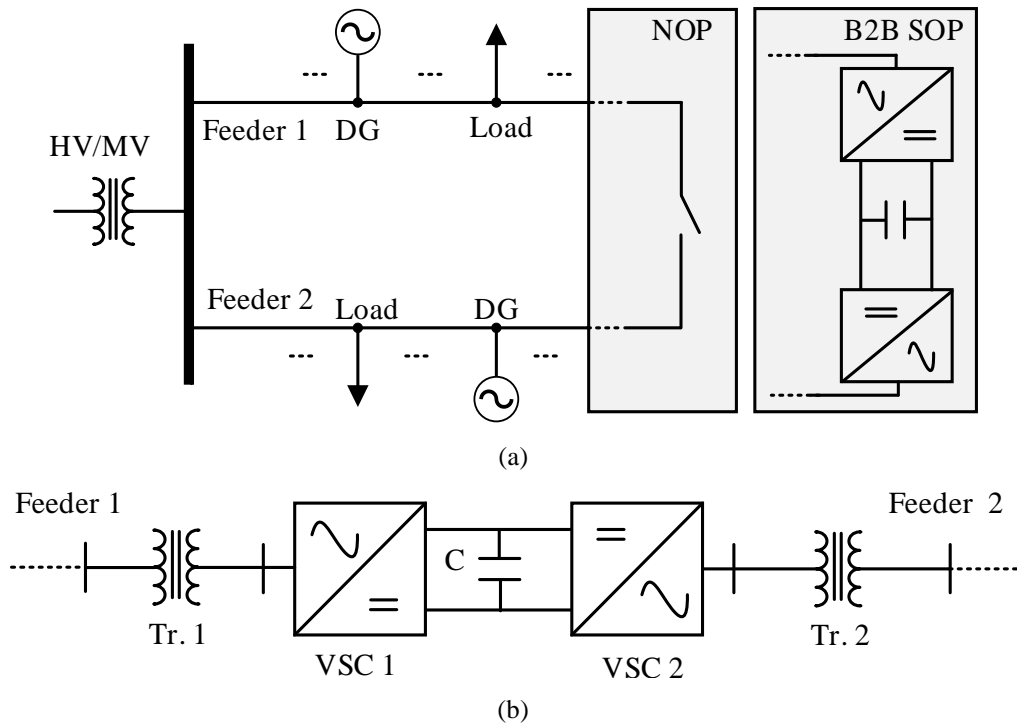
Figure 2-4 Schematic diagrams of; (a) basic configuration of a distribution network with an SOP [85], and (b) circuit configuration of a B2B SOP

The role of the interfacing transformers are 1) provide voltage matching, 2) isolate the converters from the connected AC networks, and 3) reduce the harmonic content [86]. Their main disadvantage is the bulky size.

- **Control scheme**

Figure 2-5 shows the complete control scheme of a two-terminal fully-rated B2B SOP. VSC 1 and VSC 2 are controlled independently. VSC 1 operates in P-Q control mode (i.e., inverter) to independently control active and reactive power P_1 and Q_1. VSC 2 operates in V_{dc}-Q control mode (i.e., rectifier) to regulate the DC voltage V_{dc} and provide voltage regulation Q_2.

Each VSC regulates active power (or DC voltage) and reactive power (or AC voltage) by controlling the current components I_d and I_q of the current I.
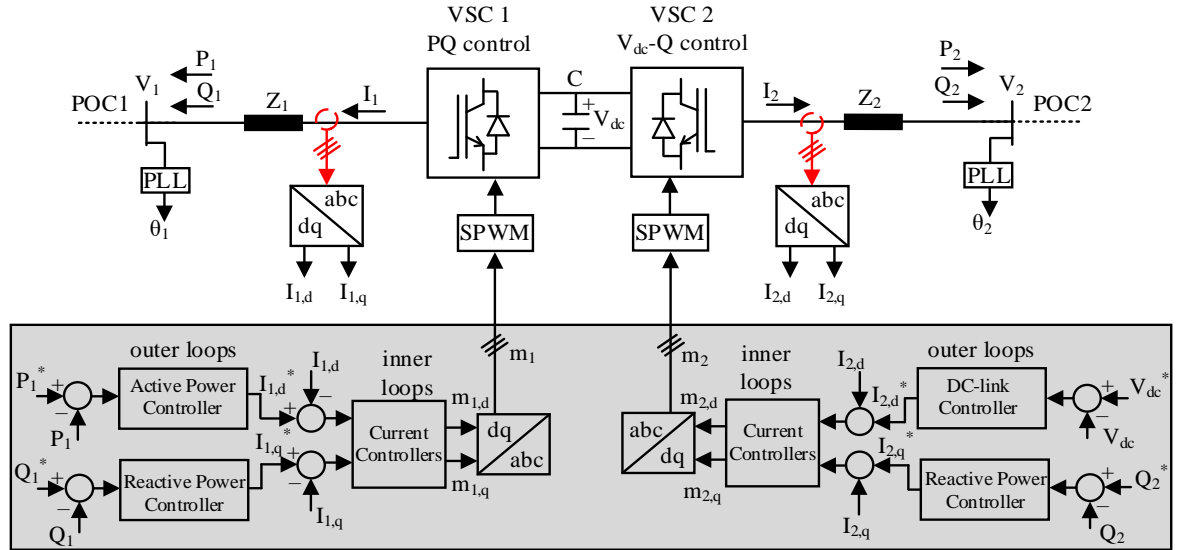
Figure 2-5 Complete control scheme of a fully-rated B2B SOP [87]

The control scheme of each VSC is realised by cascaded dq current control [88]. Outer control loops generate the reference current components I_d^* and I_q^* for inner current control loops. The measured currents I_1 and I_2 are transformed into dq current components I_d and I_q using an abc to dq transformation. Note that $I_{1,d} \propto P_1 \,\& \, I_{2,d} \propto V_{dc}$ and $I_{1,q} \propto Q_1 \,\& \, I_{2,q} \propto Q_2$.

The inner current control loops minimise the errors between the reference and measured current components using PI controllers, then generate the modulating signals (m_d) and (m_q) After transforming (m_d) and (m_q) into a three-phase quantity (m) using dq to abc transformation, the gate signals of the IGBTs are obtained using sinusoidal pulse-width modulation (SPWM).

Phase-locked loops (PLLs) are used to obtain the phase angle of the voltages at the point of connection (POC) (e.g., θ_1 and θ_2) [89], [90].

To decouple the dynamics of the inner and outer control loops, the inner current control loops are faster than the outer current control loops [91].

2.4.3 Partially rated Soft Open Points

- **Principle of operation**

Partially rated SOPs rely on the series converter(s) to control the power flow. Figure 2-6 shows the series converter that performs the main function (i.e., power flow control) of partially rated SOPs.
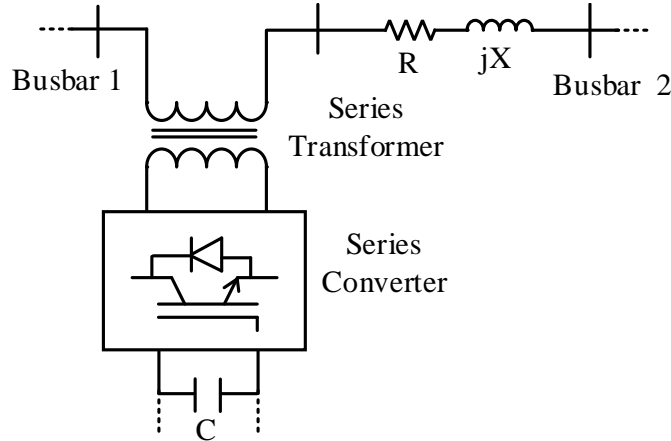
Figure 2-6 Series converter of a partially rated SOP

The shunt converter has various roles within various topologies. For example, in the conventional UPFC, the shunt converter exchanges active power with the series converter. In a Transformer-less UPFC and distributed Power flow controller (DPFC) [92], the shunt converter exchanges only reactive power with the connected AC network.

Figure 2-7 shows the equivalent circuit of a series converter connected to a two-busbar distribution network. The series converter injects a controllable voltage $\overline{V}_{se} = |\overline{V}_{se}| \angle \rho$ in series with voltage $\overline{V}_1$ making the controllable resultant voltage $\overline{V}_1^{'}$.
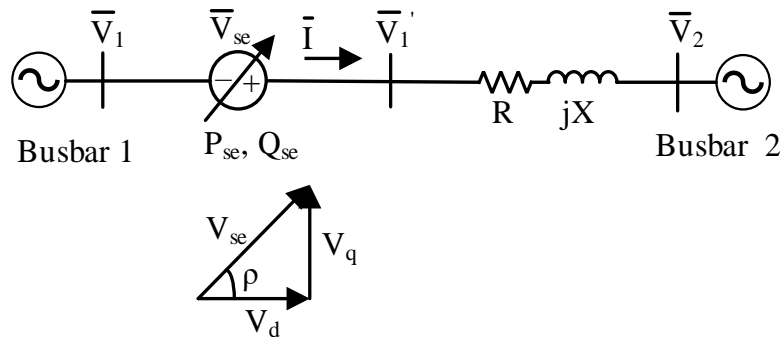
Figure 2-7 Equivalent circuit of a series converter connected to a two-busbar network

- **Control scheme**

Figure 2-8 shows a basic control scheme of a series converter in P-Q control mode.
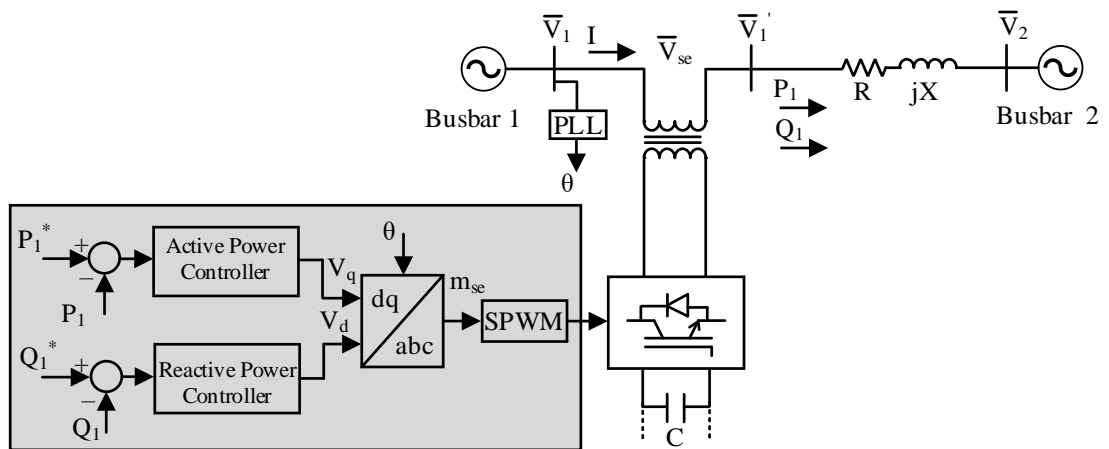
Figure 2-8 Control scheme of a series converter

The series converter controls the active and reactive power P_1 and Q_1 by manipulating the direct and quadrature voltage components V_d and V_q of the series voltage $\overline{V}_{se}$.

The X/R ratio of distribution networks is lower than transmission networks. Therefore, power P_1 and Q_1 are coupled to voltage components V_d and V_q [93], [94].

2.5 Applications of Soft Open Points and other distribution-level power electronic devices

SOPs and several power electronic devices have been trialled in distribution networks. Figure 2-9 shows a schematic diagram of the two-terminal SOP and the three-terminal SOP trialled by the UK Power Networks (UKPN) project "Flexible Urban Network" [95]. The SOPs were deployed to release the thermal and voltage constraints in low voltage networks.
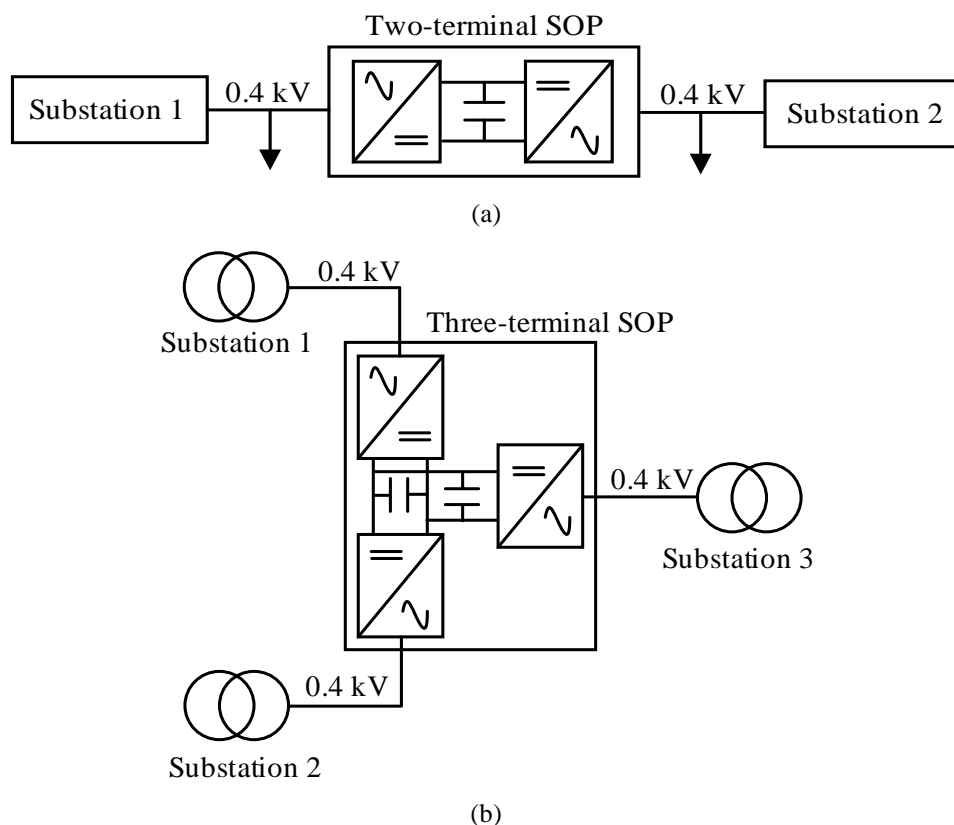
Figure 2-9 Schematic diagrams of; (a) two-terminal SOP and (b) three-terminal SOP [96]

In [97], a 33 kV, 20 MVA Flexible Power Link (FPL) was proposed by the Western Power Distribution (WPD) in the project "Network Equilibrium" to control the power flow between two 33 kV distribution areas. Figure 2-10 shows the FPL connected in the 33 kV distribution network. It was implemented using B2B VSCs installed at a normal open point. The FPL provides power flow and voltage control to maximise the amount of DGs connected to the 33 kV distribution network.
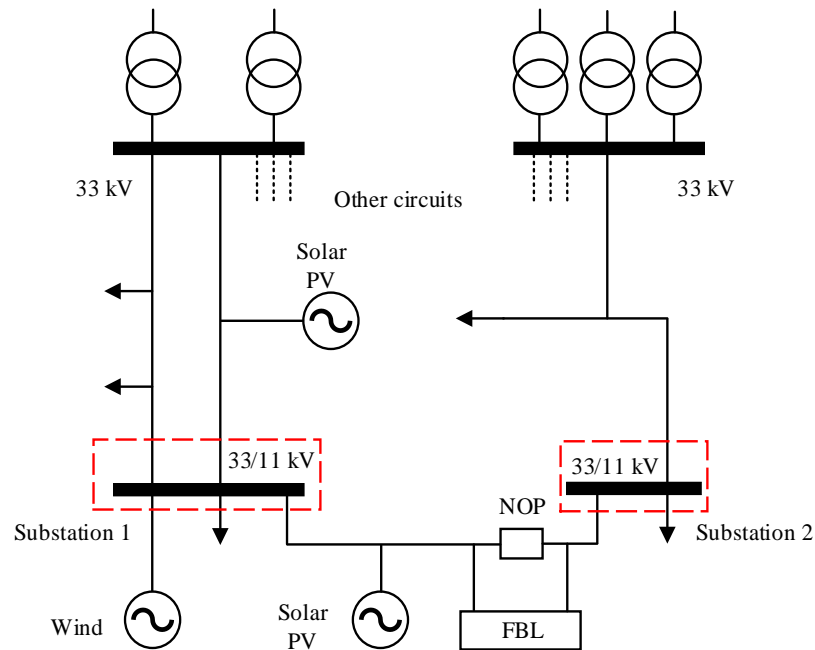
Figure 2-10 Schematic diagram of the 33 kV distribution network with the Flexible Power Link [98]

In [99], ±27 kV, 30.5 MVA medium voltage DC link (MVDC) was proposed by Scottish Power Energy Networks (SPEN) project entitled "Angle DC" to control the power flow between two 33 kV substations [100]. The DC-link is implemented using two VSC stations, inverter station and rectifier station, connected with a distribution network. The two VSC stations are installed either B2B, similar to SOPs or at different geographical locations [101]. Figure 2-11 shows the circuit configuration of the MVDC link.
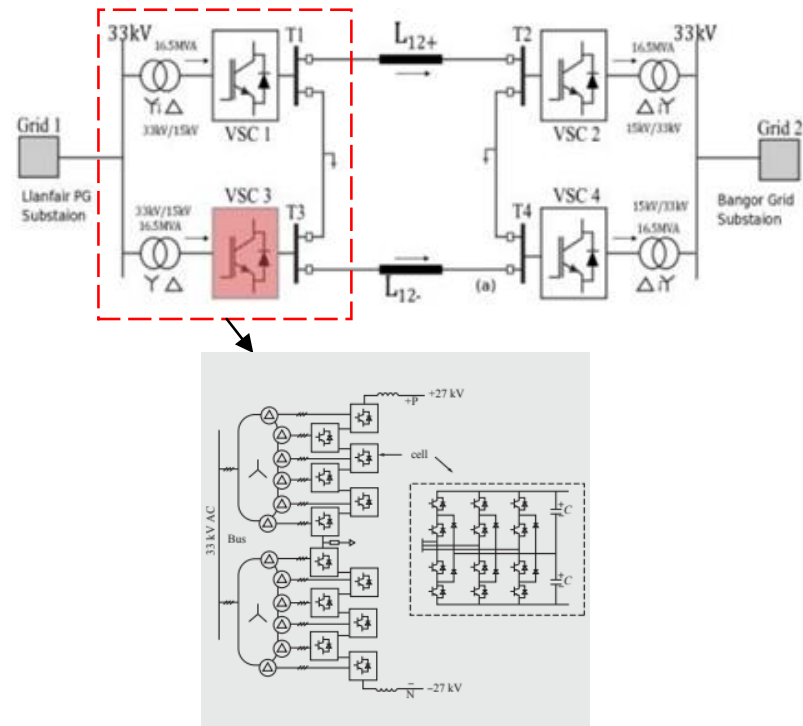
Figure 2-11 MVDC link of Angle DC project [102], [103]

In [104], 11 kV, 5 MVA Soft Power Bridge (SPB) device was proposed by the UKPN Project "Active Response to Distribution Network Constraints". The Soft Power Bridge has both series and shunt elements in similar configuration to a Unified Power Flow Controller. Figure 2-12 shows a schematic diagram of the Soft Power Bridge.
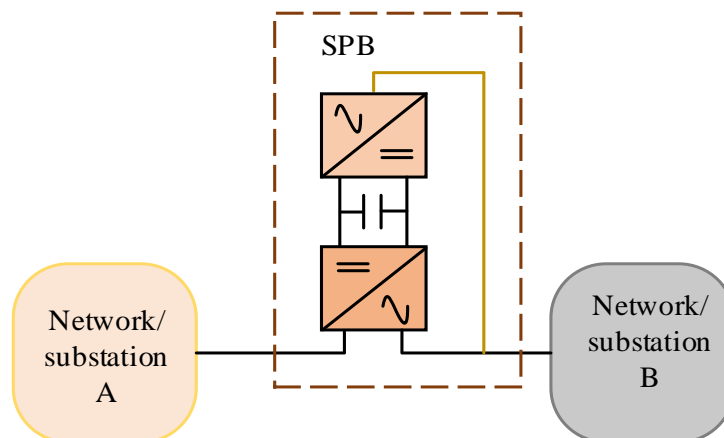
Figure 2-12 Soft Power Bridge [104]

2.6 Summary

Integrating DGs to MV distribution networks requires improving the controllability and automation of the existing distribution networks. Voltage rise in distribution networks is the main barrier for DGs connection, especially during periods of low demand. Power electronic devices such as SOPs can provide power flow management and release distribution networks' voltage and thermal constraints.

Several projects have trialled fully-rated B2B configuration of VSCs in MV distribution networks. They can provide power flow control and voltage regulation during normal operation. They have a good response during faults (e.g., limit fault propagation and faster supply restoration).

Recently, the series connection of VSCs similar to a UPFC has been investigated. The series connection of VSCs aims to provide power flow management using partially rated converters that achieve lower cost and size over the fully-rated B2B configuration.

The series connection of VSCs has not been fully addressed in MV distribution networks. More investigation is required to identify an efficient topology and examine the performance of the series converter during external faults.

Chapter 3 Multi-terminal Fully Rated Back-to-Back Soft Open Points

This chapter investigates the operational benefits of multi-terminal fully-rated back-to-back Soft Open Points in medium voltage distribution networks.

3.1 Introduction

A fully-rated back-to-back (B2B) Soft Open Point (SOP) is a power electronic device installed in distribution networks to provide power flow control and voltage regulation. Previous studies investigated the operational benefits of two-terminal B2B SOPs [105], [106]. A multi-terminal SOP offers more operational benefits by realising mutual power exchange among multiple circuits.

Figure 3-1 shows a simple distribution network with an SOP. It consists of two or multiple Voltage Source Converters (VSCs) connected B2B through a common DC link.
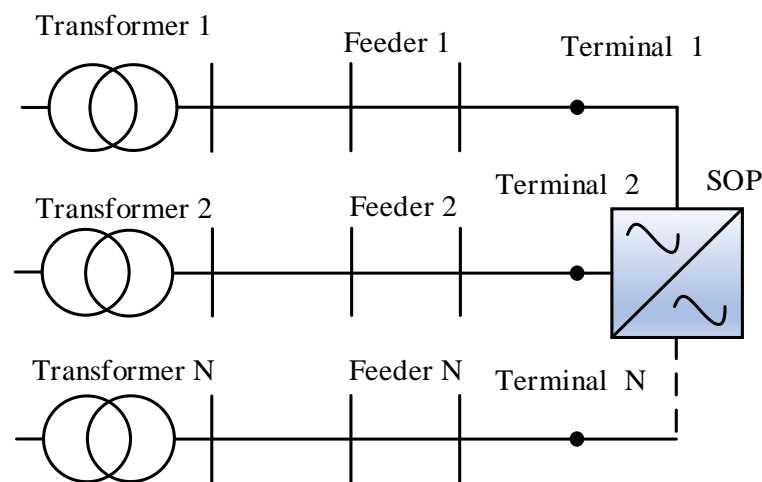
Figure 3-1 Simple distribution network with a B2B Soft Open Point

This chapter extends the analysis in the Applied Energy Journal paper entitled "Optimal Operation of Soft Open Points in Medium Voltage Electrical Distribution Networks with Distributed Generation" [107]. The operational benefits of a multi-terminal fully-rated B2B SOP were assessed. Then, a comparison of a distribution network with a three-terminal SOP, a two-terminal SOP and no SOP was undertaken.

The following points were addressed:

1. The use of sensitivity factors based on the Jacobian matrix was investigated.

2. An optimisation problem was formulated using sensitivity factors. The solution provided SOP setpoints that achieved an optimal operation of a distribution network.

3. The operational benefits of a three-terminal SOP were quantified using a 34-bus distribution network.

The results showed that the connection of a three-terminal SOP reduced the energy losses and increased the headroom of voltage limits of a distribution network more than a two-terminal SOP. In addition, the three-terminal SOP of 6 MVA total capacity enabled the distribution network to host an additional 20% of Distributed Generators (DGs) more than the two-terminal SOP of 4 MVA total capacity.

A comparison between a three-terminal SOP and a two-terminal SOP was undertaken with the same network operating conditions and the same total capacity of SOPs (i.e., a three-terminal SOP and a two-terminal SOP each of 6 MVA). The results showed that the three-terminal SOP enabled the distribution network to host more capacity of DGs and achieved lower energy losses than the two-terminal SOP.

3.2 A Two-terminal SOP in a medium voltage distribution network

3.2.1 Literature review

Figure 3-2 shows a schematic diagram of an SOP connected in place of normally open point (NOP).
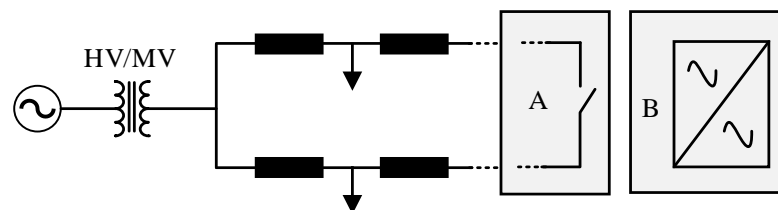
Figure 3-2 A simple distribution network; option A represents NOP and option B represents an SOP [105]

In [105], the operational benefits of installing an SOP in distribution networks were investigated compared to other voltage control strategies such as dynamic on-load tap changer (OLTC) and STATCOM. It was shown that much of the operational benefits of a B2B SOP were achieved due to its reactive power capability. In addition, active power transfer capability added some benefits. The benefits were increased with increased SOP ratings. The SOP reduced the energy curtailment of DGs, demonstrating the business benefits of adding such a device.

In [106], the operational benefits were quantified in three cases: 1) considering only SOPs, 2) considering only network reconfiguration, and 3) both of them. A combination of SOP control and network reconfiguration showed that it achieved better operational benefits with smaller SOP ratings.

In [107], the Jacobian matrix showed the correlation between the changes in active and reactive power injections of an SOP and the changes in voltage angle and magnitude of a distribution network. Three objective functions were applied separately to quantify the benefits of connecting a two-terminal SOP in a distribution network. These are Energy Loss Minimisation, Feeder Load Balancing and Voltage Profile Improvement. Results showed that the two-terminal SOP increased the hosting capacity of the distribution network. The control scheme using the objective of Voltage Profile Improvements increased the headroom of the voltage limits by the largest margin. However, it dispatched the largest amount of reactive power and was at the expense of increased energy losses.

In [108], an energy storage element was added to the DC-link of an SOP. The energy storage element mitigated the effects of output power transients of photovoltaic systems due to a fast-moving cloud cover. It was shown that integrating the SOP with a storage element reduced the voltage fluctuations and allowed more photovoltaics (PVs) uptake. However, the study did not analyse the business feasibility of adding the storage element to the SOP.

In [109], the flexibility brought by SOPs was quantified. The maximum hosting capacity of DGs described the flexibility index of SOP integration. It was shown that an SOP with a storage element achieved the greatest flexibility index.

In [110], the performance of real two-terminal and three-terminal SOPs was recorded. The SOPs were deployed by the UK Power Networks project entitled "Flexible Urban Network-Low Voltage". The visualisation techniques used to identify the candidate busbars of the SOPs were discussed in [111]. The selection criteria of SOP sites were presented in [112], for example, transfer potential of sites, space requirements and distance between substations. The control algorithm of the SOPs was presented in [113]. It was shown that transformer equalisation and voltage support modes of operation helped to improve network utilisation and reduce voltage deviation.

In [114], a coordinated voltage and VAR control method was proposed. An optimisation problem was solved considering the cooperation of an SOP and VAR devices such as OLTC and switchable CBs. This method relied on a central controller that receives all network measurements, solves the optimisation problem, and sends

the setpoints to the SOP and VAR devices. These analyses were extended in [115] to consider a distribution network with unbalanced three-phase conditions.

A combined decentralised and local voltage control strategy of SOPs was proposed in [116] to address a centralised approach's computation and communication burdens. The decentralised optimisation was used to regulate the active power exchange of SOPs in which a distribution network was divided into subnetworks. The local Q-V curve of an SOP was set using local measurements to respond quickly to frequent voltage fluctuations.

In [117], the performance of an SOP was investigated under both balanced and unbalanced network faults. Results showed that the faulted side VSC had a limited contribution to the fault current before being disabled. The un-faulted side VSC had a regulated output current and voltage that were not affected by the fault.

In [118], an SOP was used for supply restoration of a distribution network following a fault. SOPs offered a faster supply restoration compared to the traditional network reconfiguration method.

To sum up, a two-terminal B2B SOP provides operational benefits and improves the controllability and automation of MV distribution networks. It can provide independent control of active and reactive power and voltage regulation during steady-state operation. The DC-link can be equipped with a storage element to improve the flexibility of operation further. It limits the propagation of fault current during faults. Further analysis is required to investigate the operational benefits of a multi-terminal SOP in distribution networks.

3.2.2 Replicating the operational benefits of a two-terminal SOP

For this research, the optimisation and power flow models of the case study in [107] were replicated before further investigation.

Figure 3-3 shows the case study taken from [107]. The optimal operation of the test network was obtained considering Energy Loss Minimisation as an objective function. Figure 3-3(a) shows the test network. A two-terminal SOP is connected at the remote ends of Feeder 2 and Feeder 3. Figure 3-3(b) shows the P/Q injections of the two-terminal SOP. Figure 3-3 (c) shows the voltage profiles. The base voltage was 11 kV.
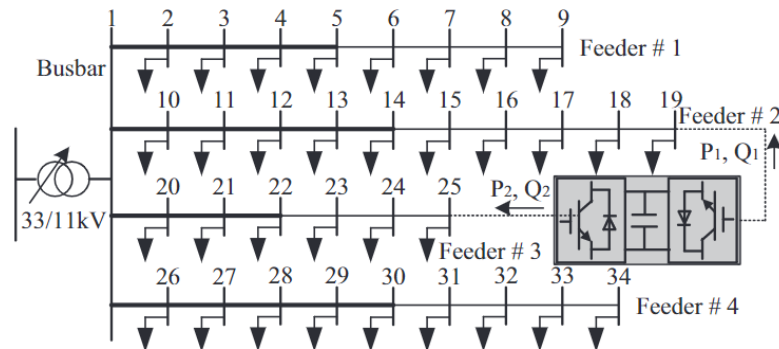
(a)
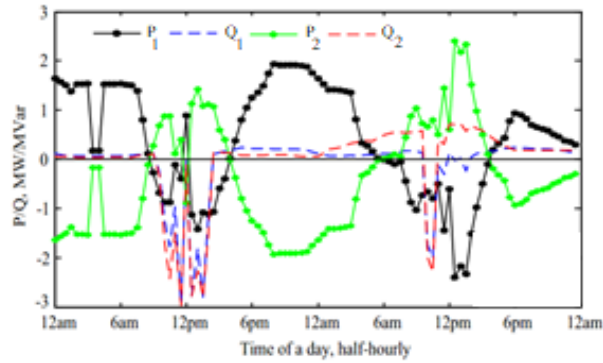
(b)
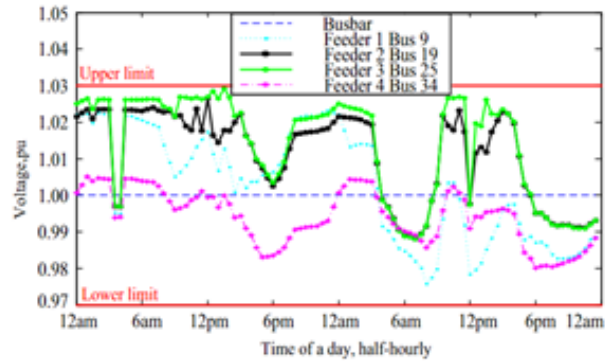
(c)

Figure 3-3 Case study taken from [107]; (a) test network, (b) P/Q setpoints, and (c) Voltage profiles

Figure 3-4 shows the replication of the results in Figure 3-3. Figure 3-4 (a) shows the active and reactive power setpoints of the two-terminal SOP. Figure 3-4 (b) shows the voltage profiles of the test network. The active and reactive power setpoints in Figure 3-4(a) are similar to that of Figure 3-3(b), and the voltage profiles in Figure 3-4(b) to that of Figure 3-3(c). These indicate the correctness of the optimisation and power flow models.
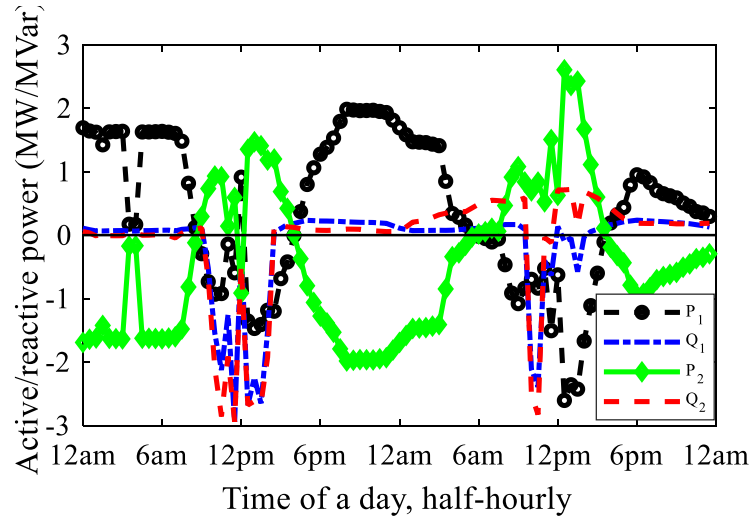
(a)
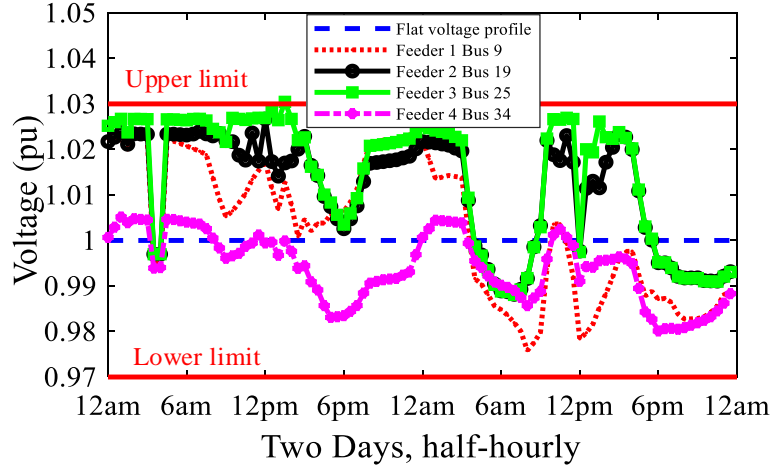
(b)

Figure 3-4 Replication of the results in Figure 3-3; (a) P/Q setpoints, and (b) voltage profiles

3.3 A multi-terminal SOP in a medium voltage distribution network

Figure 3-5 shows the circuit diagram of a three-terminal B2B SOP. VSC 1, VSC 2 and VSC 3 are interfaced to Network 1, Network 2 and Network 3 using interfacing transformers Tr.1, Tr.2 and Tr.3.
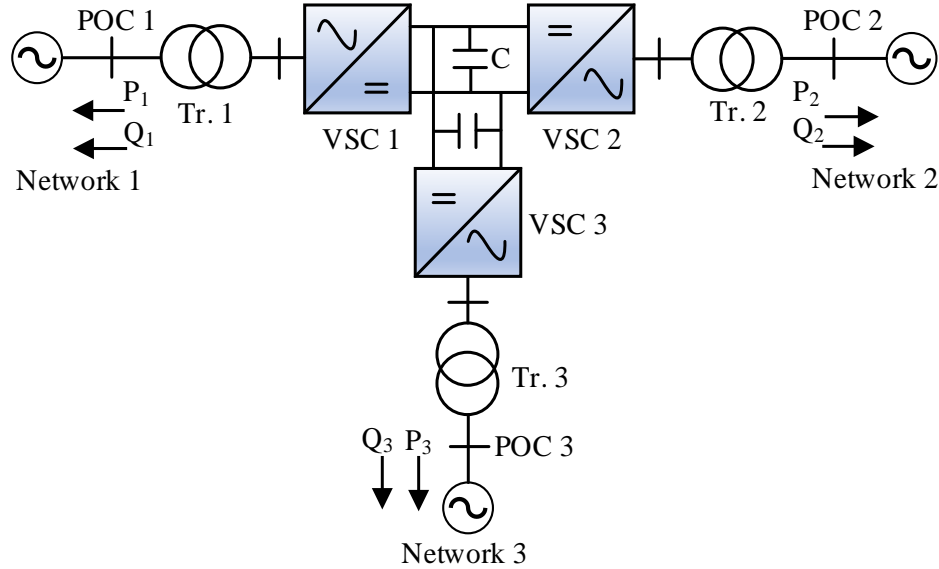
Figure 3-5 Circuit diagram of a three-terminal SOP

A three-terminal SOP controls active and reactive power independently in four-quadrant of operation. The DC bus provides galvanic isolation, which prevents fault current propagation during faults.

One of the VSC in a three-terminal SOP regulates the DC link voltage such as $\sum P_1 + P_2 + P_3 + P_{Loss} = 0$, where P_{Loss} is the power losses of an SOP. Other VSCs control active power. Each VSC independently controls reactive power.

3.4 Optimal operation of a multi-terminal Soft Open Points

The P/Q setpoints of an SOP were obtained by solving a constrained nonlinear optimisation problem using the constrained nonlinear solver f_{mincon} of MATLAB Optimisation Toolbox. The syntax of the optimisation function is $X = f_{min con}(fun, X0, A, b, A_{eq}, b_{eq}, nonlcon)$, where X is a vector of the solution, fun is the objective function, $X0$ is the initial point, A is a matrix of linear inequality constraints, b is a vector of linear inequality constraints, A_{eq} is a matrix of linear equality constraints, b_{eq} is a vector of linear equality constraints and $nonlcon$ is the nonlinear constraints [119].

The optimisation function was formulated using sensitivity factors and considered the operational limits of both an SOP and a distribution network.

Various objective functions were examined separately, such as Energy Loss Minimisation, Feeder Load Balancing and Voltage Profile Improvement.

Figure 3-6 shows a flow chart of the optimisation algorithm developed in MATLAB m-file.
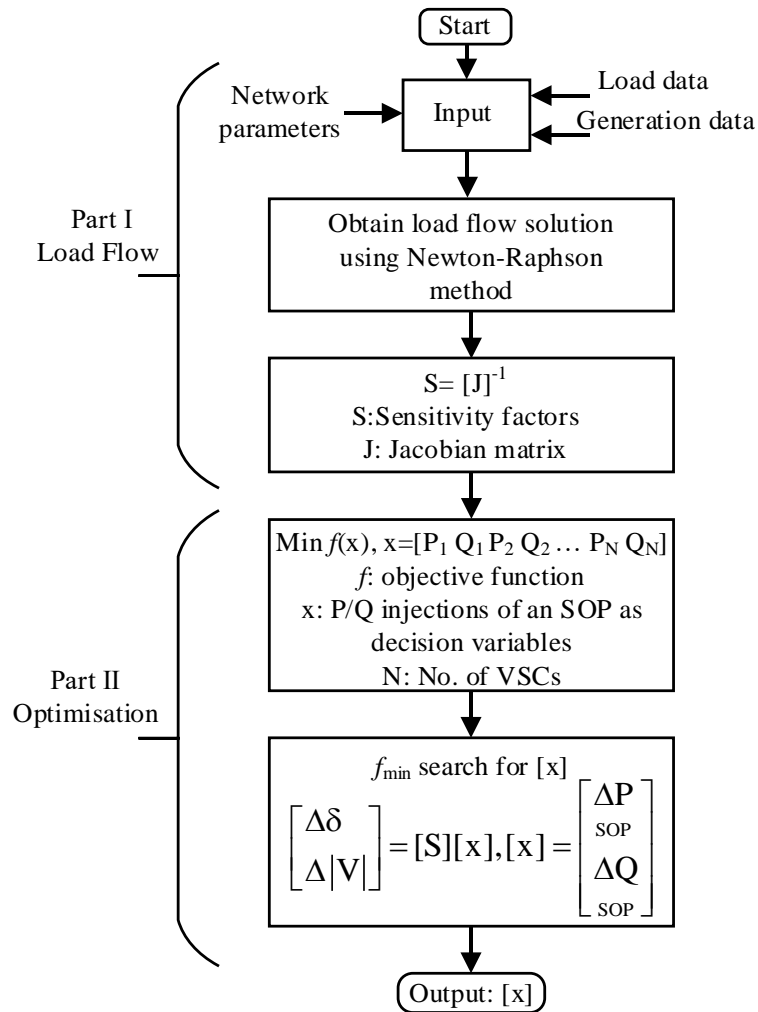
Figure 3-6 Flow chart describing the optimisation algorithm

3.4.1 Steady state modelling

Figure 3-7 shows a generic power injection model of an SOP.
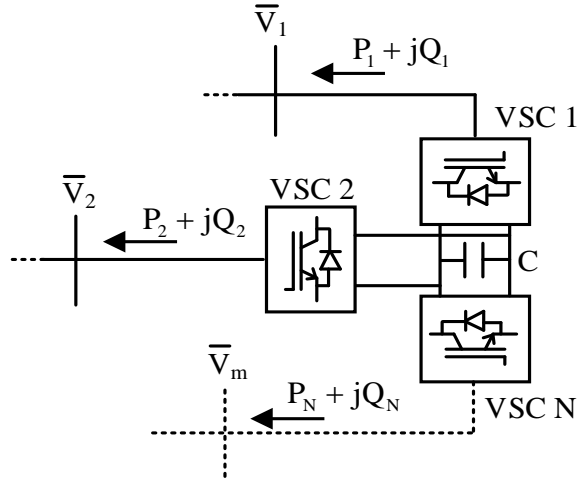
Figure 3-7 Power injection model of an SOP

3.4.2 Jacobian matrix based sensitivity analysis

For all P-Q buses, the sensitivities of voltage angle and magnitude to P/Q injections of an SOP were calculated as given in (3-1) [120].

$$
\begin{bmatrix} \Delta\delta \\ \Delta|V| \end{bmatrix} = J^{-1} \begin{bmatrix} \Delta P \\ \Delta Q \end{bmatrix} = \begin{bmatrix} \dfrac{\partial P}{\partial \delta} & \dfrac{\partial P}{\partial |V|} \\ \dfrac{\partial Q}{\partial \delta} & \dfrac{\partial Q}{\partial |V|} \end{bmatrix}^{-1} \times \begin{bmatrix} \Delta P \\ \Delta Q \end{bmatrix} \tag{3-1}
$$

For sequential steady-state power flow analysis, the Jacobian matrix was formulated describing the network conditions at every time step (t).

The sensitivity matrix was obtained by taking the Jacobina inverse as given in (3-2), where $C_{\delta,P}$ and $C_{\delta,Q}$ are the power angle sensitives in rad/MW and rad/MVAr. $C_{V,P}$ and $C_{V,Q}$ are voltage sensitives in V/MW and V/MVAr.

$$
\begin{cases} S = J^{-1} \\ S = \begin{bmatrix} C_{\delta,P} & C_{\delta,Q} \\ C_{V,P} & C_{V,Q} \end{bmatrix} \end{cases} \tag{3-2}
$$

The changes in voltage angle $\Delta\delta_i$ and magnitude $\Delta|V_i|$ at node (i) were calculated as in (3-3) and (3-4), where (m) is the total number of busbars, i = 2,3,4, … m, and j = 2,3,4, … m.

$$\Delta\delta_i = \sum_{j=2}^{m}(C_{\delta_i P_j} \cdot \Delta P_j + C_{\delta_i Q_j} \cdot \Delta Q_j) \tag{3-3}$$

$$\Delta|V_i| = \sum_{j=2}^{m}(C_{V_i P_j} \cdot \Delta P_j + C_{V_i Q_j} \cdot \Delta Q_j) \tag{3-4}$$

The voltage angle and magnitude at node (i) were obtained as given in (3-5) and (3-6), where $\delta_{i,0}$ and $|V_{i,0}|$ are the voltage angle and magnitude without SOPs.

$$\delta_i = \delta_{i,0} + \Delta\delta_i \tag{3-5}$$

$$|V_i| = |V_{i,0}| + \Delta|V_i| \tag{3-6}$$

Note that $\Delta\delta_i$ and $\Delta|V_i|$ were calculated considering only the active and reactive power injections of an SOP.

3.4.3 Problem formulation

Three objective functions were examined separately.

- **Energy Loss Minimisation**

Energy Loss Minimisation was achieved by minimising the total power losses of a distribution network $P_{T,loss}$. It was formulated as in (3-7), where r_k is the resistance of branch (k) between node (i) and (j), and (n) is the total number of branches in the network.

$$\begin{cases} P_{T,loss} = \sum_{k=1}^{n} r_k \cdot I_k^{\ 2} = \sum_{k=1}^{n} r_k \cdot [\dfrac{\left\| V_i|\angle\delta_i - |V_j|\angle\delta_j \right\|}{Z_{i,j}}]^2 \\ |V_i|\angle\delta_i = (|V_i| + \Delta|V_i|)(\cos(\delta_i + \Delta\delta_i) + j\cdot\sin(\delta_i + \Delta\delta_i)) \\ |V_j|\angle\delta_j = (|V_j| + \Delta|V_j|)(\cos(\delta_j + \Delta\delta_j) + j\cdot\sin(\delta_j + \Delta\delta_j)) \end{cases} \tag{3-7}$$

- **Feeder Load Balancing**

Feeder Load Balancing was achieved by minimising the load balance index LI_k as given in (3-8), where I_k and $I_{k,rated}$ are the actual and rated current of branch (k) [121].

$$LI_k = \sum_{k=1}^{n}(\dfrac{I_k}{I_{k,rated}})^2 \tag{3-8}$$

- **Voltage Profile Improvement**

Voltage Profile Improvement was achieved by keeping the voltages as close as possible to a flat voltage profile (i.e., 1.0 pu) as given in (3-9), where $|V_{nom}|$ is the target voltage for all nodes.

$$\sum_{i=1}^{m} (|V_i| - |V_{nom}|)^2 \tag{3-9}$$

- **Constraints**

The apparent power exchanged between VSC_x and the connected AC network should not exceed the converter's nominal apparent power as given in (3-10), where (N) is the number of converters within an SOP.

$$\sqrt{P_x^2 + Q_x^2} \leq S_x, \ \forall(x) \in N \tag{3-10}$$

During steady-state operation, the sum of the active power must equal zero, as given in (3-11).

$$\sum_{x}^{N} P_x + P_{Loss} = 0 \tag{3-11}$$

The operating losses of a VSC is relatively low. For the sake of simplicity, the losses of the SOP were neglected (i.e., $P_{Loss} = 0$). More information on power losses evaluation of VSCs can be found in [122].

The voltages and currents of a distribution network must remain within the permissible limits as given in (3-12).

$$\begin{cases} I_k \leq I_{k,rated} \\ V_{min} \leq |V_i| \leq V_{max} \end{cases} \tag{3-12}$$

3.5 Case study

3.5.1 Test network

Figure 3-8 shows a three-terminal SOP connected to a 34-bus distribution network. The three-terminal SOP was connected to the remote ends of Feeder 1, Feeder 2, and Feeder 3. It has a total capacity of 6 MVA (i.e., each VSC of 2 MVA).
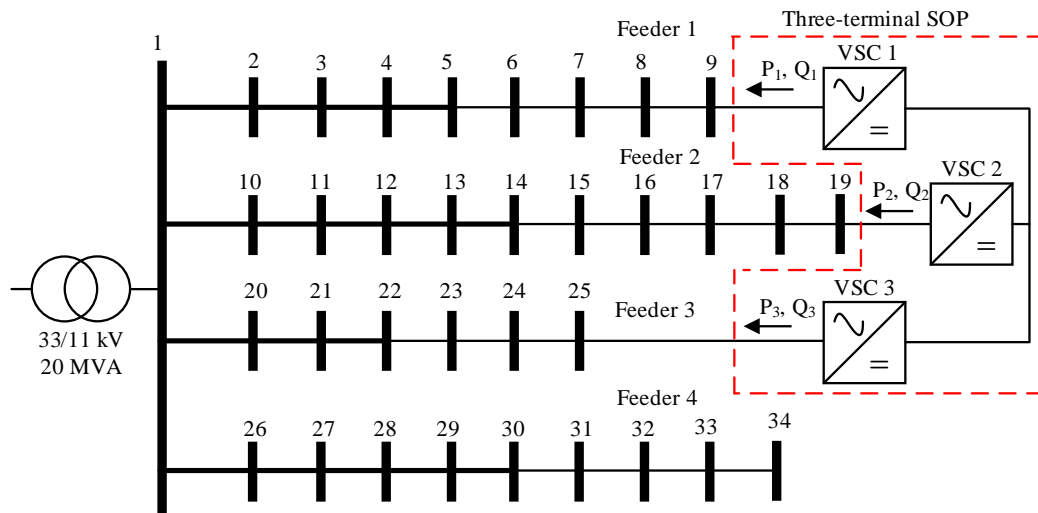
Figure 3-8 A three-terminal SOP connected in a 34-bus distribution network

The network is supplied from a 33/11 kV, 20 MVA transformer. It has four radial feeders. Various DGs and load types were considered at different locations along with the feeders. Table 3-1 shows a summary of the loads' peaks and DGs' ratings.

Table 3-1 Load and DG data [107]

Feeder #.	Load		Distributed generation		
	Type	Total peak (MVA)	Type	Locations	Ratings (MW)
1	Com.	3	Wind	5, 9	2, 0.5
2	Res.	2.5	PV	11, 14, 17	1, 2, 2.5
3	Ind.	3	Wind	22, 25	0.5, 2.5
4	Res.	2.5	PV, wind	30, 33	0.5, 0.5

The complete network information, including network parameters and load and generation data, is found in [107].

The operational benefits of the three-terminal SOP were quantified for two days (i.e., a weekend and a weekday), every step of 30 minutes and considering different DG penetration levels.

The penetration level of DGs refers to the percentage of the sum of all DGs' ratings considered relative to the rating of the 33/11 kV transformer.

Various DG penetration scenarios were considered by scaling up and down the ratings of the DGs. For instance, the DGs' ratings in Table 3-1 represents a DG penetration level of 60%.

Figure 3-9 shows the wind and PV generation profiles for the two days under study. All DGs were operated at unity power factor.
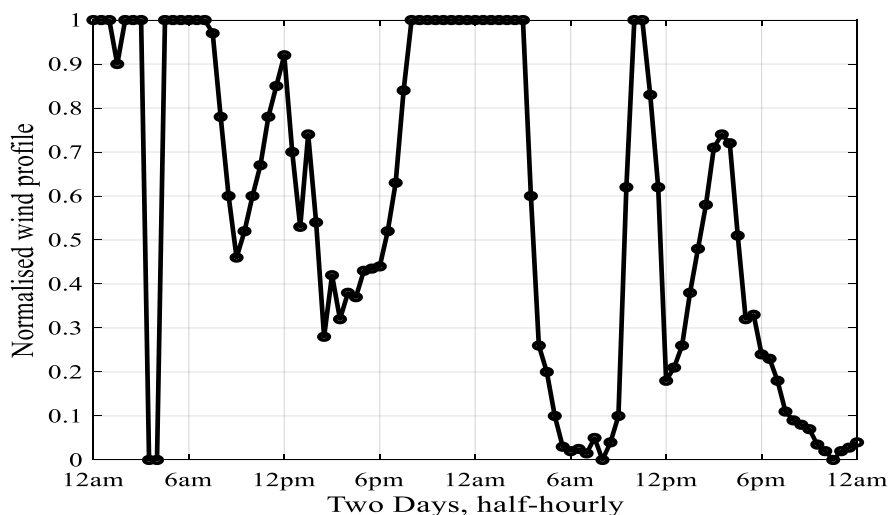
(a)
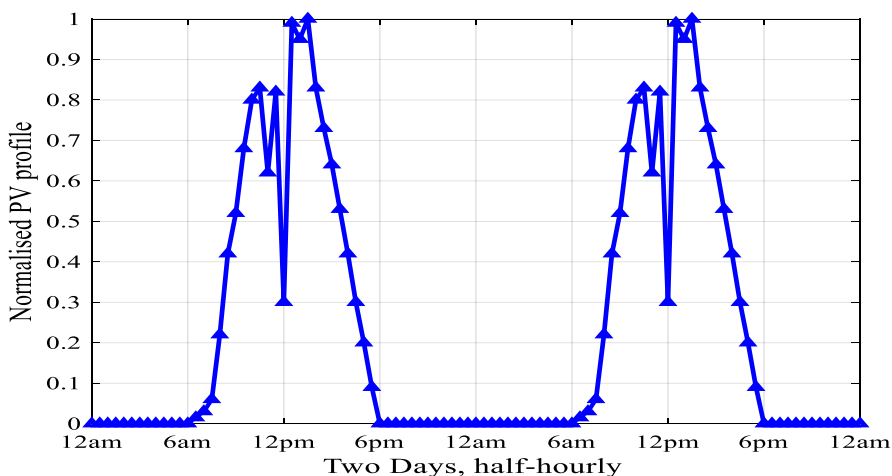
(b)

Figure 3-9 Generation profiles; (a) wind and (b) PV [107]

Figure 3-10 shows the load profiles of residential, commercial, and industrial consumers for two days, a weekend and a weekday, with lagging power factors of 0.98, 0.95 and 0.90. The load and generation profiles are normalised to their peak values mentioned in Table 3-1.
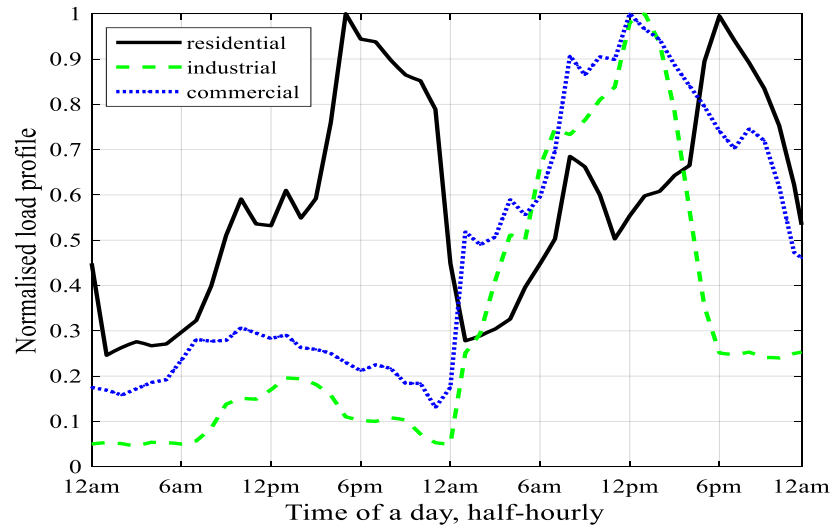
Figure 3-10 Load profiles of residential, industrial and commercial consumers [107]

For comparison, a two-terminal SOP was connected between Feeder 2 and Feeder 3. Two cases were examined; 1) the two-terminal SOP has a total capacity of 4 MVA (i.e., each VSC of 2 MVA), and 2) the two-terminal SOP has a total capacity of 6 MVA (i.e., each VSC of 3 MVA).

3.5.2 Network performance without an SOP

Figure 3-11 shows the voltage profiles without an SOP at 50% and 60% DG penetration levels. The base voltage was 11 kV. Figure 3-11(a) shows no overvoltages were reported at a 50% DG penetration level. Figure 3-11(b) shows overvoltages occurred in Feeder 2 when the DG penetration level increased to 60%. Note that Feeder 2 has a 5.5 MW installed capacity of PVs. The overvoltages happened at the instants when their PVs delivered full capacity, as shown in Figure 3-9.

(a)

(b)
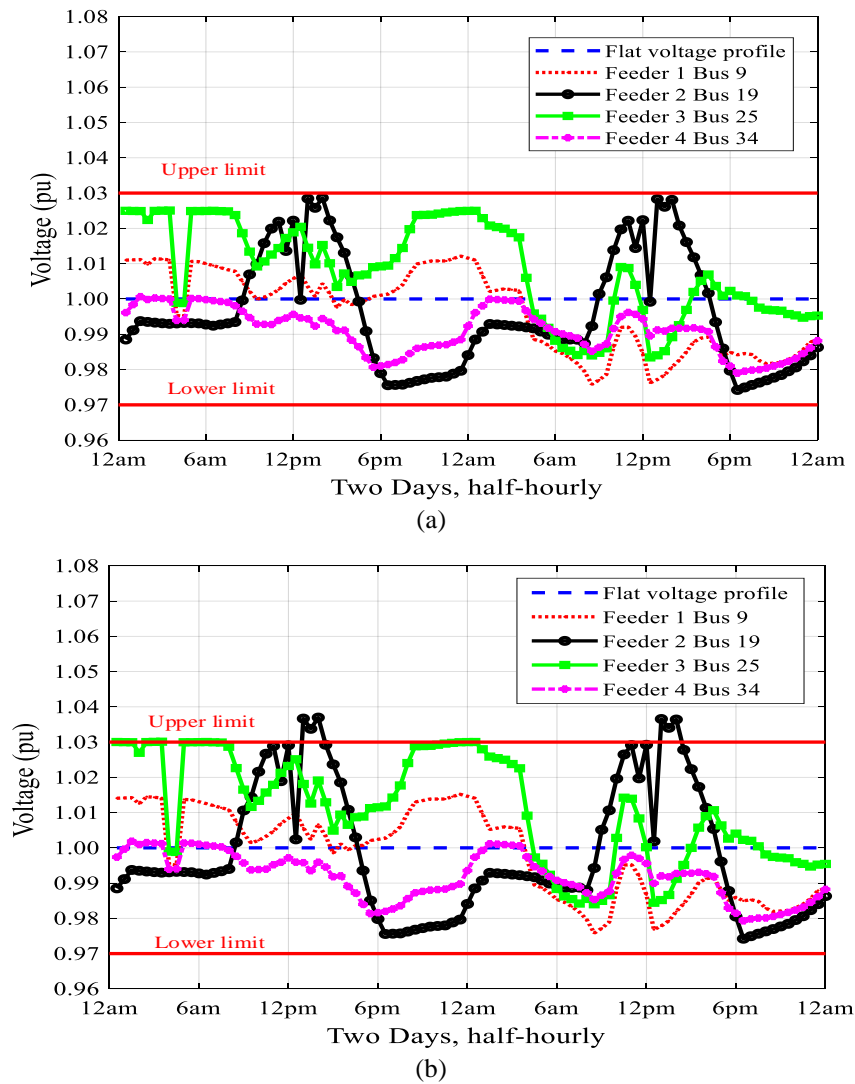
Figure 3-11 Voltage profiles without an SOP at DG penetration levels of; (a) 50%, and (b) 60%

Without an SOP, the distribution network managed to host a 50% penetration level of DGs without violating the voltage constraint. However, a further increase of DGs beyond the 50% penetration level resulted in overvoltages (See Table 3-2 for a complete simulation analysis of the test network).

Figure 3-12 shows the active power flow at the 33/11 kV transformer when the DG penetration level was 50%. The flow of active power was reversed at the instants when the DGs' output exceeded the demand.

45
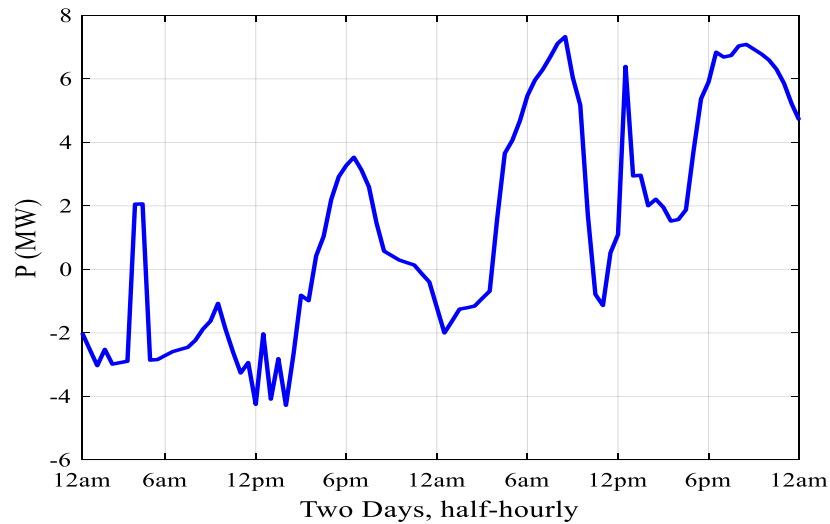
Figure 3-12 Active power at the primary transformer with a DG penetration level of 50%

3.5.3 Network performance with a three-terminal SOP

Figure 3-13 shows the P/Q setpoints of the three-terminal SOP at a DG penetration level of 90%. The setpoints P_1, Q_1, P_2, Q_2, P_3, and Q_3 were determined using Energy Loss Minimisation, Feeder Load Balancing and Voltage Profile Improvement applied separately.

The SOP dispatched active and reactive power in the four-quadrant of operation. The sum of active power at any instant (t) was zero (i.e., $P_1 + P_2 + P_3 = 0$). The reactive power was provided independently by each converter.

The setpoints of Energy Loss Minimisation and Feeder Load Balancing are similar. However, the SOP dispatched more reactive power in Voltage Profile Improvement. This came at the expense of a substantial increase in energy losses when Voltage Profile Improvement was used compared to Energy Loss Minimisation and Feeder Load Balancing (See Table 3-2).
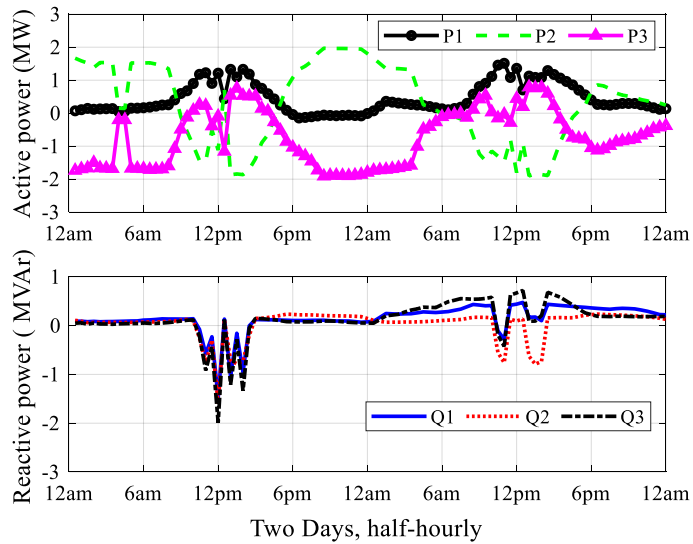
(a) Using Energy Loss Minimisation.
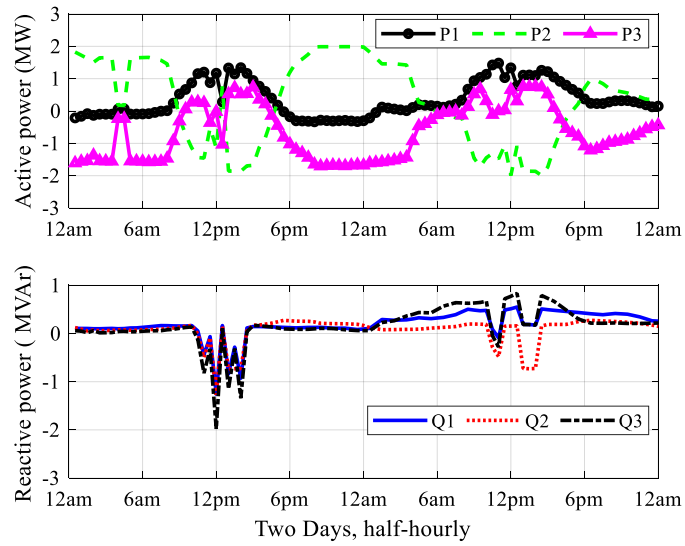
(b) Using Feeder Load Balancing.
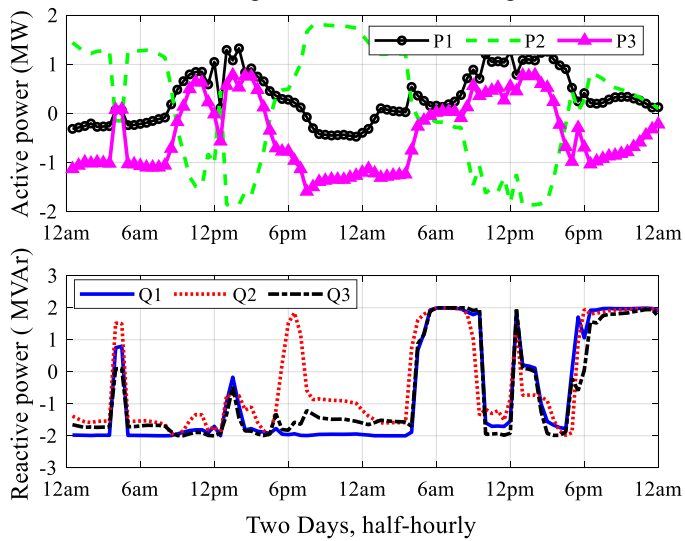
(c) Using Voltage Profile Improvement.

Figure 3-13 P/Q setpoints of a three-terminal SOP at 90% DG penetration level

Figures 3-14 shows the voltage profiles using Energy Loss Minimisation, Feeder Load Balancing and Voltage Profile Improvement at a DG penetration level of 90%. The base voltage was 11 kV. The SOP managed to keep the voltages within limits at a 90% penetration level of DGs.
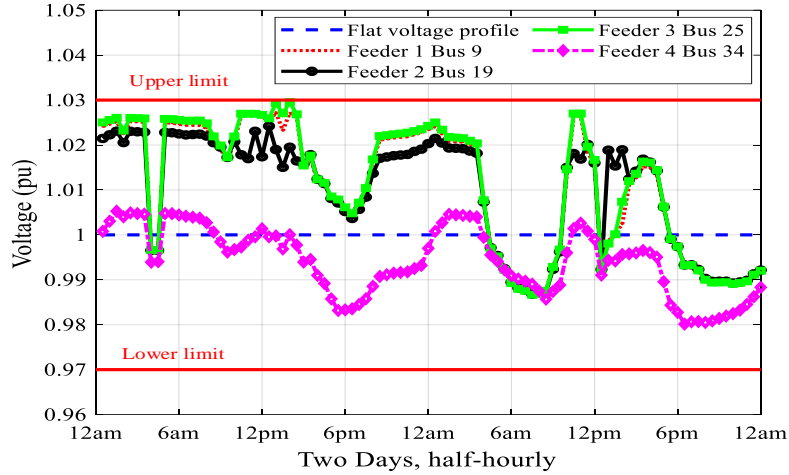
(a) Using Energy Loss Minimisation.
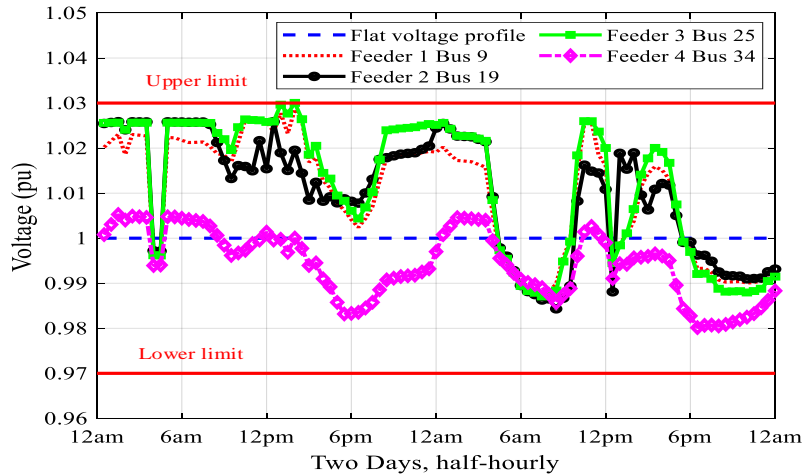
(b) Using Feeder Load Balancing.
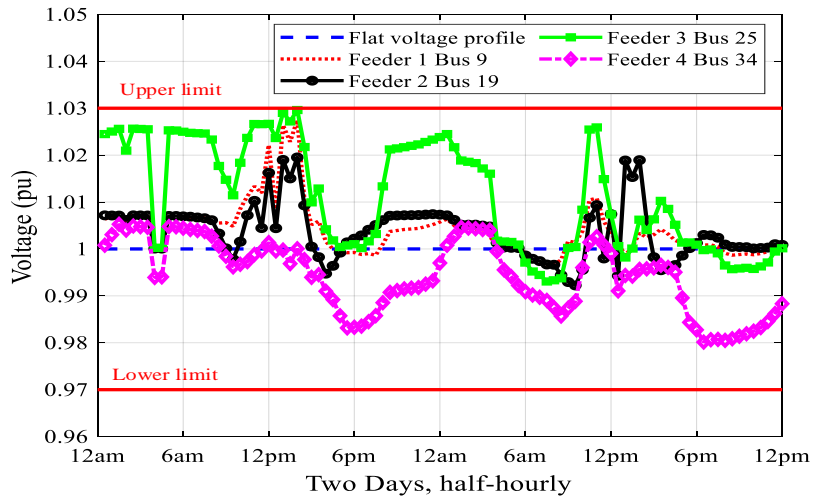
(c) Using Voltage Profile Improvement.

Figure 3-14 Voltage profiles at 90% DG penetration level

3.5.4 Comparison between a three-terminal SOP, a two-terminal SOP and no SOPs

For comparison, the control scheme using the objective of Energy Loss Minimisation was undertaken. A two-terminal SOP was connected at the remote ends of Feeder 2 and Feeder 3 in the 34-bus distribution network of Figure 3-8.

- **Case 1: a three-terminal SOP of 6 MVA and a two-terminal SOP of 4 MVA**

In this case, the three-terminal SOP has three VSCs each of 2 MVA, and the two-terminal SOP has two VSCs each of 2 MVA. The base voltage was 11 kV.

Figure 3-15 shows the maximum and minimum voltage of the test network considering Energy Loss Minimisation. The DG penetration level was increased to 100% with a step of 10%. Results show that the three-terminal SOP enabled the test network to host a DG penetration level of 90%, increasing 20% more than the two-terminal SOP.
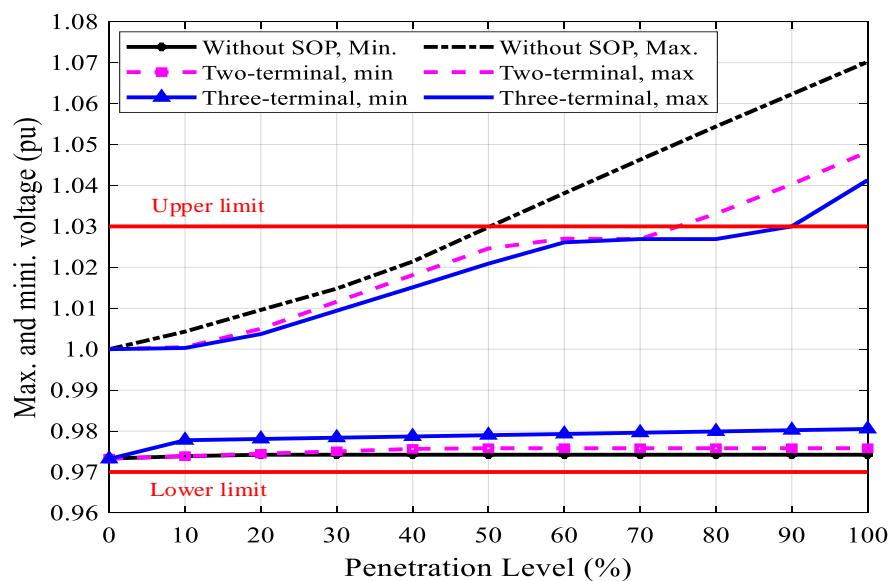
Figure 3-15 Maximum and minimum voltage of Case 1

Figure 3-16 shows the energy losses of the test network using Energy Loss Minimisation. The three-terminal SOP achieved the lowest energy losses.
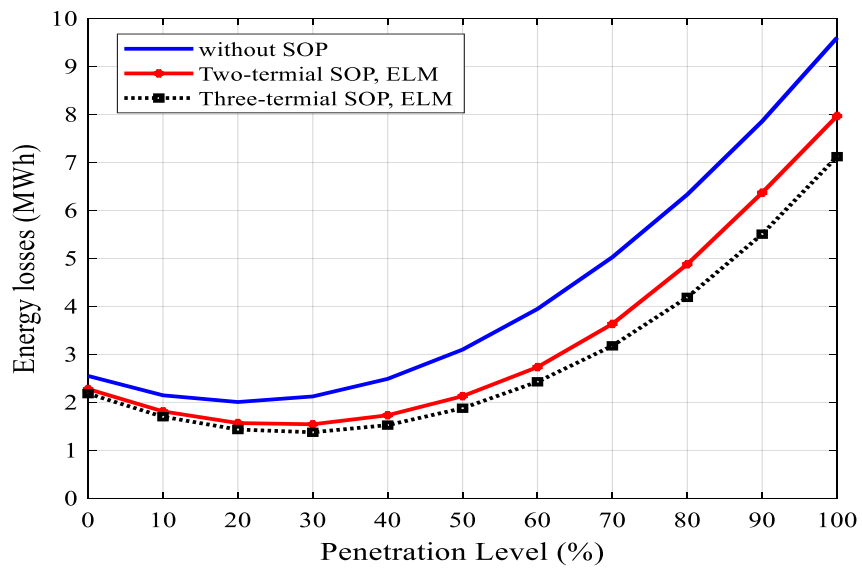
Figure 3-16 Total energy losses for the two days at different DG penetration levels

Table 3-2 provides the complete simulation analysis of the test network with the three-terminal SOP, the two-terminal SOP and no SOPs.

Table 3-2 Overall performance of the test network (Numbers in bold denote overvoltage occurred)

DG Penetration level, %	Without an SOP		Three-terminal SOP (Total capacity of 6 MVA)						Two-terminal SOP (Total capacity of 4 MVA)					
			Energy Loss Minimisation		Feeder Load Balancing		Voltage Profile Improvement		Energy Loss Minimisation		Feeder Load Balancing		Voltage Profile Improvement	
	Voltage, pu	Energy losses, MWh	Voltage, pu	Energy losses, MWh	Voltage, pu	Energy losses, MWh	Voltage, pu	Energy losses, MWh	Voltage, pu	Energy losses, MWh	Voltage, pu	Energy losses, MWh	Voltage, pu	Energy losses, MWh
	Max		Max		Max		Max		Max		Max		Max	
0	1	2.55	1.000	2.18	1.000	2.19	1.003	7.99	1.000	2.28	1.000	2.29	1.002	6.54
10	1.004	2.14	1.000	1.70	1.001	1.71	1.003	6.35	1.000	1.81	1.001	1.82	1.002	5.76
20	1.009	2.00	1.004	1.43	1.005	1.45	1.003	6.11	1.005	1.57	1.005	1.58	1.003	4.94
30	1.015	2.12	1.009	1.38	1.008	1.39	1.003	6.54	1.012	1.54	1.011	1.56	1.006	5.00
40	1.021	2.49	1.015	1.53	1.014	1.55	1.010	7.16	1.018	1.73	1.017	1.75	1.009	5.81
50	1.030	3.10	1.021	1.88	1.019	1.91	1.004	8.15	1.025	2.13	1.023	2.15	1.012	6.41
60	**1.038**	3.95	1.026	2.43	1.024	2.46	1.017	8.92	1.027	2.74	1.027	2.76	1.024	7.15
70	**1.046**	5.03	1.027	3.18	1.027	3.22	1.024	9.88	1.027	3.64	1.027	3.65	1.027	7.96
80	**1.054**	6.33	1.027	4.18	1.027	4.23	1.027	11.03	**1.033**	4.88	**1.033**	4.89	**1.040**	8.81
90	**1.062**	7.86	1.030	5.51	1.030	5.53	1.030	12.02	**1.040**	6.37	**1.042**	6.32	**1.050**	9.87
100	**1.070**	9.60	**1.041**	7.12	**1.041**	7.13	**1.041**	12.68	**1.048**	7.97	**1.049**	7.95	**1.059**	10.96

- **Case 2: A three-terminal SOP of 6 MVA and a two-terminal SOP of 6 MVA**

In this case, the three-terminal SOP has three VSCs each of 2 MVA, and the two-terminal SOP has two VSCs each of 3 MVA. The base voltage was 11 kV.

Figure 3-17 shows the maximum and minimum voltage of the test network considering Energy Loss Minimisation. The DG penetration level was increased to 100% with a step of 10%. Results show that the three-terminal SOP enabled the distribution network to host more DG capacity than the two-terminal SOP of the same total MVA capacity (i.e., the three-terminal SOP enabled a DG penetration level of 90%, while the two-terminal SOP enabled 80% of the same total MVA capacity).
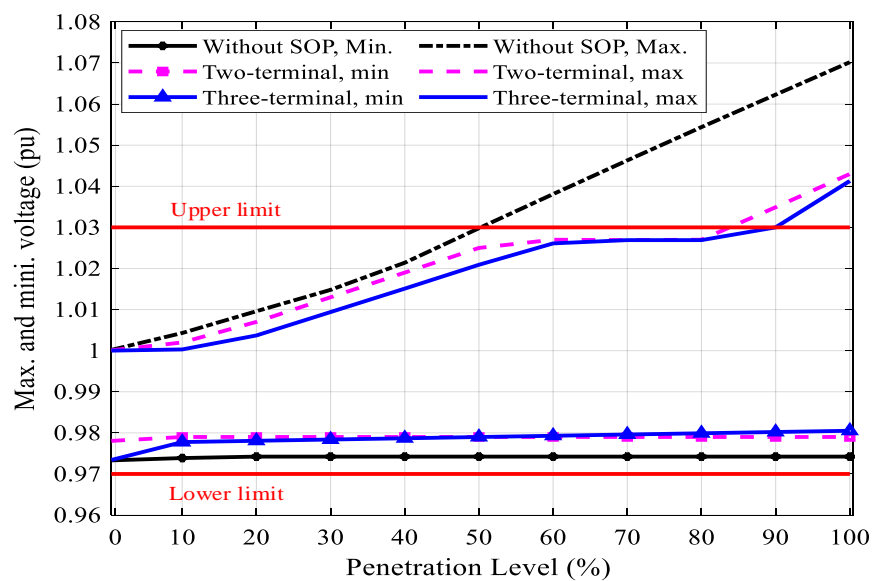
Figure 3-17 Min. and max. voltage of Case 2

Figure 3-18 shows the energy losses of the three-terminal SOP and the two-terminal SOP of the same MVA capacity and at a DG penetration level of 90%. The three-terminal SOP achieved lower energy losses than the two-terminal SOP no matter which objective function was used.
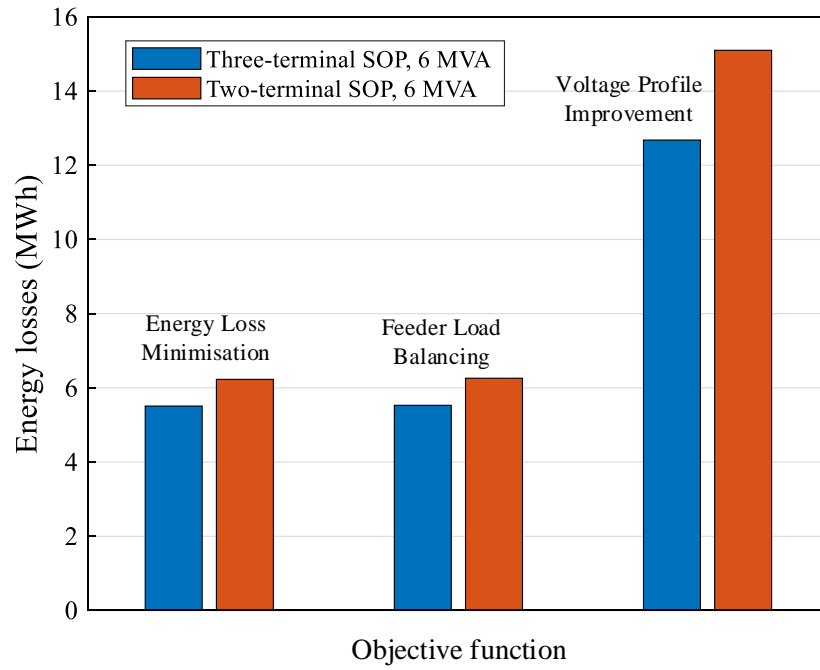
Figure 3-18 Energy losses of three-terminal SOP vs two-terminal SOP of 6 MVA each

3.6 Summary

A multi-terminal fully-rated B2B SOP enabled power flow control and voltage regulation of multiple distribution network feeders. Results showed the superiority of the three-terminal SOP over the two-terminal SOP in terms of penetration levels of DGs and the energy losses. The three-terminal SOP of 6 MVA total capacity enabled the distribution network to host a DG penetration level of 90%, increasing 20% more than the two-terminal SOP of 4 MVA and reduced the energy losses. It also achieved higher DG penetration level and lower energy losses than the two-terminal SOP of the same total MVA capacity (i.e., the three-terminal SOP enabled a DG penetration level of 90%, while the two-terminal SOP enabled 80% of the same total MVA capacity).

Despite the benefits of installing fully-rated B2B SOPs, they have not been widely deployed in MV distribution networks as they are too expensive. The cost and the size of the fully-rated converters and the interfacing transformers constitute major challenges for using the fully-rated B2B SOPs in MV distribution networks.

The series connection of VSCs is an alternative solution to provide power flow control in MV distribution networks similar to the Unified Power Flow Controller. The main advantage of the series connection of VSCs is the use of partially rated converters.

Chapter 4 A Unified Power Flow Controller in a Medium Voltage Distribution Network

This chapter investigates the basic principles of power flow control using a conventional Unified Power Flow Controller installed in a medium voltage distribution network with low X/R ratio.

4.1 Introduction

A Unified Power Flow controller (UPFC) was developed by Gyugyi from Westinghouse [123]. A UPFC is able to provide power flow control in transmission networks. It has not been widely used in transmission network due to the bulky and complicated interfacing transformers. The lower voltage level in medium voltage (MV) distribution networks compared to transmission networks and the advancement in power electronic modules makes a UPFC viable solution to control the power flow in medium voltage distribution networks [124].

In this chapter, the use of a UPFC in an MV distribution network was investigated. Power flow equations were derived for a simple two-busbar distribution network with the UPFC connected to a distribution feeder with a low X/R ratio. Procedures for sizing the series and shunt converters were developed. The control scheme was implemented using decoupled dq voltage and current control loops that were used to operate the UPFC in power flow control mode. The UPFC model was built in MATLAB Simulink using the switched representation of two-level Voltage Source Converters (VSCs).

The results demonstrated the ability of a UPFC to independently control active and reactive power flow and to regulate the voltage at the point of connection (POC).

4.2 Principle of operation

A UPFC is a power electronic device that consists of a series and shunt VSCs that are connected back-to-back through a common DC link. Figure 4-1 shows a schematic diagram of the UPFC.
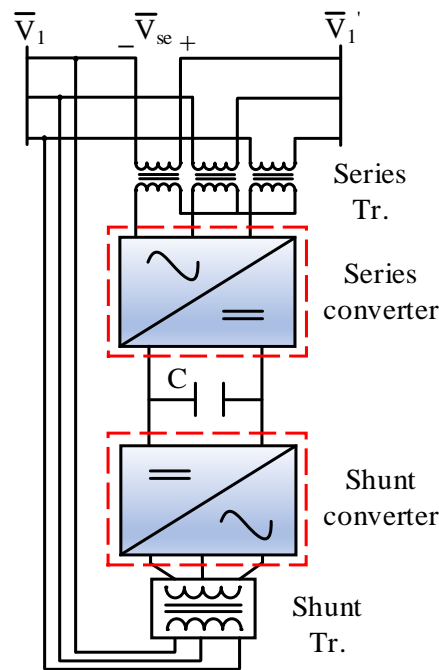
Figure 4-1 A Unified Power Flow Controller for MV applications

The series and shunt converters are interfaced to an AC system using a three-phase series transformer and a three-phase shunt transformer.

Figure 4-2 shows a simple representation of a UPFC connected to a two-busbar network. The series and shunt converters are represented by a controlled voltage source and a controlled current source.
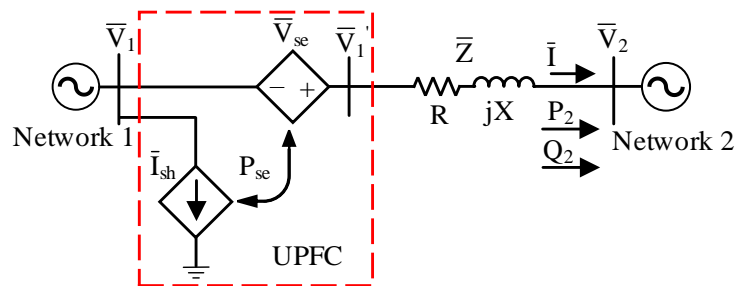
Figure 4-2 Equivalent circuit of a Unified Power Flow Controller connected to a distribution network

Figure 4-3 shows the phasor diagram developed using the equivalent circuit in Figure 4-2 to explain the role of the series converter.
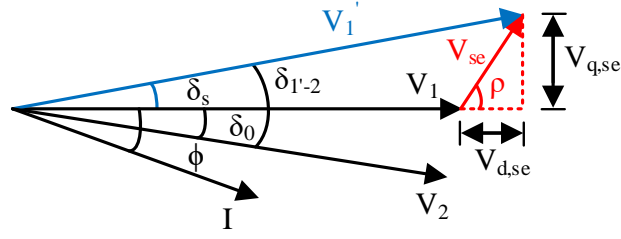
Figure 4-3 Phasor diagram explaining the role of the series converter

The sending-end voltage $\overline{V}_1$ is taken as a reference, and the angle δ_0 represents

the power angle between $\overline{V}_1$ and $\overline{V}_2$, where $\overline{V}_2$ is the receiving-end voltage.

The series converter injects a controllable voltage $\overline{V}_{se} = \left|\overline{V}_{se}\right| \angle \rho$ where

$\left|\overline{V}_{se}\right| = \sqrt{V_{d,se}^2 + V_{q,se}^2}$ and $\tan(\rho) = \dfrac{V_{q,se}}{V_{d,se}}$. Voltage $\overline{V}_{se}$ is added to voltage $\overline{V}_1$ making

the resultant voltage $\overline{V}_1' = \left|\overline{V}_1'\right| \angle \delta_s$ whose magnitude and power angle is manipulated

to achieve the target active and reactive power P_2 and Q_2.

Current $\overline{I} = \left|\overline{I}\right| \angle \phi$ flows through the series converter results in active and reactive

power exchange (P_{se}, Q_{se}) with the AC network. Only active power P_{se} flows through

the DC link.

The shunt converter regulates current $\overline{I}_{sh}$ which has an active current component

$I_{sh,d}$ and a reactive current component $I_{sh,q}$. The active current component is

determined by the requirement of balancing the real power P_{se} of the series converter.

The reactive current component can be set to achieve a reference voltage or a reference

reactive power (i.e., provide voltage regulation of $\overline{V}_1$) within the capacity of the

converter.

The distribution feeder of the two-busbar network is represented by a series

impedance $\overline{Z} = \left|\overline{Z}\right| \angle \theta$ where $\left|\overline{Z}\right| = \sqrt{R^2 + X^2}$ and $\theta = \tan^{-1}(X/R)$. The voltage $\overline{V}_1'$

and the current $\overline{I}$ are obtained as in equation (4-1).

$$\begin{cases} \overline{V}_1{}' = \overline{V}_1 + \overline{V}_{se} \\ \overline{I} = \dfrac{\overline{V}_1{}' - \overline{V}_2}{|\overline{Z}| \angle \theta} \end{cases} \tag{4-1}$$

The apparent power $\overline{S}_2$ at the receiving-end busbar is given in equation (4-2).

$$\overline{S}_2 = \overline{V}_2 \cdot \overline{I}^* = \overline{V}_2 \cdot \left(\frac{\overline{V}_1{}' - \overline{V}_2}{|\overline{Z}| \angle \theta} \right)^* = P_2 + j\,Q_2 \tag{4-2}$$

The active and reactive power P_2 and Q_2 at the receiving-end busbar are given in equation (4-3).

$$\begin{cases} P_2 = \underbrace{\dfrac{|\overline{V}_1| \cdot |\overline{V}_2|}{|\overline{Z}|} \cos(\delta_0 + \theta) - \dfrac{|\overline{V}_2|^2}{|\overline{Z}|} \cos\theta}_{\text{uncompensated active power}} + \underbrace{\dfrac{|\overline{V}_2| \cdot |\overline{V}_{se}|}{|\overline{Z}|} \cos(\delta_0 + \theta - \rho)}_{\text{controllable active power}} \\[2em] Q_2 = \underbrace{\dfrac{|\overline{V}_1| \cdot |\overline{V}_2|}{|\overline{Z}|} \sin(\delta_0 + \theta) - \dfrac{|\overline{V}_2|^2}{|\overline{Z}|} \sin\theta}_{\text{uncompensated reactive power}} + \underbrace{\dfrac{|\overline{V}_2| \cdot |\overline{V}_{se}|}{|\overline{Z}|} \sin(\delta_0 + \theta - \rho)}_{\text{controllable reactive power}} \end{cases} \tag{4-3}$$

When $\overline{V}_{se} = 0$, the active and reactive power at the receiving-end $P_2{}'$ and $Q_2{}'$ are given in equation (4-4).

$$\begin{cases} P_2{}' = \dfrac{|\overline{V}_1| \cdot |\overline{V}_2|}{|\overline{Z}|} \cos(\delta_0 + \theta) - \dfrac{|\overline{V}_2|^2}{|\overline{Z}|} \cos\theta \\[1.5em] Q_2{}' = \dfrac{|\overline{V}_1| \cdot |\overline{V}_2|}{|\overline{Z}|} \sin(\delta_0 + \theta) - \dfrac{|\overline{V}_2|^2}{|\overline{Z}|} \sin\theta \end{cases} \tag{4-4}$$

$P_2{}'$ and $Q_2{}'$ represent the uncompensated power flow when the UPFC is deactivated.

The net difference between equation (4-3), and equation (4-4) describes the effect of injecting voltage $\overline{V}_{se}$ on the power flow and it is given in equation (4-5).

$$
\begin{cases}
P_c = \dfrac{\left|\overline{V}_2\right| \cdot \left|\overline{V}_{se}\right|}{\left|\overline{Z}\right|} \cos(\delta_0 + \theta - \rho) \\[3mm]
Q_c = \dfrac{\left|\overline{V}_2\right| \cdot \left|\overline{V}_{se}\right|}{\left|\overline{Z}\right|} \sin(\delta_0 + \theta - \rho)
\end{cases}
\tag{4-5}
$$

where $P_c = P_2 - P_2^{'}$ and $Q_c = Q_2 - Q_2^{'}$ are the controllable active and reactive power of the UPFC.

Using basic algebra, voltage $\overline{V}_{se}$ is obtained from equation (4-5) and it is given in equation (4-6).

$$
\begin{cases}
\left|\overline{V}_{se}\right| = \dfrac{\left|\overline{Z}\right|}{\left|\overline{V}_2\right|} \sqrt{P_c^{\,2} + Q_c^{\,2}} \\[4mm]
\rho = (\delta_0 + \theta - \tan^{-1}(\dfrac{Q_c}{P_c}))
\end{cases}
\tag{4-6}
$$

Equation (4-6) shows that the magnitude of voltage $\overline{V}_{se}$ depends on 1) the impedance of the distribution feeder $\left|\overline{Z}\right|$, 2) the controllable power P_c and Q_c of the UPFC, and 3) voltage $\left|\overline{V}_2\right|$.

4.3 Procedure for sizing the series and the shunt converters

The size of the series and the shunt converters is determined by the maximum apparent power that is exchanged by the converters with an AC network. The apparent power of the series and shunt converters is given in equation (4-7).

$$
\begin{cases}
\overline{S}_{se} = \overline{V}_{se} \cdot \overline{I}^{*} = P_{se} + jQ_{se} \\[2mm]
\overline{S}_{sh} = \overline{V}_1 \cdot \overline{I}_{sh}^{\;*} = P_{sh} + jQ_{sh}
\end{cases}
\tag{4-7}
$$

Assuming lossless converters, the active power exchanged by the series and shunt converters is equal (i.e., $P_{se} = P_{sh}$). The series and shunt converters independently exchange reactive power with the network.

4.3.1 Series converter

Voltage $\left|\overline{V}_{se}\right|$ is advantageously small in an MV distribution network compared to a transmission network. This is because the impedance is usually small in the MV

60

distribution network compared to the transmission network. Using equation (4-6), the voltage $\left|\overline{V}_{se}\right|$ can be estimated by considering the controllable power P_c and Q_c, the impedance $\left|\overline{Z}\right|$ and the voltage $\left|\overline{V}_2\right|$.

To determine the size of the series converter, it is required to calculate the term $\sqrt{P_c^2 + Q_c^2}$. Figure 4-4 shows P-Q diagrams of the power transfer through an AC distribution feeder which are used to present two examples for the magnitudes of P_c and Q_c where the term $\sqrt{P_c^2 + Q_c^2}$ is maximum. Figure 4-4(a) shows power flow reversal occurs from point A of 1.0 pu active power and zero reactive power to point B of -1.0 pu active power and zero reactive power. Figure 4-4(b) shows power flow reversal occurs from point A' of 0.8 pu active power and 0.6 pu reactive power to point B' of -0.8 pu active power and -0.6 pu reactive power. In both cases, the term $\sqrt{P_c^2 + Q_c^2}$ has a maximum value of 2.0 pu.

(a)   (b)
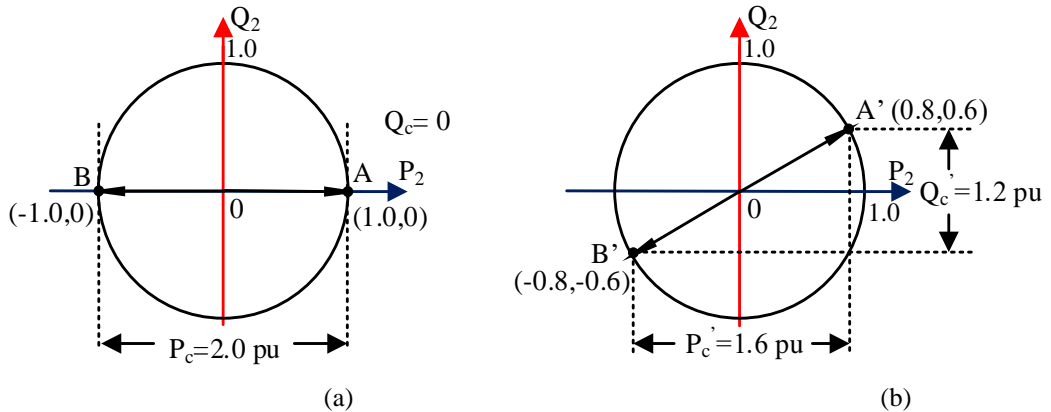
Figure 4-4 P-Q diagrams of the power transfer through an AC distribution feeder showing P_c and Q_c when power flow reversal occurs; (a) from point A to point B, and (b) from point A' to point B'

Assuming $\left|\overline{V}_2\right|$ is 0.95 pu, and $\left|\overline{Z}\right|$ ranges between 5% to 10%. From equation (4-6), $\left|\overline{V}_{se}\right|$ ranges between 0.105 pu to 0.210 pu.

As the current $\left|\overline{I}\right|$ is 1.0 pu, the apparent power of the series converter ranges between 0.105 pu to 0.210 pu.

4.3.2 Shunt converter

Current $\bar{I}_{sh} = I_{sh,d} + jI_{sh,q}$ has a direct current component $I_{sh,d}$ which is proportional to the active power P_{sh}, and a quadrature current component $I_{sh,q}$ which is proportional to the reactive power Q_{sh} (i.e., $P_{sh} \propto I_{sh,d}$ and $Q_{sh} \propto I_{sh,q}$).

The size of the shunt converter must be at least as large as the active power of the series converter. Assuming the series converter operates at the full load and unity power factor, the apparent power of the shunt converter is at least equal to the apparent power of the series converter (i.e., $\left|\bar{S}_{sh}\right| = \left|\bar{S}_{se}\right|$). In this case, the minimum apparent power of the shunt converter ranges between 0.105 pu to 0.210 pu. Additional capacity is required to provide the reactive current needed for voltage regulation.

4.4 Control scheme of a Unified Power Flow Controller

Figure 4-5 shows the single line diagram of a UPFC connected to a two-busbar network. The UPFC is controlled to operate in the power flow control mode. The series converter operates in the P-Q control scheme to regulate the active and reactive power P_1 and Q_1. The shunt converter operates in the V_{dc}-Q control scheme to maintain a constant DC voltage of the DC link and provide voltage regulation at busbar $\bar{V}_1$.

Figure 4-5 Single line diagram of a UPFC connected to a two-busbar network

Unlike the case in transmission networks, distribution networks have low X/R ratio, and the flow of active and reactive power is coupled to the power angle $\delta_{1'-2}$ and the voltage difference $(\left|\overline{V}_1'\right| - \left|\overline{V}_2\right|)$.

The control scheme is based on vector control where PI controllers are used to regulate the AC quantities that are transformed into dq rotating reference frame. Phase locked loop (PLL) tracks the phase angle of voltage $\overline{V}_1$.

4.4.1 Series converter

The control of P_1 and Q_1 is achieved by injecting voltage $\overline{V}_{se}$. Figure 4-6 shows the decoupled voltage control loops of the series converter [125]. The errors between the reference and the measured active and reactive power $(P_1^* - P_1)$ and $(Q_1^* - Q_1)$ are manipulated using PI controllers and transformed into dq voltage components $V_{q,se}^*$ and $V_{d,se}^*$. Voltage component $V_{d,se}^*$ is in-phase with voltage $\overline{V}_1$ and voltage component $V_{q,se}^*$ is in quadrature to voltage $\overline{V}_1$. A dq-abc transformation is used to transform $V_{d,se}^*$ and $V_{q,se}^*$ into a reference abc voltage $\overline{V}_{se}^*$. The gate signals for the IGBTs are obtained using SPWM. The gain parameters of the PI controllers are given in Appendix A.
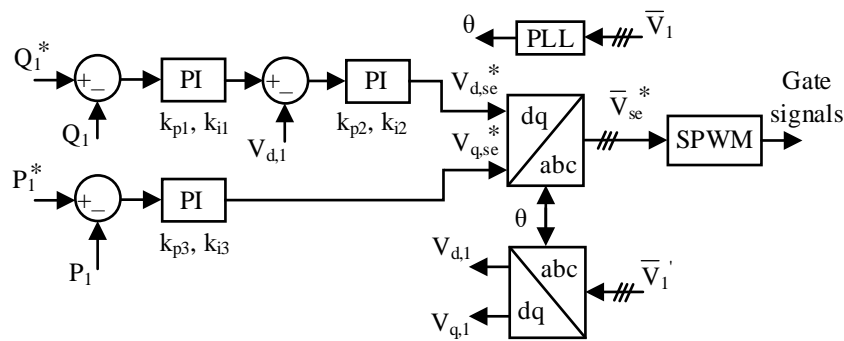
Figure 4-6 Series converter decoupled dq voltage control loops [125]

4.4.2 Shunt converter

Figure 4-7 shows the control scheme of the shunt converter. It regulates current $\overline{I}_{sh}$ by controlling voltage $\overline{V}_c$, where $\overline{V}_c$ is the terminal voltage of the shunt converter. Figure 4-7(a) shows the outer power control loops. The DC voltage control loop

63

ensures balanced active power transfer through the DC link (i.e., $P_{se} = P_{sh}$). The error $(V_{dc}^* - V_{dc})$ is manipulated using PI controller to generate the reference current component $I_{sh,d}^*$. The reactive power control loop regulates Q_{sh}. The error $(Q_{sh}^* - Q_{sh})$ is manipulated using PI controller to generate the reference current component $I_{sh,q}^*$. Current limiters are used for limiting the reference currents during abnormal conditions such as faults.

Figure 4-7(b) shows the inner dq current control loops. The measured current $\bar{I}_{sh}$ is transformed into direct and quadrature current components $I_{sh,d}$ and $I_{sh,q}$ using an abc-dq transformation. The errors between the reference and the measured currents $(I_{sh,d}^* - I_{sh,d})$ and $(I_{sh,q}^* - I_{sh,q})$ are manipulated using PI controllers and transferred into voltage components $V_{c,d}^*$ and $V_{c,q}^*$. A dq-abc transformation is used to transform $V_{c,d}^*$ and $V_{c,q}^*$ to a reference abc voltage $\bar{V}_c^*$. SPWM is used to generate the gate signals for the IGBTs.

(a)

(b)
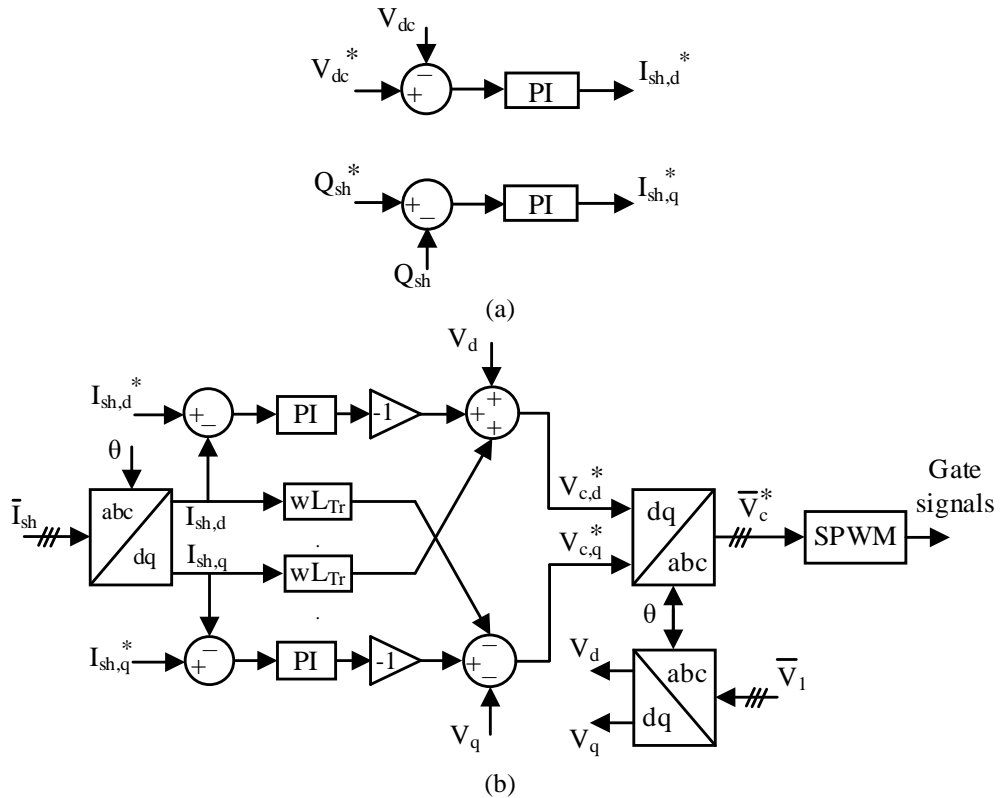
Figure 4-7 Shunt converter decoupled dq current control loops; (a) outer power control loops and (b) inner current control loops

The parameters of the controllers (i.e., gain and time constant) are determined using Internal Model Control technique [126]. The gain parameters of the PI controllers are given in Appendix A. The speed of response of the outer control loop is slower than that of the inner control loop. This decouples the dynamics of both control loops.

4.5 Simulation results

A UPFC model was built in MATLAB Simulink using the switched representation of two-level VSCs. The system configuration shown in Figure 4-5 was used for the simulation and for generating the results in Figure 4-8 to Figure 4-10. The UPFC was connected to 12.66 kV, 5 MVA distribution feeder of a two-busbar network. Network 1 was modelled as a voltage source with an internal impedance (i.e., $\overline{V}_1 = 12.66 \angle 0$ kV and $\overline{Z}_s = 0.02 + j0.1\Omega$) and Network 2 was modelled as a constant voltage source. Table 4-1 summarises the circuit parameters of the Simulink model.

Table 4-1 Parameters of the Simulink model

Parameters	Value
Network power rating	5 MVA
Network voltage	12.66 kV
Impedance of the feeder, $\overline{Z}$	0.966+j 1.140 Ω
Series transformer (Phase voltage)	460/460 V, 630 kVA, $Z_{tr,se}$= 4%
Shunt transformer (Line voltage)	12.66/0.8 kV Δ/Y, 750 kVA, $Z_{tr,sh}$=6%
DC capacitance	2 mF

A step change of active and reactive power was performed to test the ability of the control system to independently control the active and reactive power flow.

Figure 4-8 shows the performance of the UPFC model in response to control signals to change the reactive power from 1 MVAr to 3 MVAr at t = 1 s and the active power from 2 MW to 4 MW at t = 2 s.

Figure 4-8(a) shows the response to step change of active and reactive power. At t = 1 s, the reactive power was increased from 1 MVAr to 3 MVAr while the active power was maintained unchanged at 1 MW. At t = 2 s, the active power was increased from 2 MW to 4 MW while the reactive power was maintained unchanged at 3 MVAr.

Figure 4-8(b) shows the current $|\bar{I}|$. After $t = 2$ s, the distribution feeder was operating at the full load and the peak value of current $|\bar{I}|$ was 322 A (i.e., $|\bar{I}| = 228$ A rms).

Figure 4-8(c) shows the active and reactive power of the series converter P_{se} and Q_{se}. At $t = 1$ s and $t = 2$ s, power P_{se} and Q_{se} was increased in response to the control signals.

Figure 4-8(d) shows the DC voltage. At $t = 1$ s and $t = 2$ s, the DC voltage slightly dropped upon the change in active power P_{se} which caused instantaneous imbalance in the active power flow through the DC link. The DC voltage controller of the shunt converter responded to the deviation in voltage V_{dc} by generating current $I_{sh,d}^{*}$ to meet the active power demand by the series converter and to bring the DC voltage to its reference value.

(a)

(b)

(c)

(d)
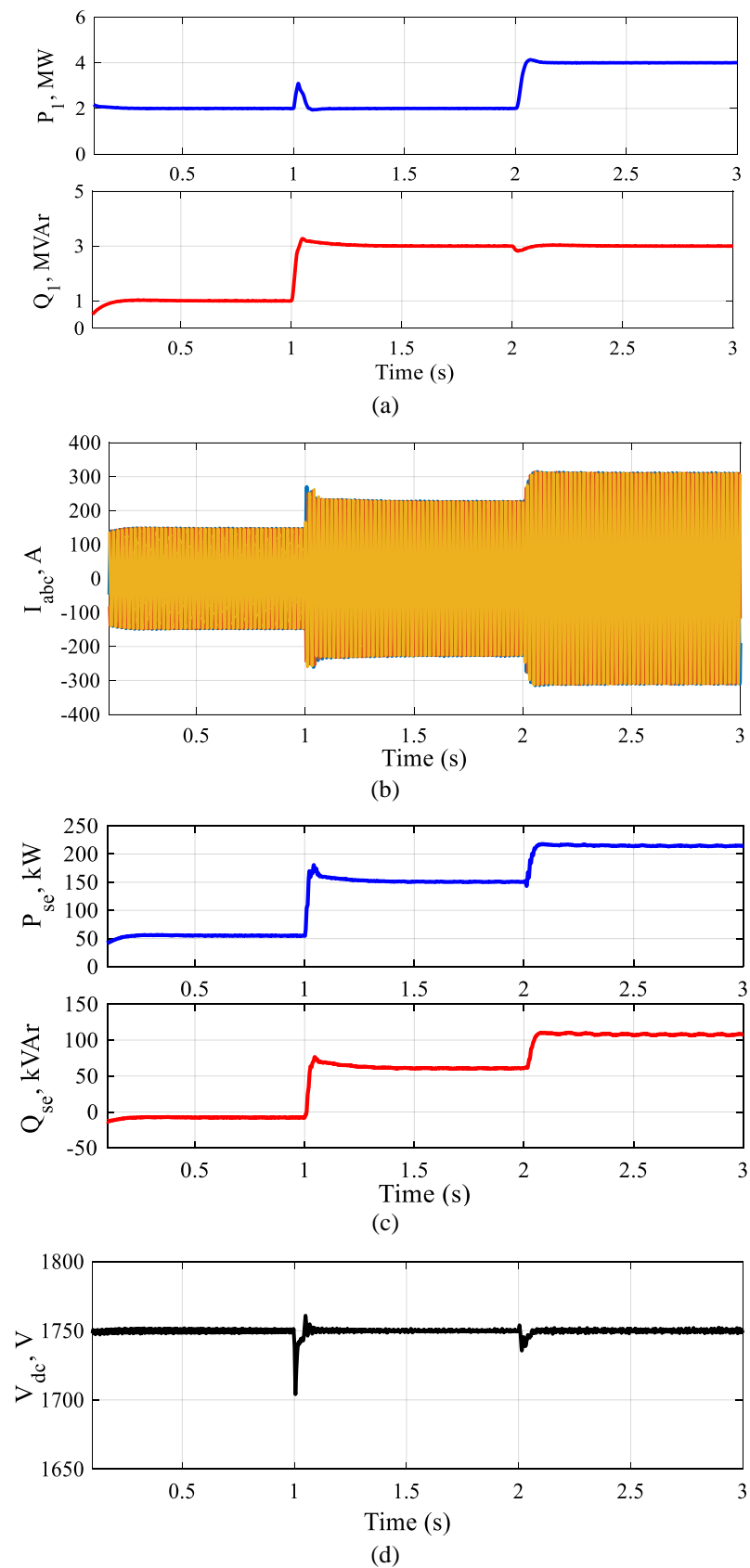
Figure 4-8 Performance of UPFC in response to step change of active and reactive power; (a) power P_1 and Q_1, (b) feeder current, (c) P_{se} and Q_{se}, and (d) voltage V_{dc}

Figure 4-9 shows the active and reactive power of the shunt converter P_{sh} and Q_{sh} . At t = 1 s and t = 2 s, the active power P_{sh} was increased to meet the active power demand of the series converter P_{se} . After t = 1 s, the shunt converter supplied reactive power Q_{sh} (i.e., source of reactive power) of 178 kVAr which then increased to 200 kVAr after t = 2 s. This provision of reactive power Q_{sh} aimed to compensate for the voltage drop across the internal impedance of Network 1 and to maintain voltage $\left|\overline{V}_1\right|$ constant (i.e., $\left|\overline{V}_1\right|$ = 1.0 pu).
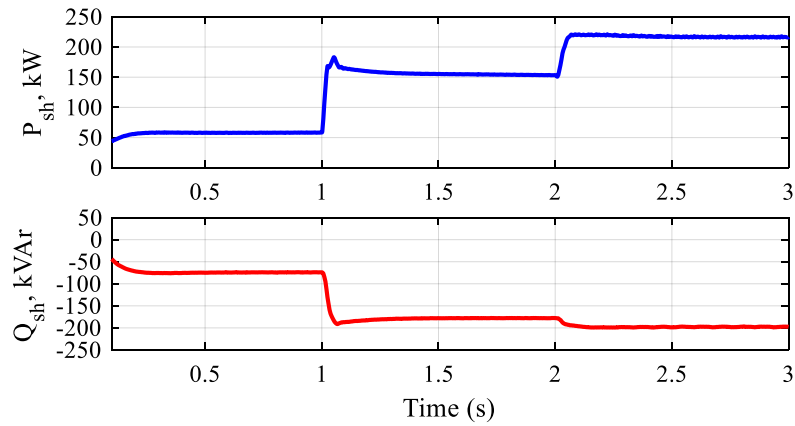
Figure 4-9 Active and reactive power of the shunt converter

Figure 4-10 shows the performance of the series converter in response to a sudden change in impedance $\overline{Z}$. At t = 4 s, impedance $\overline{Z}$ was increased by 50%.

Figure 4-10(a) shows the series voltage $\overline{V}_{se}$. Before t = 4 s, the peak voltage $\left|\overline{V}_{se}\right|$ was 500 V (i.e., $\left|\overline{V}_{se}\right|$ = 353 V rms) and the apparent power $\left|\overline{S}_{se}\right|$ was 241 kVA (i.e., $\left|\overline{S}_{se}\right| = 3*353V*228A$). After t = 4 s, the peak voltage $\left|\overline{V}_{se}\right|$ was increased by approximately 50% to 721 V (i.e., $\left|\overline{V}_{se}\right|$ = 510 V rms) and the apparent power $\left|\overline{S}_{se}\right|$ was increased to 349 kVA.

Figure 4-10(b) shows the power P_1 and Q_1 . The controller maintained the power flow to its reference values.

(a)

(b)
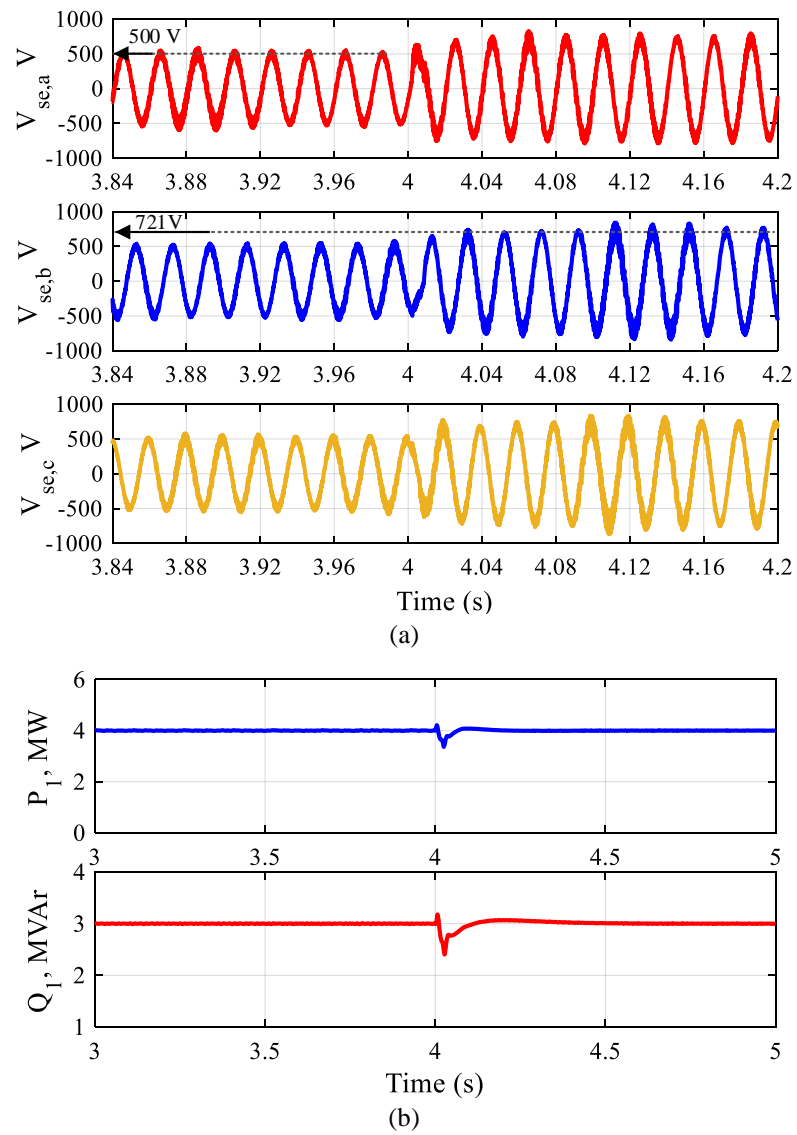
Figure 4-10 Performance of the series converter when feeder's impedance was increased

4.6 Summary

A UPFC in an MV distribution network is able to independently control active and reactive power flow and provide voltage regulation using partially rated B2B VSCs that are interfaced to a medium voltage AC network using series and shunt interfacing transformers.

A UPFC model was built in MATLAB Simulink. The response to control signals to step change the active and reactive power flow demonstrated the ability of the UPFC to independently control active and reactive power and provide voltage regulation.

The size of a UPFC connected to the distribution feeder of a two-busbar network was shown to depend on the impedance of the distribution feeder, the receiving-end voltage, and the controllable power.

Chapter 5 Transformer-less Unified Power Flow Controller in Medium Voltage Distribution Networks

This chapter investigates the use of a Transformer-less Unified power Flow Controller in Medium Voltage Distribution Networks.

5.1 Introduction

A Transformer-less Unified Power Flow Controller (UPFC) is a power electronic device consisting of series and shunt Voltage Source Converters (VSCs) that are not connected to a common DC bus. It was proposed in [127] to control power flow in transmission networks and was based on the concepts of Flexible AC Transmission Systems (FACTs). Figure 5-1 shows the structure of a Transformer-less UPFC.
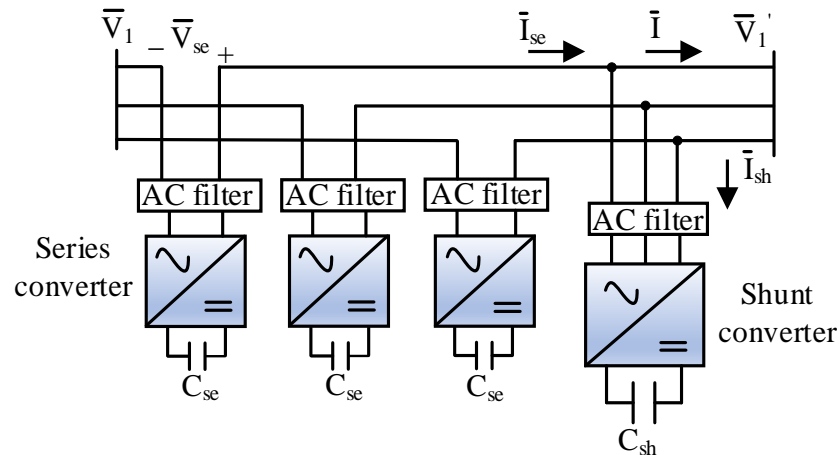
Figure 5-1 Structure of a Transformer-less UPFC

The main advantage of a Transformer-less UPFC over a conventional UPFC is the complete removal of interfacing transformers, hence a significant reduction in its size and cost.

In this chapter: (1) the use of a Transformer-less UPFC in transmission networks was reviewed, and then (2) the use of a Transformer-less UPFC considered for distribution networks was investigated.

The following points were addressed:

1) The operation of a Transformer-less UPFC in a distribution circuit was investigated. Distribution circuits are different from transmission circuits and the low X/R ratio of distribution circuits makes the analysis more complex than transmission circuits.

2) The operating range of a Transformer-less UPFC and the required power ratings of the series and shunt converters were investigated. The analyses were carried out considering both active and reactive power control.

3) A simulation and a small-scale experimental setup were used to validate
the theoretical analysis.

The results showed that a Transformer-less UPFC in MV distribution network is a
good choice for applications that require controlling active power exchange. However,
it has limited control of reactive power as this requires a large shunt current (i.e., >1.0
pu).

5.2 Transformer-less UPFC in transmission networks

5.2.1 Literature review

A literature review for a Transformer-less UPFC in transmission networks was
undertaken.

A Transformer-less UPFC was proposed in 2014 to control active power, while
maintaining reactive power flow minimal over long-distance lines [127]. The main
advantage of the Transformer-less UPFC over the conventional UPFC is the complete
removal of the interfacing transformers such as the complicated zigzag transformers
used with 48-pulse gate turn-off (GTO) converters [128], [129] and the transformers
used with the modular multilevel converters (MMCs) [130]. Figure 5-2 shows the
structure of the Transformer-less UPFC in transmission networks. Figure 5-2(a) shows
a Transformer-less UPFC connected to a two-busbar transmission network. The series
and shunt converters were built using cascaded multilevel inverters (CMIs) to reach
high-voltage level without transformers [131]. Figures 5-2 (b) and (c) show CMIs built
using H-bridge and half-bridge modules.
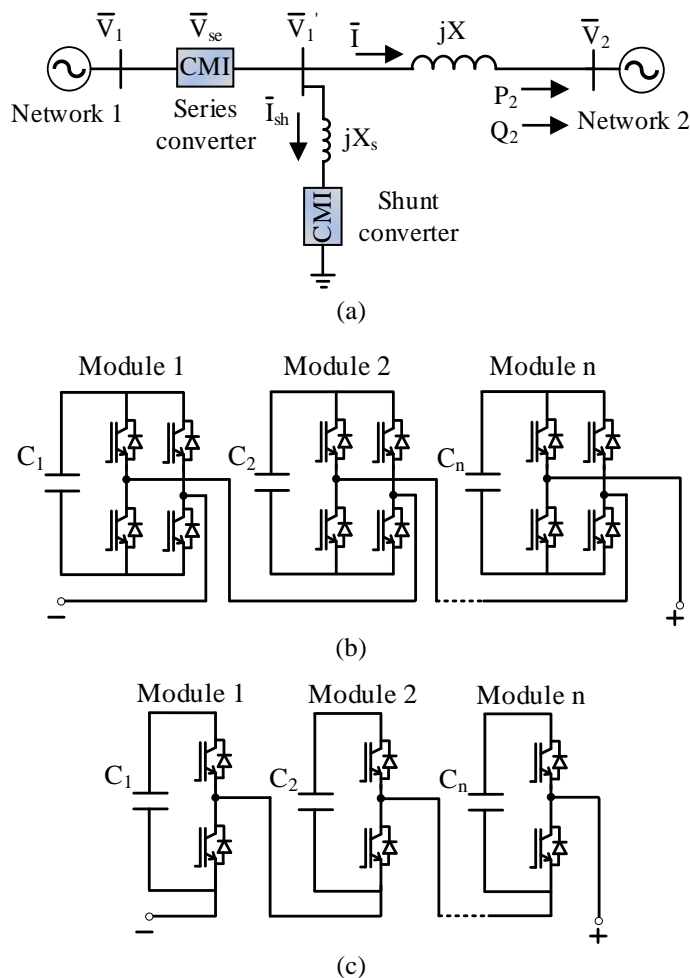
Figure 5-2 Circuit diagram of a Transformer-less UPFC in transmission networks; (a) system configuration, (b) CMI based on H-bridge modules, and (c) CMI based on half-bridge modules [132]

In [132], a Transformer-less UPFC was investigated to increase the transfer capability of a transmission grid. It connected two separate transmission grids with a large phase difference that could not be previously connected. Results showed the ability of the Transformer-less UPFC to maximise power flow over the transmission grid, hence improving the utilisation of transmission lines.

In [133], the performance of a 2 MVA, 13.8 kV prototype Transformer-less UPFC demonstrated the ability of a Transformer-less UPFC to control power flow in an inductive line. It was shown that the voltages and currents of the series and shunt converters were 90° phase shift (i.e., they only exchanged reactive power).

In [134], semiconductor device power ratings (SDPRs) was used to demonstrate the cost-benefit of a Transformer-less UPFC using CMIs when compared to a back-to-back (B2B) topology based on MMCs. Calculations of SDPR showed significant

reduction in the required SDPRs of the Transformer-less UPFC based CMIs compared to the B2B based MMCs.

In [135], the ratings of the series and shunt converters were investigated. Analysis showed that the ratings of the series and shunt converters are small and of 0.2 pu and 0.5 pu. However, this analysis only considered active power control while keeping the reactive power unchanged.

In [136], [137], the control schemes of the series and shunt converters were presented and used to test the performance of a Transformer-less UPFC in response to a step change of active power.

The control scheme of a Transformer-less UPFC is quite complex. The series and shunt converters of the Transformer-less UPFC regulate their floating DC bus voltages. In contrast to a B2B configuration, one converter is dedicated to regulating the DC-link voltage [138].

To sum up, a Transformer-less UPFC can provide independent control of active and reactive power using partially rated converters and with complete elimination of the interfacing transformers. However, the capability of the Transformer-less UPFC to control active and reactive power has not been fully investigated.

5.2.2 Replicating a Transformer-less UPFC in transmission networks

Figure 5-3 shows the shunt current's magnitudes in [135] when the Transformer-less UPFC was used to increase the power flow from various uncompensated active and reactive power to 1.0 pu target active power while keeping the reactive power unchanged.
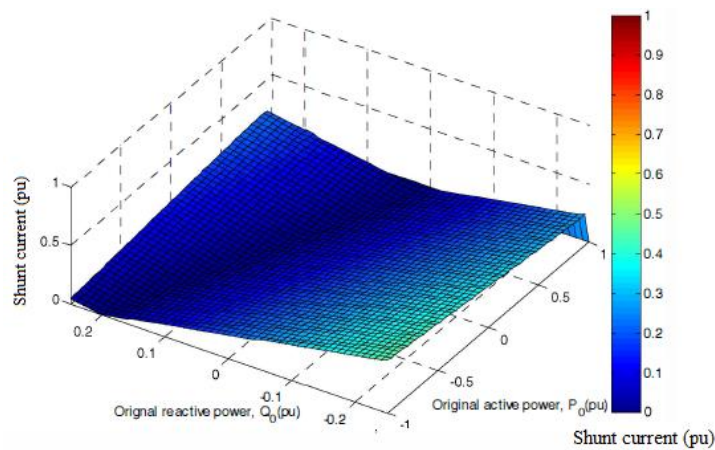
Figure 5-3 Shunt current for various uncompensated power [135]

An algorithm was developed using MATLAB m-file (see Figure 5-8) to calculate the magnitude of the shunt current at various operating conditions of active and reactive power control.

The algorithm was used to replicate the results in [135], for example, Figure 5-3. This is to ensure the correctness of the algorithm before undertaking more investigation. Figure 5-4 shows the replication of Figure 5-3 given in [135].
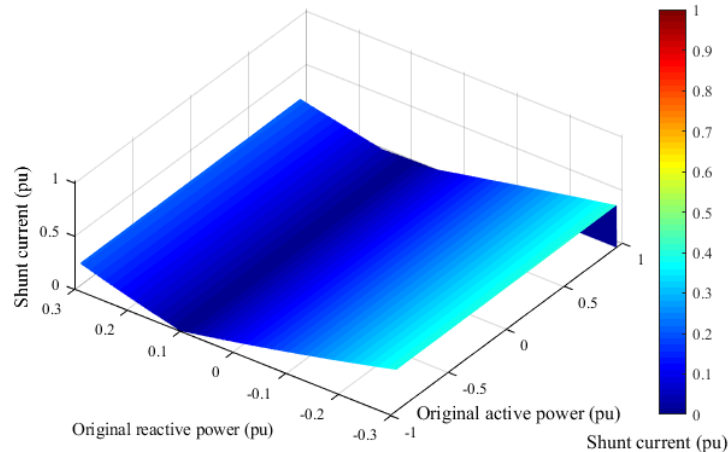
Figure 5-4 Replication of shunt current's magnitude

Figures 5-3 and 5-4 show similar shunt current magnitudes when a Transformer-less UPFC was used to control active. However, the unavailable information in [135], such as the X/R ratio of the transmission line, constitutes a challenge to exactly replicate Figure 5-3.

A Transformer-less UPFC model was built in MATLAB/Simulink using the same parameters as in [127]. The base voltage and apparent power were 13.8 kV and 2 MVA. Figure 5-5 shows a complete replication of the Simulink results in [127].

77

Figure 5-5(a) shows the results of the Simulink model. Figure 5-5(b) shows snapshots of the results in [127]. The waveforms show similar steady-state values. However, the dynamics and the total harmonic distortion (THD) are different due to different gain parameters and different converters' topologies.

(a)   (b)
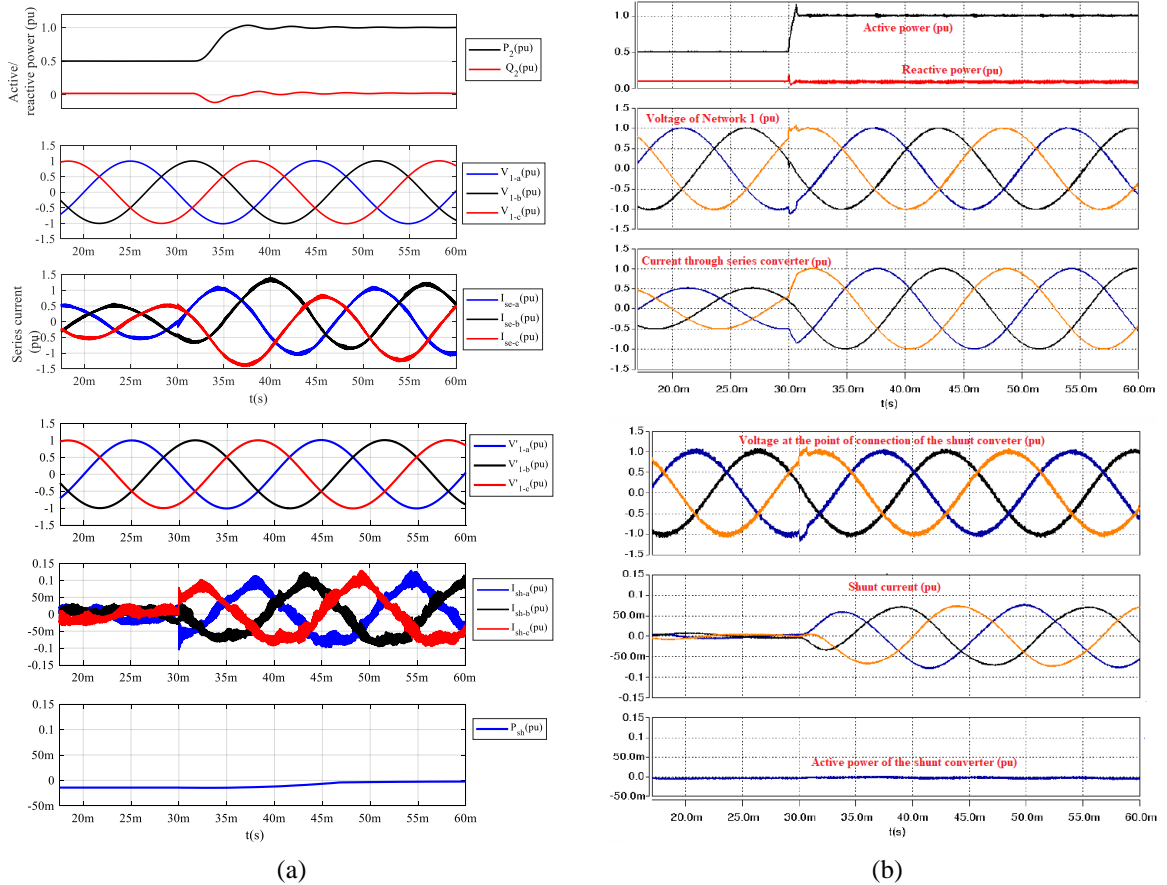
Figure 5-5 Step change of active power: (a) replication of the results and (b) the results in [127]

5.3 Transformer-less UPFC in MV distribution networks

Figure 5-6 shows the equivalent circuit of a Transformer-less UPFC connected in a two-busbar distribution network. The series converter is modelled as a controlled voltage source and the shunt converter as a controlled current source.
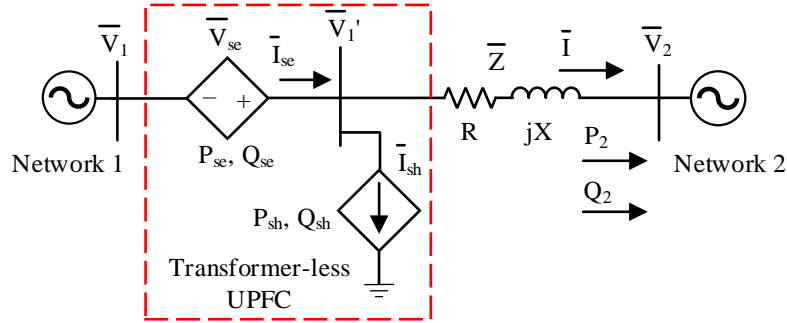
Figure 5-6 Equivalent circuit of a Transformer-less UPFC connected to a two-busbar distribution network

The voltage and current at busbar $\overline{V}_1{}'$ are given in (5-1)

$$\begin{cases} \overline{V}_1{}' = \overline{V}_1 + \overline{V}_{se} \\ \overline{I}_{se} = \overline{I} + \overline{I}_{sh} \end{cases} \tag{5-1}$$

Figure 5-7 shows a phasor diagram developed using the equivalent circuit in Figure 5-6. It explains the role of the series and shunt converters, where voltage $\overline{V}_1$ of Network 1 is taken as a reference, and angle δ_0 represents the power angle between $\overline{V}_1$ and voltage $\overline{V}_2$ of Network 2.
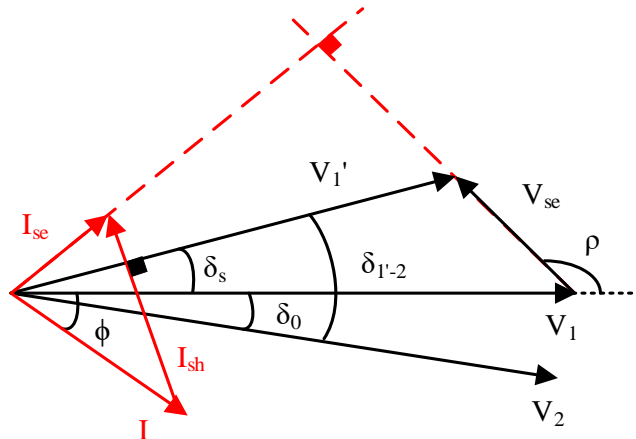
Figure 5-7 Principle of operation of a Transformer-less UPFC

The role of the series converter in a Transformer-less UPFC is similar to that in a conventional UPFC. It injects a controllable voltage $\overline{V}_{se} = \left|\overline{V}_{se}\right| \angle \rho$ whose magnitude and phase angle are given in equation (4-6) and rewritten, as given in (5-2).

$$\begin{cases} \overline{V}_{se} = \dfrac{\left|\overline{Z}\right|}{\left|\overline{V}_2\right|} \sqrt{P_c^2 + Q_c^2} \\ \rho = (\delta_0 + \theta - \tan(\dfrac{Q_c}{P_c})) \end{cases} \tag{5-2}$$

Voltage $\overline{V}_{se}$ is added to voltage $\overline{V}_1$ making the resultant voltage $\overline{V}_1^{'} = \left|\overline{V}_1^{'}\right| \angle \delta_s$ which is regulated to achieve the target active and reactive power P_2 and Q_2 as shown by the voltage phasors in Figure 5-7.

The role of the shunt converter in a Transformer-less UPFC is different from that in a conventional UPFC. The shunt converter ensures that each converter can only exchange reactive power Q_{se} and Q_{sh} with the connected AC network (i.e., $P_{se} = 0$ and $P_{sh} = 0$).

The shunt current $\bar{I}_{sh}$ is controlled to be perpendicular to voltage $\overline{V}_1^{'}$ (i.e., $\bar{I}_{sh} \perp \overline{V}_1^{'}$), and it must make the series current $\bar{I}_{se}$ perpendicular to voltage $\overline{V}_{se}$ (i.e., $\bar{I}_{se} \perp \overline{V}_{se}$) as shown by the current phasors in Figure 5-7 and is given in (5-3), where ϕ is the angle between voltage $\overline{V}_1$ and current $\bar{I}$. Note that the series current is the resultant of the shunt current and the current of the distribution feeder (i.e., $\bar{I}_{se} = \bar{I}_{sh} + \bar{I}$).

$$\left|\bar{I}_{sh}\right| \angle (\delta_s + 90°) = \left|\bar{I}_{se}\right| \angle (\rho - 90°) - \left|\bar{I}\right| \angle \phi \tag{5-3}$$

Equation (5-3) is used to obtain an expression of $\bar{I}_{sh}$, as in (5-4). Detailed derivation of (5-4) is provided in the Appendix B.

$$\bar{I}_{sh} = \left|\bar{I}\right| \cdot \dfrac{\cos(\rho - \phi)}{\sin(\rho - \delta_s)} \angle (\delta_s - 90°) \tag{5-4}$$

Equations (5-2) and (5-4) are used to calculate the reference voltage and current $\overline{V}_{se}^{*}$ and $\bar{I}_{sh}^{*}$ for the series and shunt converters (i.e., the series and shunt converters are in voltage and current control mode).

Given that the feeder's impedance is available, a Transformer-less UPFC relies on the measurements of $\overline{V}_1$ and $\overline{V}_2$ to calculate its $\overline{V}_{se}^{\ *}$ and $\overline{I}_{sh}^{\ *}$. $\overline{V}_1$ is measured locally. However, $\overline{V}_2$ requires communication.

5.4 Operating range of a Transformer-less UPFC in MV distribution networks

The operating range of a Transformer-less UPFC describes its capability to control active and reactive power in an MV distribution network, and it is directly related to the power ratings of the series and shunt converters.

The series and the shunt converters' power ratings must fulfil the maximum apparent power $\left|\overline{S}_{se}\right|$ and $\left|\overline{S}_{sh}\right|$ exchanged between the converters and the connected AC network such as $\left|\overline{V}_{se}\right| \cdot \left|\overline{I}_{se}\right| \le \left|\overline{S}_{se}\right|$ and $\left|\overline{V}_1^{'}\right| \cdot \left|\overline{I}_{sh}\right| \le \left|\overline{S}_{sh}\right|$.

5.4.1 Series converter

The power rating of the series converter can be estimated using equation (5-2). Assuming $\left|\overline{V}_2\right|$ is 0.95 pu, the term $\sqrt{P_c^{\ 2} + Q_c^{\ 2}}$ is 2.0 pu (e.g., the series converter can reverse the power flow from (1 pu, 0 pu) to (-1 pu, 0 pu)) and impedance $\left|\overline{Z}\right|$ ranges between 5% to 10%, then substituting in equation (5-2), voltage $\left|\overline{V}_{se}\right|$ ranges between 0.105 pu to 0.210 pu. As current $\left|\overline{I}_{se}\right|$ is 1.0 pu, the power rating of the series converter ranges between 0.105 pu to 0.210 pu.

5.4.2 Shunt converter

The shunt converter has the full network voltage applied across its terminal. The power rating of the shunt converter is determined based on $\left|\overline{I}_{sh}\right|$. Therefore, it is required to calculate the maximum shunt current required to ensure zero active power exchange between each of the series and shunt converters and the connected AC network.

An algorithm was developed to calculate the shunt current as shown in Figure 5-8. It calculates current $\left|\overline{I}_{sh}\right|$ when the power flow changes from various uncompensated active and reactive power $P_2^{'}$ and $Q_2^{'}$ (i.e., prior to connecting the

Transformer-less UPFC) to an arbitrary target active and reactive power P_2 and Q_2.
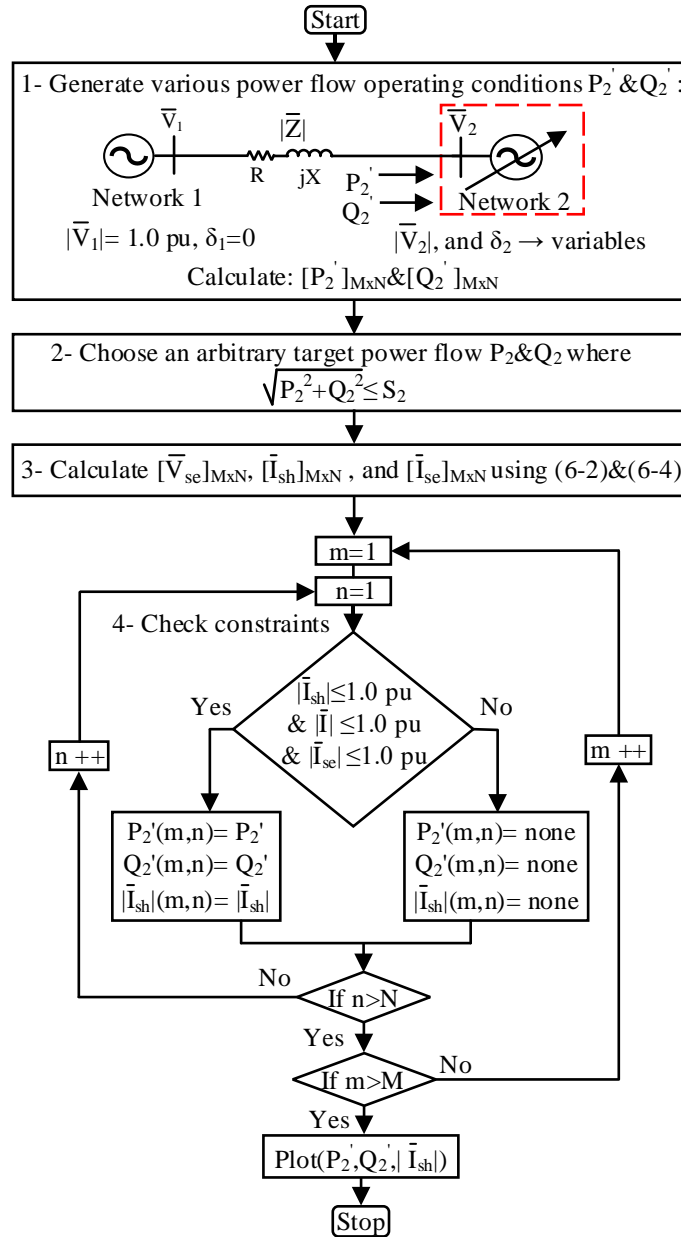
Figure 5-8 The algorithm used to determine the shunt current

Firstly, various operating conditions of the uncompensated power $P_2^{'}$ and $Q_2^{'}$ are generated by hypothetically changing voltage $\left|\overline{V}_2\right|$ and phase angle δ_2 while maintaining voltage $\left|\overline{V}_1\right|$ and phase angle δ_1 constant at $1.0\angle 0°$ pu. Power $P_2^{'}$ and $Q_2^{'}$ are calculated using equation (4-4) and rewritten, as in (5-5).

$$\begin{cases} P_2^{'} = \dfrac{\left|\overline{V}_1\right| \cdot \left|\overline{V}_2\right|}{\left|\overline{Z}\right|} \cos(\delta_0 + \theta) - \dfrac{\left|\overline{V}_2\right|^2}{\left|\overline{Z}\right|} \cos\theta \\[4ex] Q_2^{'} = \dfrac{\left|\overline{V}_1\right| \cdot \left|\overline{V}_2\right|}{\left|\overline{Z}\right|} \sin(\delta_0 + \theta) - \dfrac{\left|\overline{V}_2\right|^2}{\left|\overline{Z}\right|} \sin\theta \end{cases} \qquad (5\text{-}5)$$

Various operating points of $P_2^{'}$ and $Q_2^{'}$ are stored in matrices $\left[P_2^{'}\right]_{M \times N}$ and $\left[Q_2^{'}\right]_{M \times N}$ where M and N are the range of $\left|\overline{V}_2\right|$ and δ_2, for example $\left|\overline{V}_2\right|$ changes from 0.95 pu to 1.03 pu and δ_2 changes from $-5°$ to $+5°$ such as $\sqrt{(P_2^{'})^2 + (Q_2^{'})^2} \leq S_2$ where S_2 is the maximum apparent power of the distribution feeder.

Secondly, an arbitrary target power P_2 and Q_2 is chosen such as $\sqrt{(P_2)^2 + (Q_2)^2} \leq S_2$. Thirdly, voltage $\left[\overline{V}_{se}\right]_{M \times N}$, current $\left[\overline{I}_{sh}\right]_{M \times N}$ and current $\left[\overline{I}_{se}\right]_{M \times N}$ are calculated using equations (5-2) and (5-4). Finally, the algorithm checks the current constraints (i.e., $\left|\overline{I}_{sh}\right| \,\&\, \left|\overline{I}\right| \,\&\, \left|\overline{I}_{se}\right| \leq 1.0$ pu).

Figure 5-9 shows current $\left|\overline{I}_{sh}\right|$ mapped against uncompensated power $P_2^{'}$ and $Q_2^{'}$. The base voltage and apparent power were 12.66 kV and 10 MVA. The distribution feeder has impedance of 8 % and X/R of 2.0. A circle of 1.0 pu radius represents all the values of the uncompensated power $P_2^{'}$ and $Q_2^{'}$. The color map provides the shunt current's magnitude at every power $P_2^{'}$ and $Q_2^{'}$ to the Target Power of (0.6 pu, 0.2 pu) such as dark blue area represents zero shunt current, while dark red area represents 1.0 pu shunt current. The areas with black circles and red crosses are inoperable as either current $\left|\overline{I}_{sh}\right|$ and current $\left|\overline{I}_{se}\right|$ exceeded 1.0 pu or current $\left|\overline{I}_{se}\right|$ exceeded 1.0 pu.

Three cases were selected to demonstrate the shunt current's magnitude by changing the uncompensated power "A", "B" and "C" to the same Target Power. These cases are:

Case A: the change of power flow from A (0.2 pu, 0.2 pu) to Target Power (0.6 pu, 0.2 pu), where the per-unit values in each bracket are the active and reactive power.

Case B: the change of power flow from B (0.6 pu, 0 pu) to Target Power (0.6 pu, 0.2 pu).

Case C: the change of power flow from C (0.2 pu, 0 pu) to Target Power (0.6 pu, 0.2 pu).
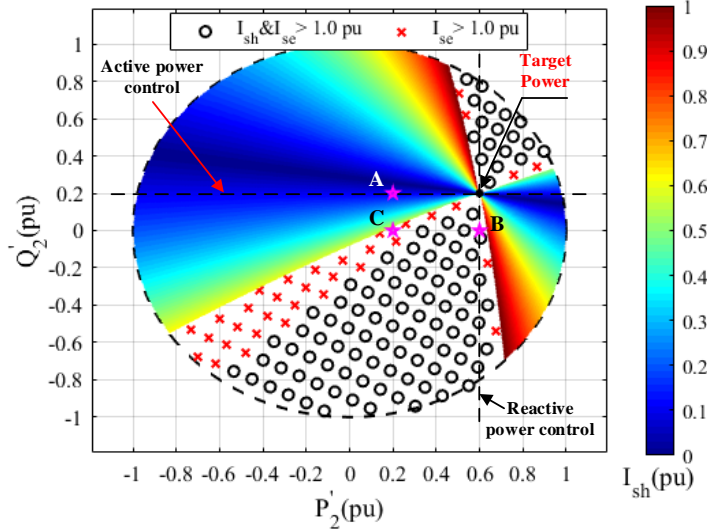
Figure 5-9 Current $\left|\bar{I}_{sh}\right|$ mapped when the uncompensated power P_2' and Q_2' within 1.0 pu circle changed to point A (0.6 pu, 0.2 pu)

It can be observed that in Case A, current $\left|\bar{I}_{sh}\right|$ was only 0.1 pu when the power flow changed from "A to Target Power" (i.e., step change of active power from 0.2 pu to 0.6 pu while the reactive power was maintained constant).

In Case B, the change of power flow from "B to Target Power " (i.e., step change of reactive power from 0 to 0.2 pu while the active power was maintained constant) was in the area with black circles as currents $\left|\bar{I}_{sh}\right| \& \left|\bar{I}_{se}\right|$ exceeded 1.0 pu.

In Case C, the change of power flow from "C to Target Power" (i.e., step change of active power from 0.2 pu to 0.6 pu and reactive power from 0 pu to 0.2 pu) was in the area with red crosses as current $\left|\bar{I}_{se}\right|$ exceeded 1.0 pu.

Note that in all cases, the power flow was changed from either "A", "B" or "C" to "Target Power" because of injecting the corresponding voltage $\overline{V}_{se}$. While $\left|\bar{I}_{sh}\right|$ is required to guarantee zero active power exchange between each of the series and shunt converters and the connected AC network.

A horizontal line was drawn to Target Power of (0.6 pu, 0.2 pu), where $P_2^{'}$ changes while $Q_2^{'}$ is constant (i.e., active power control). The points along the horizontal line show a maximum shunt current's magnitude of 0.1 pu. This demonstrates the ability of the Transformer-less UPFC to control active power using a small shunt current. Similarly, a vertical line was drawn to Target Power of (0.6 pu, 0.2 pu), where $Q_2^{'}$ changes while $P_2^{'}$ is constant (i.e., reactive power control). The vertical line is entirely in the areas with red crosses and black circles. Hence, the Transformer-less UPFC is inoperable.

Table 5-1 shows steady-state voltages and currents of the series and shunt converters for Cases B and C when the Transformer-less UPFC was inoperable. These values were calculated using equations (5-1), (5-2) and (5-4) and used to develop the scaled phasor diagrams in Figure 5-10.

Table 5-1 Voltage and current of the series and shunt converters (Numbers in bold denote the currents exceed 1.0 pu). The base voltage and apparent power were 12.66 kV and 10 MVA.

Point	$\overline{V}_{se}$ (pu)	$\overline{I}_{se}$ (pu)	$\overline{V}_1^{'}$ (pu)	$\overline{I}_{sh}$ (pu)
"B to Taregt Power"	$0.016\angle-29°$	$\mathbf{1.26}\angle 61°$	$1.014\angle-0.5°$	$\mathbf{1.33}\angle89.5°$
"C to Target Power"	$0.035\angle 37°$	$\mathbf{1.03}\angle-53°$	$1.03\angle1.2°$	$0.61\angle-88.8°$

Although the principle of operation of the Transformer-less UPFC was fulfilled as shown by the scaled phasor diagrams in Figure 5-10 (i.e., $\overline{I}_{sh} \perp \overline{V}_1^{'} \ \& \ \overline{I}_{se} \perp \overline{V}_{se}$), Cases B and C are inoperable.

| (a) | (b) |
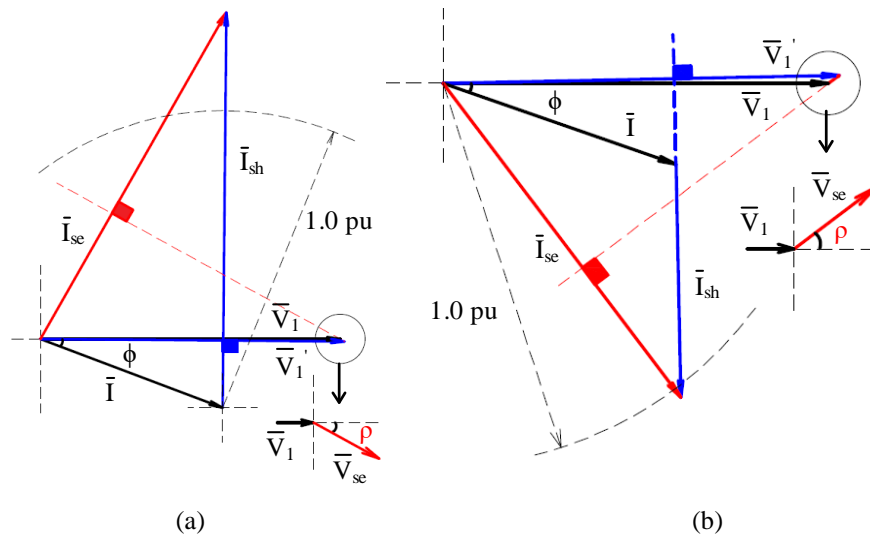
Figure 5-10 Scaled phasor diagrams; a) $\left|\bar{I}_{sh}\right| \& \left|\bar{I}_{se}\right| > 1.0$ pu, and b) $\left|\bar{I}_{se}\right| > 1.0$ pu

5.4.3 Shunt current for several Target Power

Figure 5-11 shows the shunt current's magnitude against power $P_2^{'}$ and $Q_2^{'}$ for several Target Power points. Figures 5-11(a) to (c) show similar characteristics when the Target Power was changed to several arbitrary points in four-quadrant of operation, and indicate that current $\left|\bar{I}_{sh}\right|$ has a maximum value of 0.5 pu for active power control, while either currents $\left|\bar{I}_{sh}\right|$ and $\left|\bar{I}_{se}\right|$ exceeded 1.0 pu or current $\left|\bar{I}_{se}\right|$ exceeded 1.0 pu for reactive power control.

(a)

(b)

(c)
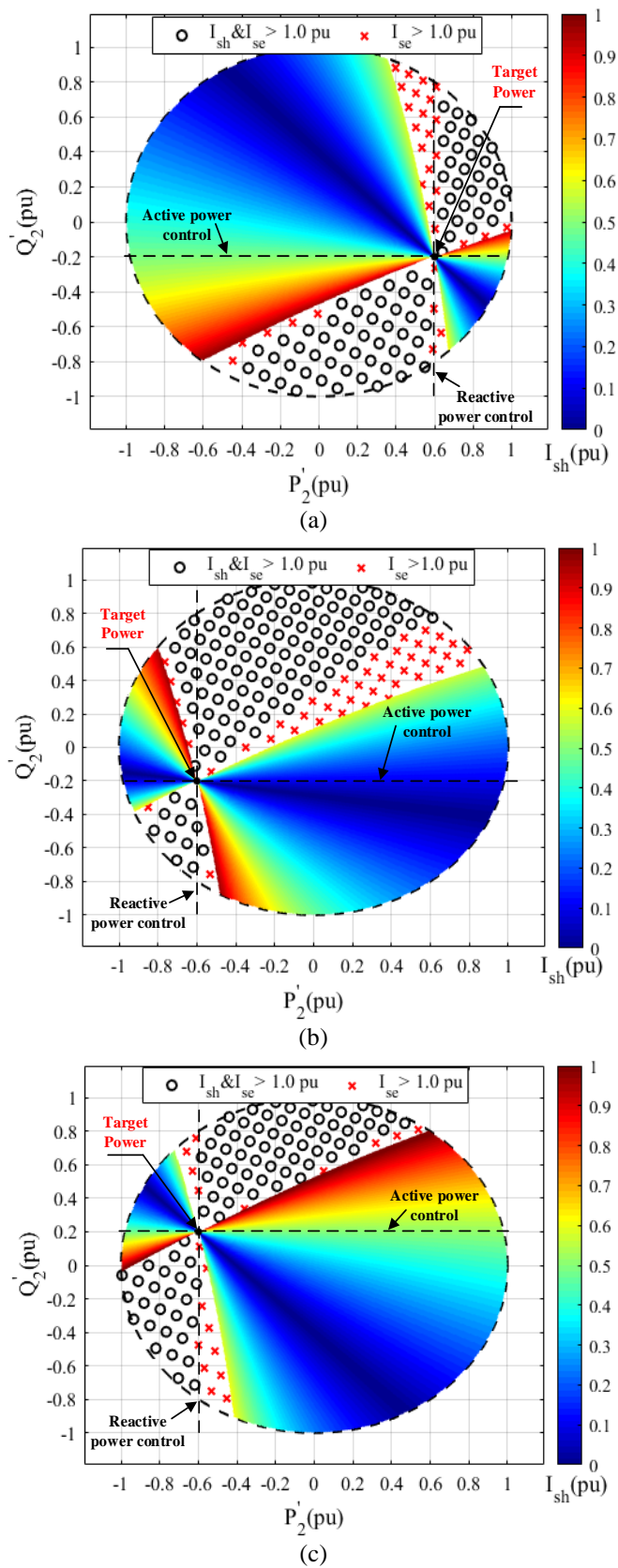
Figure 5-11 Current $\left|\bar{I}_{sh}\right|$ against power $P_2^{'}$ and $Q_2^{'}$ for several Target Power; (a) (0.6 pu, -0.2 pu), (b) (-0.6 pu, -0.2 pu) and (c) (-0.6 pu, 0.2 pu).

5.4.4 Theoretical analysis of the shunt current

Simplified expressions of $\left|\bar{I}_{sh}\right|$ can be obtained in two cases: 1) active power control (i.e., $Q_c = 0$), and 2) reactive power control (i.e., $P_c = 0$).

Firstly, an approximate expression of current $\left|\bar{I}_{sh}\right|$ can be obtained from (5-4) by neglecting angle δ_s which is usually small in MV distribution networks as given in (5-6).

$$\left|\bar{I}_{sh}\right| = \left|\bar{I}\right| \cdot (\frac{\cos(\phi)}{\tan(\rho)} + \sin(\phi)) \tag{5-6}$$

Secondly, the controllable power P_c and Q_c was obtained in (4-5) and rewritten in equation (5-7).

$$\begin{cases} P_c = \dfrac{\left|\bar{V}_2\right| \cdot \left|\bar{V}_{se}\right|}{\left|\bar{Z}\right|} \cos(\delta_0 + \theta - \rho) \\[4mm] Q_c = \dfrac{\left|\bar{V}_2\right| \cdot \left|\bar{V}_{se}\right|}{\left|\bar{Z}\right|} \sin(\delta_0 + \theta - \rho) \end{cases} \tag{5-7}$$

Approximate equations for the controllable power P_c and Q_c can be obtained from (5-7) by neglecting angle δ_0, as in (5-8), where V_d and V_q are the direct and quadrature components of voltage $\bar{V}_{se}$.

$$\begin{cases} P_c \cong \dfrac{V_2 R}{Z^2} V_d + \dfrac{V_2 X}{Z^2} V_q \\[4mm] Q_c \cong \dfrac{V_2 X}{Z^2} V_d - \dfrac{V_2 R}{Z^2} V_q \end{cases} \tag{5-8}$$

When $Q_c = 0$, then substituting in (5-8) obtains $V_q / V_d = X/R$ or $\tan(\rho) = X/R$. In this case, current $\left|\bar{I}_{sh}\right|$ in (5-6) can be rewritten as given in (5-9).

$$\left|\bar{I}_{sh}\right| \approx \left|\bar{I}\right| \cdot (\frac{\cos(\phi)}{X/R} + \sin(\phi)) \tag{5-9}$$

Since the feeder is utilised for active power control, hence angle ϕ is close to zero. Therefore, current $\left|\bar{I}_{sh}\right|$ is a fraction of current $\left|\bar{I}\right|$ considering a distribution feeder of an X/R ratio greater than 1.0.

Similarly, when $P_c = 0$, then substituting in (5-8) obtains $V_q / V_d = -R / X$. In this case, current $\left|\bar{I}_{sh}\right|$ in (5-6) can be rewritten as given in (5-10).

$$\left|\bar{I}_{sh}\right| \approx \left|\bar{I}\right| \cdot (\frac{\cos(\phi)}{R / X} + \sin(\phi)) \qquad (5\text{-}10)$$

Equation (5-10) demonstrates that current $\left|\bar{I}_{sh}\right|$ is very likely to exceed 1.0 pu especially when the X/R ratio of a distribution feeder increases.

The above analysis demonstrates that a Transformer-less UPFC can control active power with a partially rated shunt converter. Assume the full-load operation of current $\left|\bar{I}\right|$, angle ϕ is zero, and the X/R is 2.0, using (5-9), the power rating of the shunt converter is 0.5 pu when used to control active power. However, its ability to control reactive power is limited by the converters' current ratings.

5.5 Simulation study

In this section, the control methodology of a Transformer-less UPFC was taken from the IEEE Transaction on Power Electronics paper entitled "Modulation and Control of Transformer-less UPFC" [136].

5.5.1 Control scheme of the simulated Transformer-less UPFC

Figure 5-12 shows the test system implemented in MATLAB Simulink.
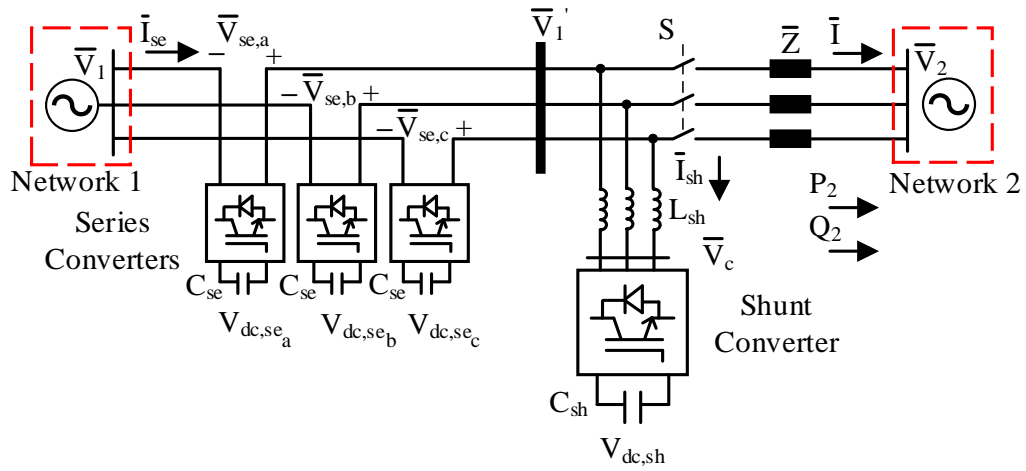
Figure 5-12 Simulated Transformer-less UPFC

The Transformer-less UPFC was connected to a 10 MVA, 12.66 kV distribution feeder whose impedance was 8%, X/R ratio of 2.0. The base voltage and apparent power were 12.66 kV and 10 MVA. The series converters were implemented using single-phase two-level VSCs, while the shunt converter was implemented using a three-phase two-level VSC.

The minimum capacitance of the single-phase series converters and three-phase shunt converter was calculated as given in (5-11) [139], where ΔV_{dc} is the maximum ripple voltage and was considered 5%.

$$\begin{cases} C_{se} \geq \dfrac{S_{se}/3}{2\omega\, V_{dc,se}\, \Delta V_{dc,se}} \\[4mm] C_{sh} \geq \dfrac{S_{sh}}{\omega\, V_{dc,sh}\, \Delta V_{dc,sh}} \end{cases} \tag{5-11}$$

Table 5-2 summarises the parameters of the Transformer-less UPFC model.

Table 5-2 Parameters of the Transformer-less UPFC model

	Parameter	Value
Series converter	nominal power, S_{se}	1.5 MVA
	DC voltage, $V_{dc,se}$	1750 V
	DC capacitance, C_{se}	6 mF
Shunt converter	nominal power, S_{sh}	10 MVA
	DC voltage, $V_{dc,sh}$	30 kV
	DC capacitance, C_{sh}	5 mF
	filter inductance, L_{sh}	20 mH

- **Overall control**

The Transformer-less UPFC was operated to control active and reactive power P_2 and Q_2 at Network 2 independently. Figure 5-13 shows the overall control structure.
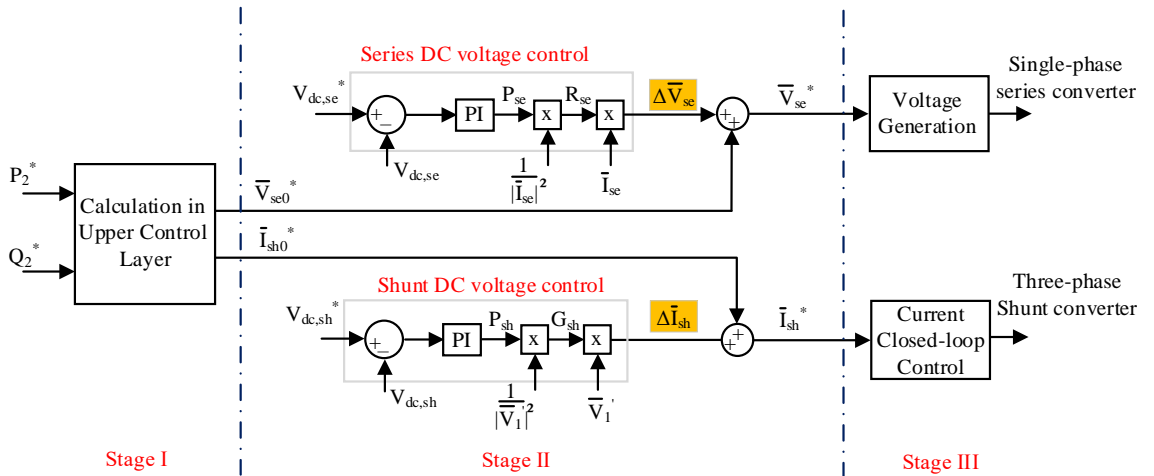
Figure 5-13 Overall control scheme of a Transformer-less UPFC [136]

In stage I, the desired active and reactive power at Network 2 (P_2^* and Q_2^*) were used to calculate the reference voltage $\overline{V}_{se0}^*$ of the series converter and the reference current $\overline{I}_{sh0}^*$ of the shunt converter according to (5-12) and (5-13).

$$\begin{cases} P_c^* = P_2^* - P_2, Q_c^* = Q_2^* - Q_2 \\ \left|\overline{V}_{se0}\right|^* = \dfrac{\left|\overline{Z}\right|}{\left|\overline{V}_2\right|}\sqrt{(P_c^*)^2 + (Q_c^*)^2}, \rho^* = (\delta_0 + \theta - \tan^{-1}(\dfrac{Q_c^*}{P_c^*})) \end{cases} \tag{5-12}$$

$$\begin{cases} \overline{I}^* = \text{conj}(\dfrac{P_2^* + jQ_2^*}{\overline{V}_2}) \\ \left|\overline{I}_{sh0}\right|^* = \left|\overline{I}\right|^* \cdot \dfrac{\cos(\rho^* - \phi^*)}{\sin(\rho^* - \delta_s^*)}, \phi_{sh}^* = (\delta_s^* - 90)^\circ \end{cases} \tag{5-13}$$

Equations (5-12) and (5-13) are derived from (5-2) and (5-4). When both $\overline{V}_{se}$ and $\overline{I}_{sh}$ are regulated effectively, P_2 and Q_2 will be maintained close to P_2^* and Q_2^*.

In stage II, the DC voltage control loops of the series and shunt converters are found. Their outputs are $\Delta\overline{V}_{se}$ and $\Delta\overline{I}_{sh}$ which are added to $\overline{V}_{se0}^*$ and $\overline{I}_{sh0}^*$.

In stage III, the series and shunt converters generate the switching signals of the IGBTs.

- **Individual converter control**

    a. **Series converter**

Figure 5-14 shows the control loop of the single-phase series converter. In total, three identical control loops were used for the series converters.

The DC voltage controller (in the red dash box) maintains the DC voltage $V_{dc,se}$ of the series converter at its reference value $V_{dc,se}^*$. The PI controller eliminates the error between $V_{dc,se}$ and $V_{dc,se}^*$ and generates an output power P_{se} which equals the power losses of the converter (i.e., $P_{se} = P_{loss}$). This ensures the active power is balanced within the converter.

The output (P_{se}) is then divided by I_{se}^2 to obtain a virtual resistance R_{se}. The value of R_{se} is equal to the equivalent resistance of the converter. R_{se} is further multiplied by the vector $\overline{I}_{se}$ to obtain the AC voltage drop across the converter $\Delta\overline{V}_{se}$ caused by the equivalent resistance of the converter. $\Delta\overline{V}_{se}$ needs to be added to $\overline{V}_{se0}^*$ to compensate for the AC voltage drop. The sum $(\overline{V}_{se0}^* + \Delta V_{se})$ is the reference voltage

$\overline{V}_{se}^{*}$ that is forwarded to the PWM block, generating the switching signals $S_1 \to S_4$ [136]. The gain parameters of the PI controller are given in Appendix A.
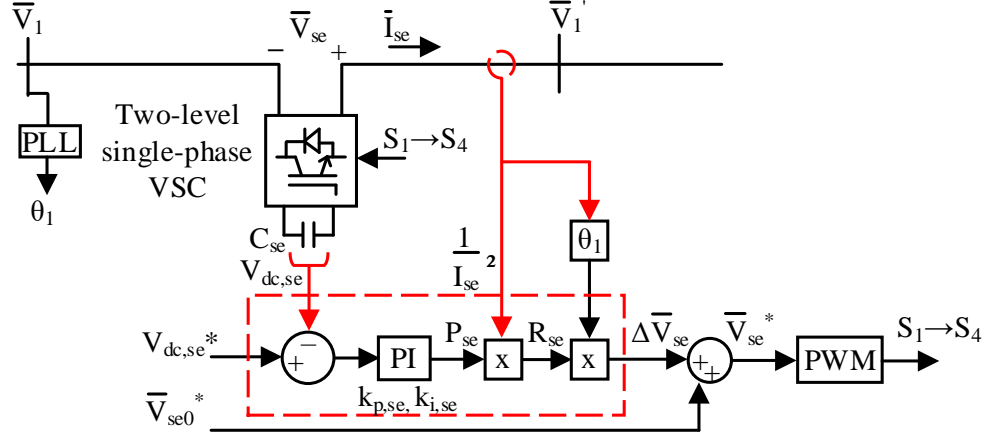
Figure 5-14 Control scheme of the single-phase series converter [136]

b. Shunt converter

Figure 5-15 shows the control loops of the three-phase shunt converter. The DC voltage controller (in the red dash box) maintains the DC voltage $V_{dc,sh}$ of the shunt converter at its reference value $V_{dc,sh}^{*}$. It has similar control structure to the DC voltage controller of the series converter.

The shunt current is regulated in the dq frame using abc to dq transformation. The dq current errors ($I_{sh,d}^{*} - I_{sh,d}$) and ($I_{sh,q}^{*} - I_{sh,q}$) are sent to the PI controllers of the current control loops.

The PI controllers minimise the dq current errors and generate the reference dq voltage signals $V_{c,d}$ and $V_{c,q}$, which are then transformed to abc frame using dq to abc transformation. The PWM block generates the gate signals of the IGBTs ($S_1 \to S_6$). The gain parameters of the PI controllers are given in Appendix A.
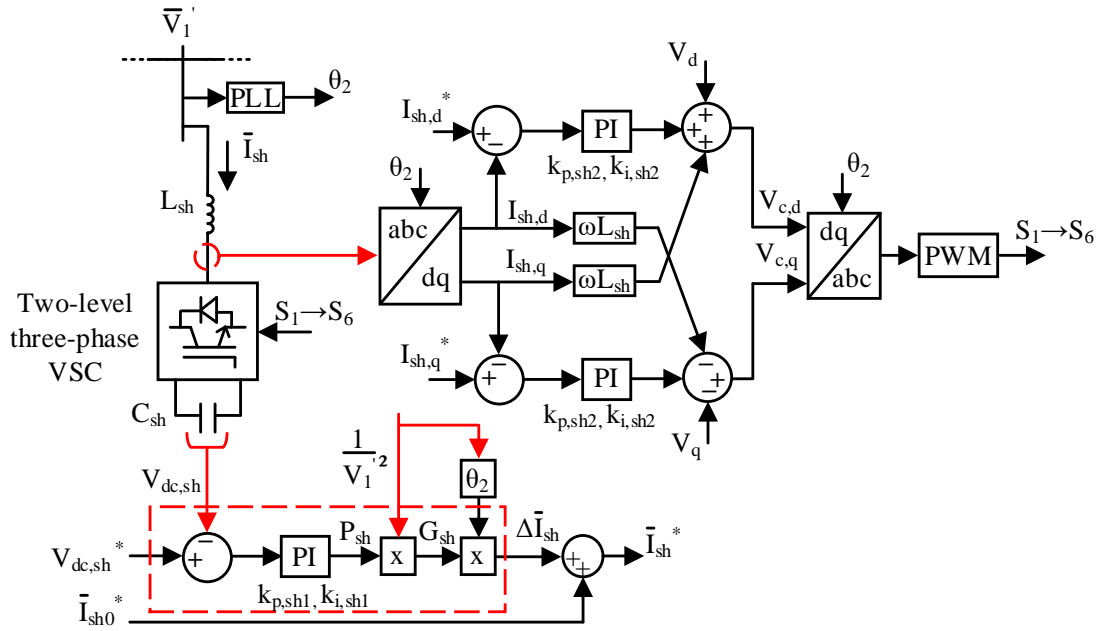
Figure 5-15 Control scheme of the three-phase shunt converter [140]

5.5.2 Results

The same three cases (Case A, Case B and Case C) shown in Figure 6-9 were simulated.

- **Case A**

Figure 5-16 shows the voltages and currents of the series and shunt converters when a step change of active power occurred at $t = 0.2$ s in response to a change in active power control signal. Before $t = 0.2$ s, the uncompensated active power was 0.2 pu and the uncompensated reactive power was 0.2 pu.

Figure 5-16(a) shows that P_2 was increased from 0.2 pu to 0.6 pu while Q_2 was maintained unchanged at 0.2 pu in steady-state. This demonstrates the ability of the Transformer-less UPFC to independently control active and reactive power.

Figures 5-16(b) and (c) show that after $t = 0.2$ s, currents $\left|\bar{I}_{sh}\right|$ and $\left|\bar{I}_{se}\right|$ were 0.11 pu and 0.69 pu and both with 90° phase shift in respect of voltages $\bar{V}_1^{'}$ and $\bar{V}_{se}$. This small shunt current matches with the analysis in Section 5.4.2 (i.e., Case A). Thus, it demonstrates the ability of the Transformer-less UPFC to regulate active power with a small requirement of shunt current (i.e., partially rated shunt converter).

(a)

(b)

(c)
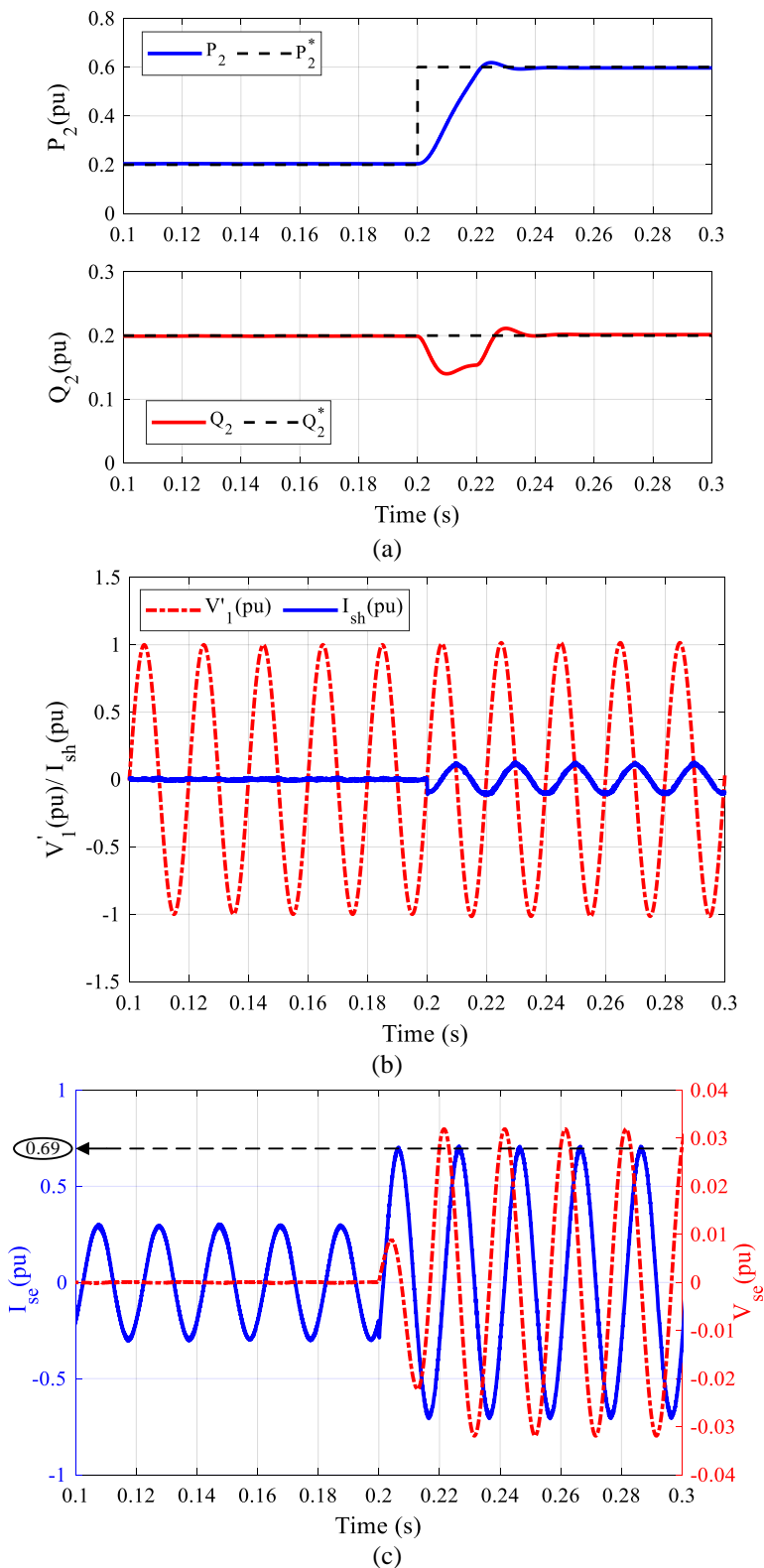
Figure 5-16 Simulation waveforms of Case A;(a) P_2 and Q_2, (b) $\overline{V}_1^{'}$ and $\overline{I}_{sh}$ and (c) $\overline{V}_{se}$ and $\overline{I}_{se}$

- **Case B**

Figure 5-17 shows the voltages and currents of the series and shunt converters when a step change of reactive power occurred at t = 0.2 s in response to a change in reactive power control signal. Before t = 0.2 s, the uncompensated active power was 0.6 pu and the uncompensated reactive power was zero.

Figure 5-17(a) shows that Q_2 was increased from zero to 0.2 pu while P_2 was maintained constant at 0.6 pu in steady-state. In response to this step change of reactive power, current $\left|\bar{I}_{sh}\right|$ was increased to 1.31 pu and current $\left|\bar{I}_{se}\right|$ to 1.21 pu in steady-state as shown in Figures 5-17(b) and (c). Both $\left|\bar{I}_{sh}\right|$ and $\left|\bar{I}_{se}\right|$ exceeded 1.0 pu. These magnitudes match with Case B in Section 5.4.2 and the phasor diagram in Figure 5-10(a).
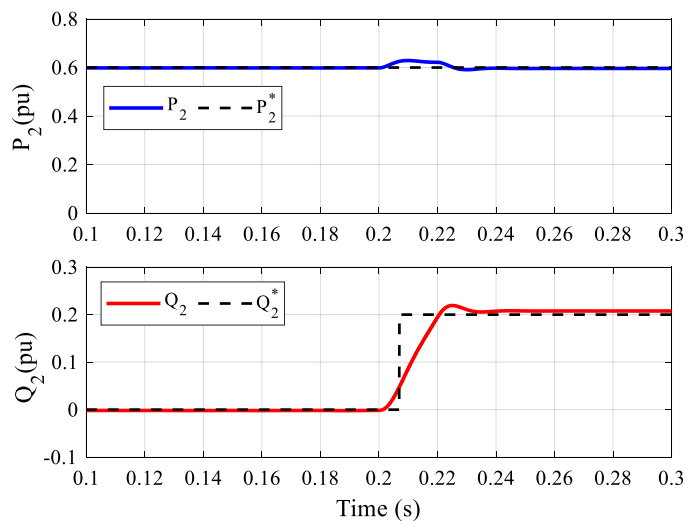
(a)
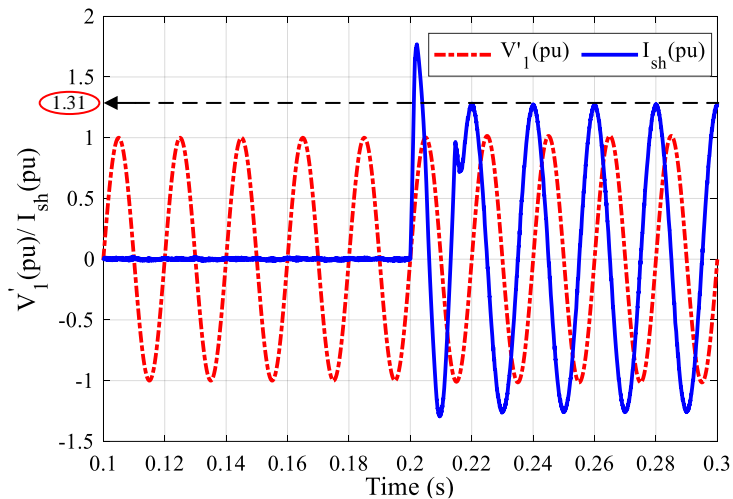
(b)
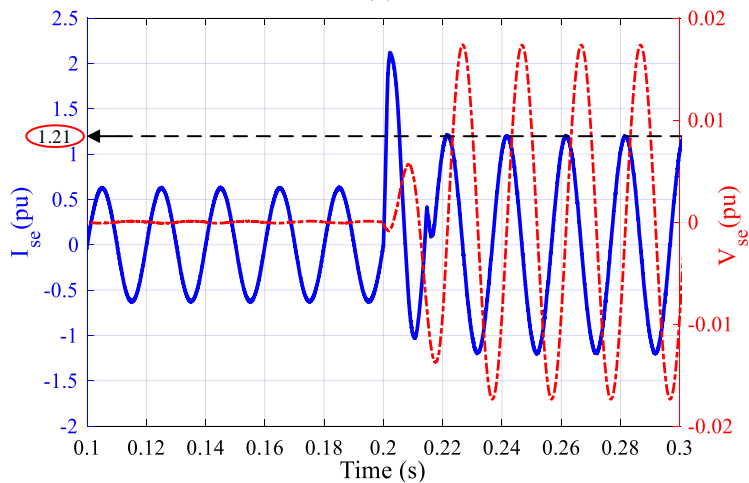
(c)

Figure 5-17 Simulation waveforms of Case B;(a) P_2 and Q_2, (b) $\overline{V}_1^{'}$ and $\overline{I}_{sh}$ and (c) $\overline{V}_{se}$ and $\overline{I}_{se}$

- **Case C**

Figure 5-18 shows the voltages and currents of the series and shunt converters when a step change of active and reactive power occurred at t = 0.2 s in response to changes in active and reactive power control signals. Before t = 0.2 s, the uncompensated active power was 0.2 pu and the uncompensated reactive power was zero.

Figure 5-18(a) shows that P_2 was increased from 0.2 pu to 0.6 pu, and Q_2 was increased from zero to 0.2 pu in steady-state.

Figure 5-18(b) and (c) show that current $\left|\bar{I}_{sh}\right|$ was increased to 0.64 pu, and current $\left|\bar{I}_{se}\right|$ was 1.06 pu. Although current $\left|\bar{I}_{sh}\right|$ was below 1.0 pu, current $\left|\bar{I}_{se}\right|$ exceeded 1.0 pu. These results match with Case C in Section 5.4.2 and the phasor diagram in Figure 5-10(b).
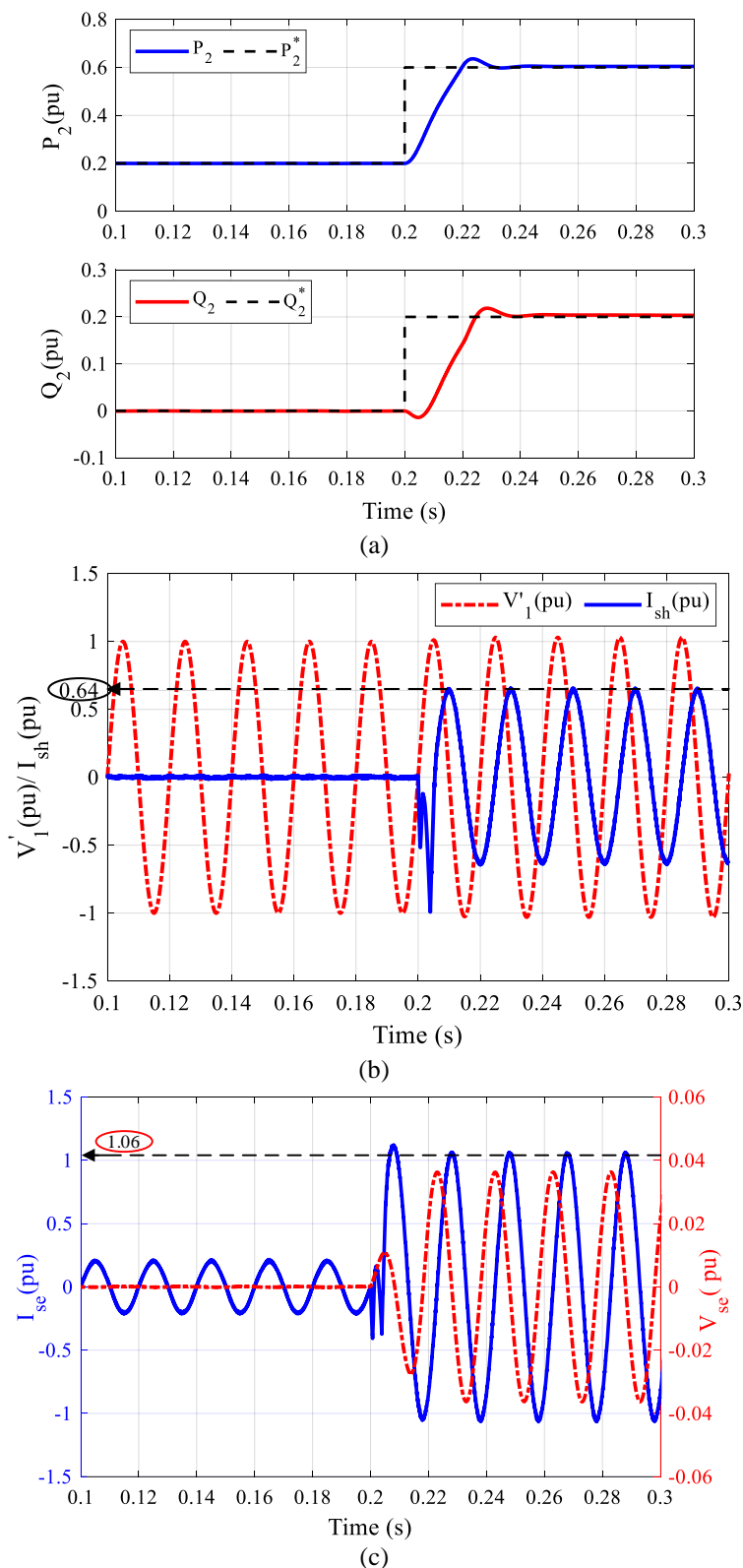
Figure 5-18 Simulation waveforms of Case C;(a) P_2 and Q_2, (b) $\overline{V}_1^{'}$ and $\overline{I}_{sh}$ and (c) $\overline{V}_{se}$ and $\overline{I}_{se}$

5.6 Experimental results

5.6.1 Experimental equipment

A physical experiment was used to demonstrate the shunt current's magnitude of a Transformer-less UPFC, as shown in Figure 5-19. It consists of;

1) an Imperix power electronic rig [141]. (See Appendix C for more information on the Imperix power electronic rig)

2) two power amplifiers [142]. (See Appendix D for more information on the power amplifier)

3) a series impedance.
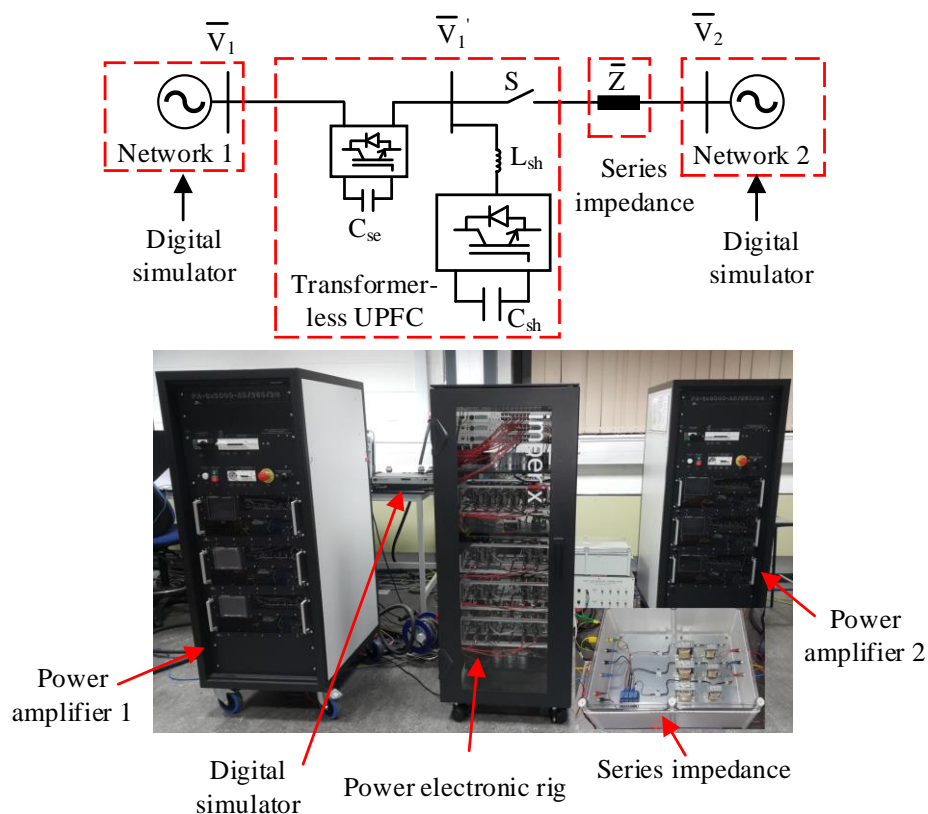
Figure 5-19 Physical set-up of the test system

The Imperix power electronic rig has half-bridge modules that were connected to form the single-phase series converters and the three-phase shunt converter. Two half-bridge modules were used to implement each two-level single-phase series converter and were directly connected to Network 1. Three half-bridge modules were used to implement a two-level three-phase shunt converter interfaced to the AC network through a filter inductance L_{sh}.

100

The power amplifiers were used to emulate Network 1 and Network 2, and both were controlled using an OPAL-RT digital simulator [143]. The series impedance represents the distribution feeder connecting Network 1 and Network 2.

Table 5-3 shows the parameters of the test setup.

Table 5-3 System parameters of the test setup

	Parameter	Value
Network	rated apparent power	0.75 kVA
	Phase voltage	$50V\angle0°, 50\,Hz$
	Feeders' impedance	$0.68 + j1.57\,\Omega$
PWM	switching frequency	20 kHz
	dead time band	$1\,\mu s$
Series converter	DC voltage, $V_{dc,se}$	20 V
	DC capacitance, C_{se}	$750\,\mu F$
Shunt converter	DC voltage, $V_{dc,sh}$	150 V
	DC capacitance, C_{sh}	$750\,\mu F$
	filter inductance, L_{sh}	2.5 mH

5.6.2 Tests conducted and results

The start-up of the experiment required starting the series converters and shunt converter and both are physically connected to the same point (i.e., busbar $\overline{V}_1'$). Then, synchronisation procedures were followed to connect Network 1 and Network 2. For the sake of simplicity, the experiment was conducted at low voltage.

Figure 5-20 shows the DC voltage across the DC buses of the series and shunt converters from start-up until steady-state. In Step 1, the series converters were connected and charged through the anti-parallel diodes. In Step 2, the DC voltage controllers of the series converters were activated, and V_{dc,se_a}, V_{dc,se_b} and V_{dc,se_c} were maintained constant at 20 V. In Step 3, the shunt converter was connected and charged

through the anti-parallel diodes. In Step 4, the DC voltage controller of the shunt converter was activated, and $V_{dc,sh}$ was maintained constant at 150 V.
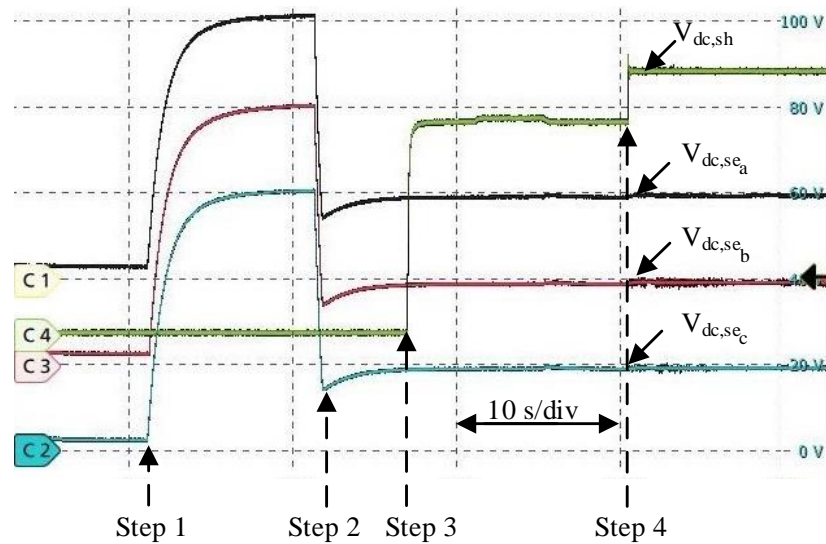
Figure 5-20 DC voltages of the three single-phase converters with 20 V/div (C1-C3), and the DC voltage of the shunt converter with 50 V/div (C4)

Figure 5-21 shows the experimental waveform of voltage $\overline{V}_1^{'}$ after closing the Switch "S".
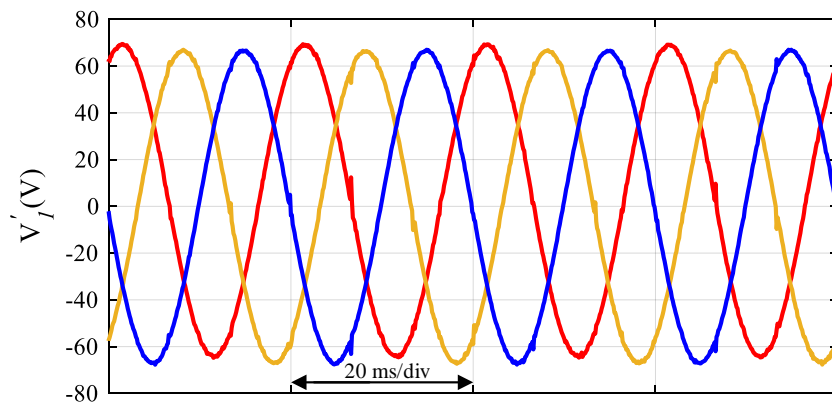
Figure 5-21 Experimental waveform of the phase voltage $\overline{v}_1^{'}$

Two cases were tested: 1) step change of active power while the reactive power was kept unchanged. 2) step change of reactive power while the active power was maintained constant.

Figure 5-22 shows the experimental results of the Transformer-less UPFC in response to a control signal to step change the active power flow. The base voltage and apparent power were $\sqrt{3}(50)$ V and 750 VA.

Figure 5-22(a) shows the measured active power P_2 at Network 2. P_2 was increased from 0.36 pu to 0.8 pu, while the reactive power Q_2 was maintained unchanged at 0.12 pu.

Figure 5-22(b) shows a small shunt current of approximately 0.63 A rms (i.e., 0.13 pu) provided by the shunt converter.
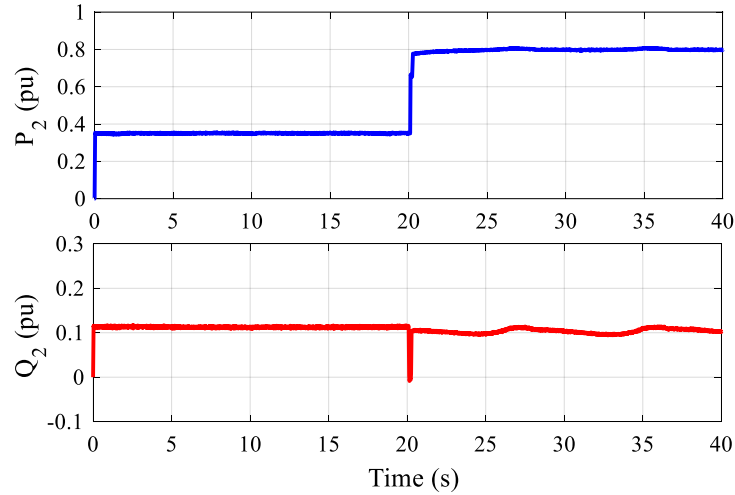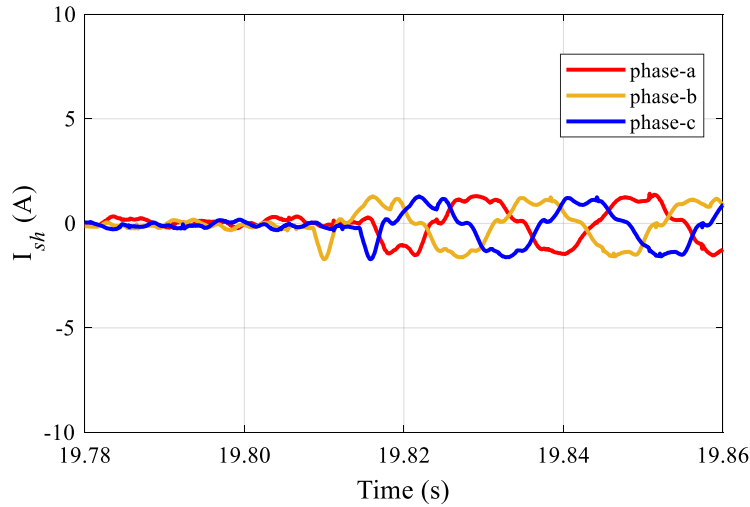
Figure 5-22 Experimental waveforms in response to step change of active power; (a) active and reactive power at Network 2, and (b) shunt current

Figure 5-23 shows the experimental results of the Transformer-less UPFC in response to a control signal to step change the reactive power flow. Figure 5-23(a) shows that Q_2 was increased from 0.12 pu to 0.3 pu while P_2 was kept unchanged at 0.36 pu. Figure 5-23(b) shows a large shunt current of 5.16 A rms (i.e., 1.03 pu).

(a)

(b)
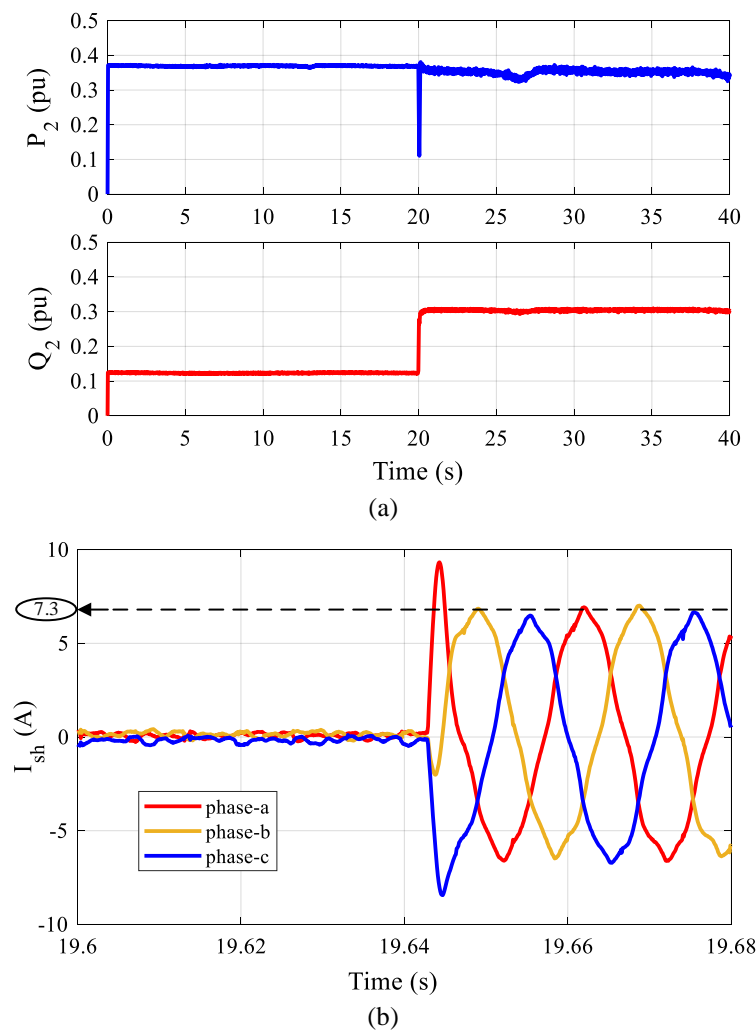
Figure 5-23 Experimental waveforms in response to step change of reactive power; (a) active and reactive power at Network 2, and (b) shunt current

5.6.3 Discussion of results and limitations

The lower voltage used with the experiment did not provide the same operating points as in the Simulation section. However, it highlights the most important findings of this work that are; 1) a small shunt current when a Transformer-less UPFC controls active power (see Figure 5-22(b)). 2) a large shunt current when a Transformer-less UPFC controls reactive power (see Figure 5-23(b)).

The series converter controls the power flow by injecting series voltage up to 5 V (approximately 10 % of the phase-voltage). It was difficult to replicate the results in the Simulation section, considering the voltage drop of the wires, the IGBTs, and other passive components.

5.7 Summary

A Transformer-less UPFC was investigated as a candidate for power electronic devices in MV distribution networks. It can provide power flow control using series and shunt converters that are not connected to a common DC-link and with complete removal of the interfacing transformers.

The operation of a Transformer-less UPFC relies on controlling the series and shunt converters together such that both converters exchange only reactive power with the AC network.

The shunt current of the Transformer-less UPFC was small when it was used to control active power. In contrast, the use of the Transformer-less UPFC to control reactive power required a large shunt current (i.e., > 1.0 pu).

A Transformer-less UPFC in MV distribution network is a good choice for applications that require controlling active power. However, its ability to control reactive power is limited by the converters' current ratings.

Chapter 6 Improved Unified Power Flow Controller for a Distribution Circuit

This chapter introduces an Improved Unified Power Flow Controller for power flow management in medium voltage distribution networks.

6.1 Introduction

The Improved Unified Power Flow Controller (UPFC) can provide power flow management similar to a UPFC. It does not need an interfacing series transformer with a unique design such as small capacity, high insulation level, large short-circuit current and an over-excitation tolerance. Hence it offers a smaller size and less cost. Figure 6-1 shows the Improved UPFC in comparison to a UPFC.
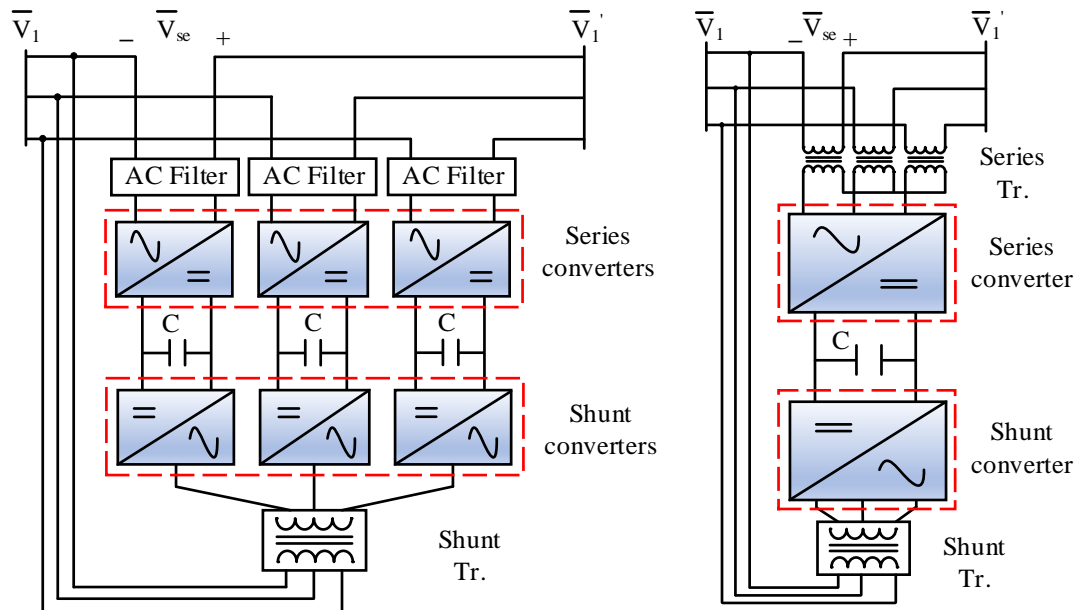
Figure 6-1 Circuit configurations of (a) Improved UPFC and (b) UPFC

The series connection of the Improved UPFC is performed using three separate single-phase converters directly connected in series to an MV distribution network instead of a three-phase converter interfaced using a three-phase series transformer in a UPFC. The Improved UPFC has three separate DC-link buses. The shunt converters are connected back-to-back (B2B) to the series converters, and they are interfaced to an AC network using a three-phase interfacing shunt transformer. The shunt converters of the Improved UPFC can be either single-phase or three-phase converters. In this work, single-phase shunt converters were used. Three-phase converters require smaller DC-link capacitance, though they require more IGBT modules and a more complex multi-winding three-phase shunt transformer.

The Improved UPFC can be built using three-level converters that are widely used for MV motor drive applications [144]. It has a similar configuration to the Soft Power Bridge (SPB) being implemented by UK Power Networks (UKPN) as part of the NIC project entitled "Active Response to Distribution Network Constraints" [145].

107

The Improved UPFC was modelled in MATLAB Simulink using the switched representation of single-phase three-level NPC Voltage Source Converters (VSCs). The Simulink model of the Improved UPFC aims to test the performance of single-phase series and shunt converters operate in P-Q and V_{dc}-Q control schemes to regulate the power flow of 5 MVA, 11 kV distribution feeder of a two-busbar network. The performance was tested by performing step changes of active and reactive power and power flow reversal.

The results demonstrated the ability of the control scheme to independently control active and reactive power flow and maintains the DC-link voltages constant.

6.2 Principle of operation

The Improved UPFC is a power electronic device with the same functionality as a UPFC. It consists of three single-phase series converters connected B2B to three single-phase shunt converters through three separate DC-link buses. The series converters are directly connected to an AC network with no need for interfacing series transformers. The shunt converters are interfaced to the AC network using a three-phase shunt transformer. Figure 6-2 shows a single line of the Improved UPFC.

Figure 6-2 Single line diagram of the Improved UPFC

Three-level topology was selected to reduce the blocking voltage of the IGBTs, reduce the harmonics in the output voltage and current, and it has been used for MV motor drive applications [146]. Although the series voltage is small (e.g., 10% of the

full network voltage), the insulation level of the IGBT modules should match the network voltage.

6.3 Control scheme of the Improved Unified Power Flow Controller

6.3.1 SPWM of a single-phase three-level NPC converter

Figure 6-3 shows the circuit configuration of a single-phase three-level full-bridge NPC converter. The DC voltage V_{dc} is split into three voltage levels $+1/2\,V_{dc}$, $-1/2\,V_{dc}$ and zero by two series-connected capacitors.
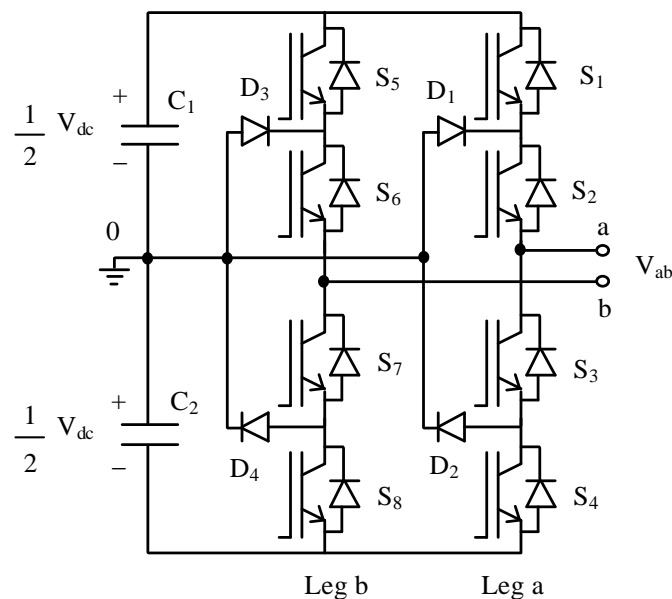
Figure 6-3 A single-phase three-level full-bridge NPC converter

Sinusoidal PWM was used to generate the gate signals $(S_1 \rightarrow S_8)$ for the IGBTs. Figure 6-4 shows the operating principles of SPWM for a single-phase three-level full-bridge NPC converter. Figure 6-4(a) shows two modulating signals (m_a) and (m_b) that are compared with two triangle signals C_1 and C_2 to generate the gate signals $(S_1 \rightarrow S_4)$ and $(S_5 \rightarrow S_8)$ of leg a and leg b. Figure 6-4(b) shows the output voltage V_{a0} of leg a, and voltage V_{b0} of leg b of the single-phase NPC converter. Figure 6-4(c) shows the output voltage V_{ab} of the single-phase NPC converter.
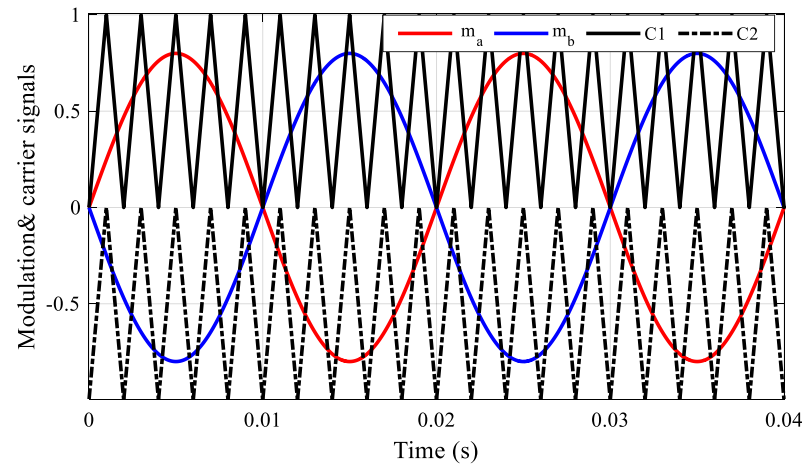
(a)
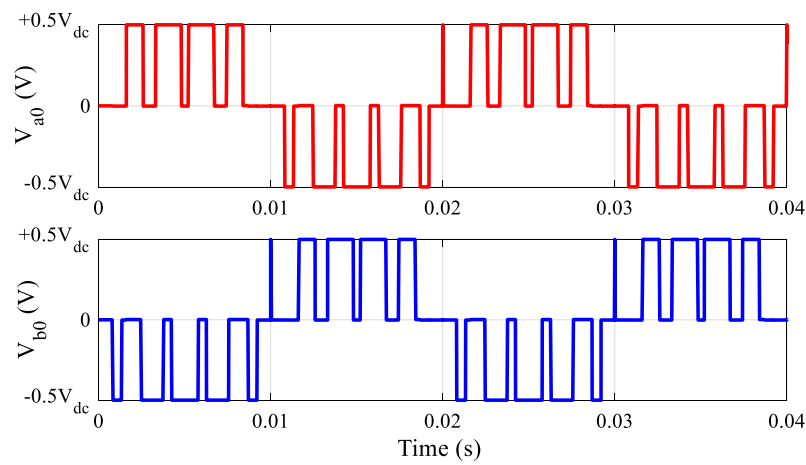
(b)
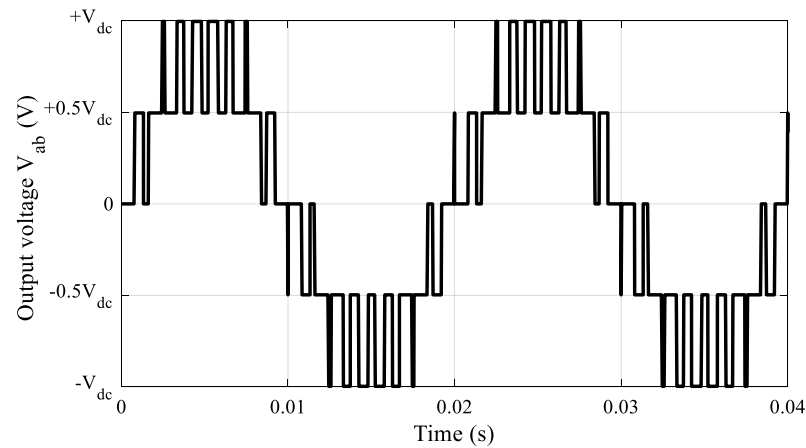
(c)

Figure 6-4 Operating principles of SPWM; (a) reference and carrier signals (b) voltage V_{a0} and voltage V_{b0} and (c) the output voltage V_{ab}

6.3.2 Power flow control mode

The Improved UPFC was controlled to operate in power flow control mode. Figure 6-5 shows the schematic diagram of the Improved UPFC connected to a two-busbar distribution network.
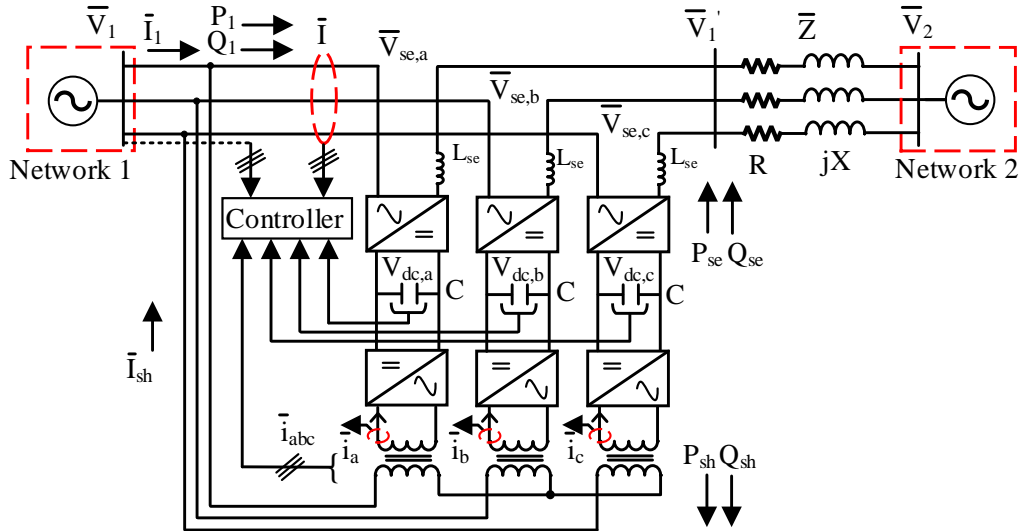
Figure 6-5 Schematic diagram of the test system built in MATLAB/Simulink

The series converters operate in P-Q control scheme to regulate the active and reactive power P_1 and Q_1. The shunt converters operate in V_{dc}-Q control scheme to maintain constant DC voltages across the DC-link buses and to provide/absorb reactive power Q_{sh} at busbar $\overline{V}_1$.

PI controllers are not well suited for single-phase converters as they require a computational effort to provide an orthogonal component (i.e., β axis component) of voltages and currents in the αβ frame [147]. An alternative to synchronous dq frame PI controllers is stationary frame Proportional-Resonant (PR) controllers.

A PR controller is a combination of proportional gain and resonant path tuned at a desired frequency. The basic transfer function of a PR controller $G_c(s)$ is given in (6-1).

$$G_c(s) = k_p + \frac{k_i s}{s^2 + w_r s + w_0^2} \tag{6-1}$$

where k_p and k_i are the proportional gain and integral gain, w_r and w_0 are the resonant cut-off frequency and the resonant target frequency.

Figure 6-6 shows the control loops of the Improved UPFC. Figure 6-6(a) shows the control loops of the series converter. The reference power P_1^* and Q_1^* are transformed into dq current components $I_d^* = P_1^* / 1.5V_d$ and $I_q^* = Q_1^* / 1.5V_d$ where V_d is the direct component of voltage $\overline{V}_1$. The dq current components I_d^* and I_q^* are transformed into αβ current components I_α^* and I_β^* using dq-αβ transformation. A PLL is used to generate the phase information θ of voltage $\overline{V}_1$. Two separate anti-windup PR digital controllers are used to regulate the αβ current components I_α and I_β of current $\overline{I}$ [148]. The output of the PR controllers is the modulating signals $m_{\alpha,se}$ and $m_{\beta,se}$ in αβ frame, and they are converted into $m_{se,abc}$ in abc frame using αβ-abc transformation. SPWM is used to generate the gate signals $(S_{1,abc} \rightarrow S_{8,abc})$ to drive the IGBTs of the three single-phase series converters.

Figure 6-6(b) shows the three separate control loops that are used to control the three single-phase shunt converters. The error signals of the DC voltages $\Delta V_{dc,a}$, $\Delta V_{dc,b}$ and $\Delta V_{dc,c}$ and of the reactive power $\Delta Q_{sh,a}$, $\Delta Q_{sh,b}$ and $\Delta Q_{sh,c}$ are manipulated using PI controllers to generate the reference direct and quadrature current components $I_{d,a}^* + jI_{q,a}^*$, $I_{d,b}^* + jI_{q,b}^*$ and $I_{d,c}^* + jI_{q,c}^*$ of the single-phase shunt converters. The reference current of each single-phase shunt converter is determined as given in equation (6-2).

$$i_{abc}^*(t) = I_{d,abc}^* \sin(\theta_{abc}) + I_{q,abc}^* \cos(\theta_{abc}) \tag{6-2}$$

The PR controllers track the reference currents $i_{abc}^*(t)$ and generate the modulating signals $m_{sh,abc}$ before being converted into PWM signals to drive the IGBTs.

(a)

(b)
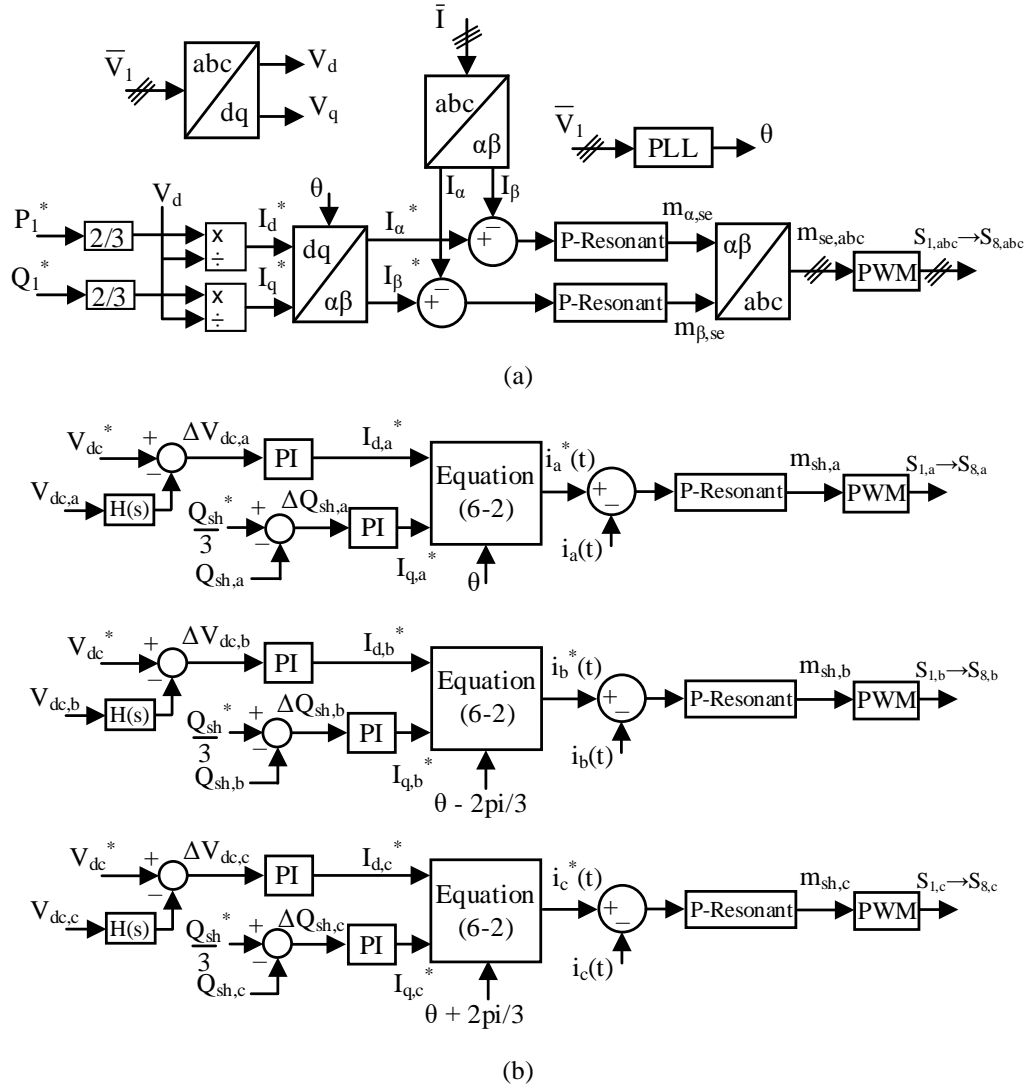
Figure 6-6 Control loops of the Improved UPFC; (a) series converters, and (b) shunt converters

6.3.3 Second order filter

The measured feedback DC voltage signal (i.e., $V_{dc,a}$, $V_{dc,b}$ and $V_{dc,c}$) has a DC voltage component and a ripple component. The ripple component is mainly double frequency harmonics that inherently exist with single-phase converters.

Second-order digital filters $H(s)$ are connected to the measured feedback voltage signals to extract the DC voltage components and prevent the ripple components from being introduced to the control loops, hence improving the control loops' performance. The transfer function $H(s)$ is given in equation (6-3).

$$H(s) = 1 - \frac{2\xi w_0 S}{S^2 + 2\xi w_0 S + w_0{}^2} \tag{6-3}$$

where w_0 and ξ are the desired double frequency harmonics and the damping factor.

Using $w_0 = 200\pi$ and $\xi = 0.05$, the Bode diagram in Figure 6-7 was obtained and the magnitude (dB) shows that the transfer function $H(s)$ provided very low gain around the resonant frequency $w_0 = 200\pi$.
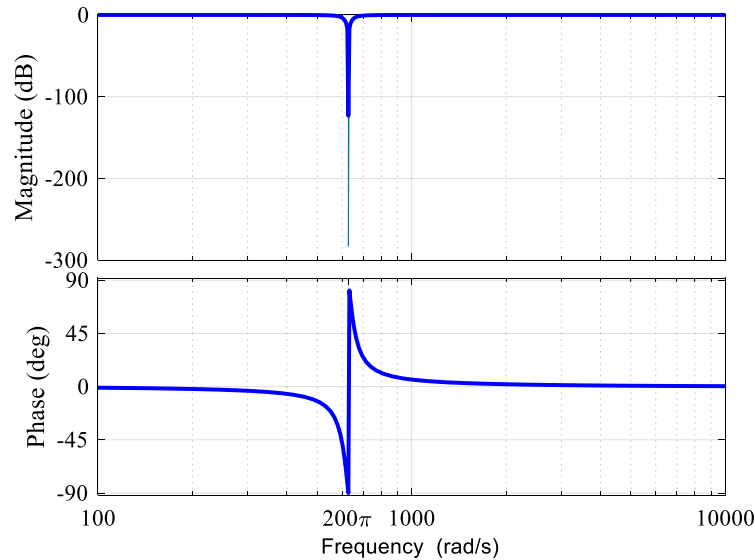
Figure 6-7 Bode diagram of second order filter

6.4 Simulation results

6.4.1 Case study

The system configuration shown in Figure 6-5 was used for the simulation. The simulation aims to test the performance of Improved UPFC with single-phase converters operating in P-Q and V_{dc}-Q control schemes. This was conducted by performing several step changes of active and reactive power and power flow reversal.

The model of the Improved UPFC was built in MATLAB Simulink using the switched representation of single-phase three-level NPC converters. The gain parameters of the anti-windup PR controllers were calculated as in [149].

The Improved UPFC was connected to an 11 kV, 5 MVA distribution feeder of a two-busbar network. Table 6-1 shows the circuit parameters of the Simulink model.

Table 6-1 Circuit parameters of the Simulink model

Parameters		Value
Network power rating		5 MVA
Network voltage		11 kV
Impedance of the feeder, $\overline{Z}$		0.57+j 1.140 Ω
Filter inductance, L_{se}		150 μH
DC capacitance, C		12 mF
DC voltage, V_{dc}		1200 V
Rated power of series converter, S_{se}		600 kVA
Rated power of shunt converter, S_{sh}		600 kVA
Shunt transformer		11/1.4 kV, 600 kVA, $Z_{tr,sh}$=6%
PR controller gain	proportional gain	0.022
	time constant	1.4 ms
PI controller gain	proportional gain	33
	time constant	2.5 ms

The minimum DC voltage for a single phase VSC was obtained from $V_{ph}(\text{peak}) = mV_{dc}$, where (m) is the modulating index. A 10% reserve voltage was considered together with the minimum DC voltage to ensure proper operation during transients and to consider the voltage drop across the interfacing impedance (i.e., series AC filter and shunt transformer) [150]. Considering $\left|\overline{V}_{se}\right|$ = 750 V rms and the maximum modulation index of SPWM is 1.0, the DC voltage was selected to be 1200 V.

The voltage rating of the IGBTs was selected such that the summation of the DC voltage, ripple voltage and turn off overshoot voltage is restricted to 70% of IGBT's nominal voltage rating [150]. Given that the blocking voltage of the IGBTs is half of the DC voltage (i.e., 600 V) and the feeders' nominal power is 5 MVA, IGBTs of 1.2 kV, 300 A were selected [151].

The DC capacitance was calculated from $C \geq \dfrac{S_{1-ph}}{\omega\, V_{dc}\, \Delta V_{dc}}$ [152]. Given that $S_{1\text{-}ph}$ = 210 kVA, ΔV_{dc} = 4%, and V_{dc} = 1200 V, the capacitance of the DC link is 12 mF.

6.4.2 Results

Figure 6-8 shows the response of the Improved UPFC to control signals to change active and reactive power P_1 and Q_1 at 0.4 s, 0.8 s and 1.2 s, and conduct power reversal at 1.6 s, 2.0 and 2.4 s.

Figure 6-8(a) shows accurate and fast-tracking performance to the target active and reactive power. At t = 0.4 s, P_1 was increased to 4 MW while Q_1 was maintained constant at 1 MVAr. At t = 0.8 s, Q_1 was increased to 3 MVAr and the distribution feeder transferred its full capacity (i.e., 5 MVA). At t =1.2 s, P_1 and Q_1 were decreased to 2 MW and 1 MVAr.

At t = 1.6 s, P_1 was reversed to -2 MW while Q_1 was maintained constant, then at t = 2.0 s, Q_1 was reversed to -1 MVAr while P_1 was kept unchanged at -2 MW. At = 2.4 s, P_1 was reversed to 2 MW while Q_1 was maintained constant at -1 MVAr. These demonstrate the ability of the Improved UPFC to independently control active and reactive power of the distribution feeder.

Figure 6-8(b) shows the active and reactive power of the series and shunt converters. The active power supplied or absorbed by the series converters approximately equals the active power absorbed by the shunt converters (i.e., $P_{se} + P_{sh} \approx 0$) in the steady-state, apart from the active losses absorbed to supply internal losses. The series converters provided the requested reactive power Q_{se} while the reactive power of the shunt converters Q_{sh} was set to zero.

Figure 6-8(c) shows that the DC voltage controllers well-regulated the DC voltages across the DC-link buses.
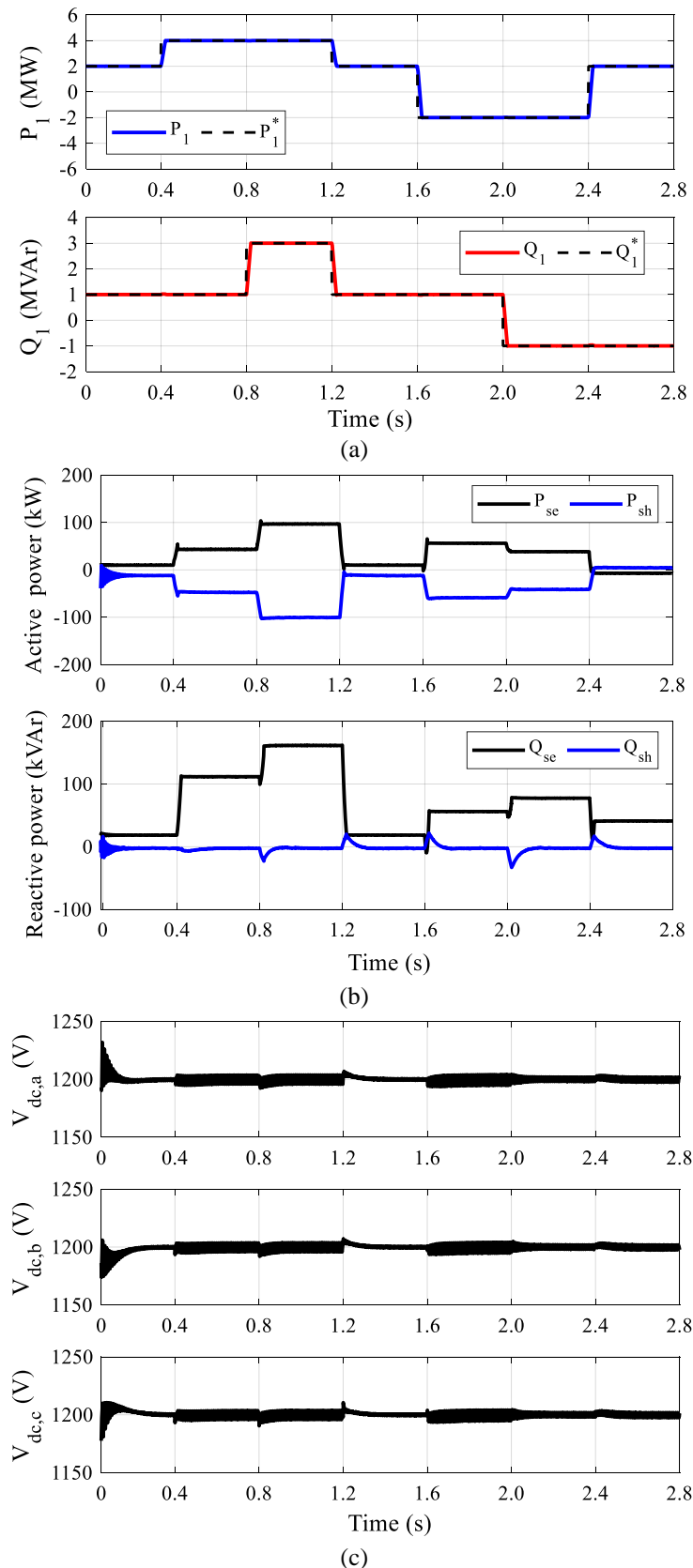
Figure 6-8 Response of the Improved UPFC; (a) active and reactive power of the feeder, (b) active and reactive power of the converters, and (c) DC-link voltages

Figure 6-9 shows the response of the Improved UPFC to a control signal to reverse the power flow at t = 0.5 s. Before t = 0.5 s, uncompensated power of 4 MW and 3 MVAr flows from Network 1 to Network 2.

Figure 6-9(a) shows that the active power P_1 was changed from 4 MW to -4 MW with a rate of 0.4 MW/ms, and the reactive power Q_1 was changed from 3 MVAr to - 3 MVAr with a rate of 0.3 MVAr/ms. In this case, the controllable power was maximum (i.e., $\sqrt{P_c^2 + Q_c^2} = 2.0$ pu, $S_{base} = 5$ MVA).

Figure 6-9(b) shows active and the reactive power of the series and shunt converters P_{se}, Q_{se}, P_{sh}, and Q_{sh}. Before t = 0.5 s, the converters injected zero active and reactive power. After t = 0.5 s, the series converters operated at full-load and injected active power of 261 kW and reactive power of 500 kVAr. The shunt converters absorbed 276 kW to supply the active power requested by the series converters, while no reactive power was provided at busbar $\overline{V}_1$ (i.e., $Q_{sh} = 0$).

Figure 6-9(c) shows the DC voltage across the DC-link buses. The DC voltage controllers maintained a constant DC voltage across the DC-link buses. The DC voltage has double frequency oscillations. which inherently exist with single-phase converters.

(a)

(b)

(c)
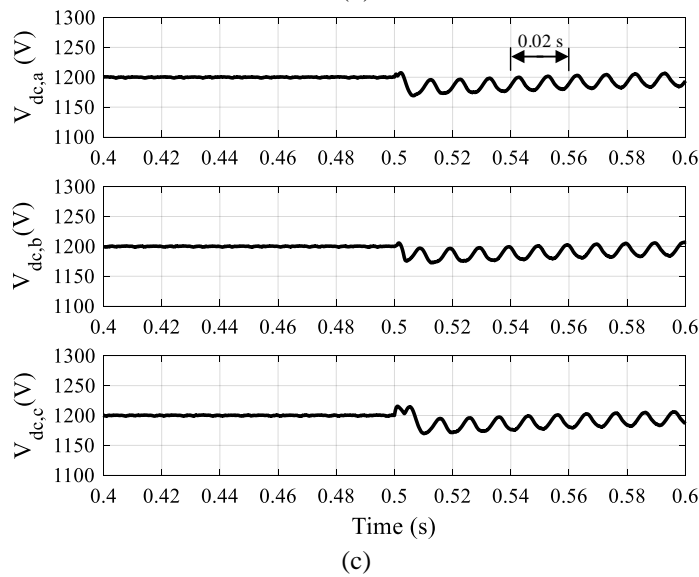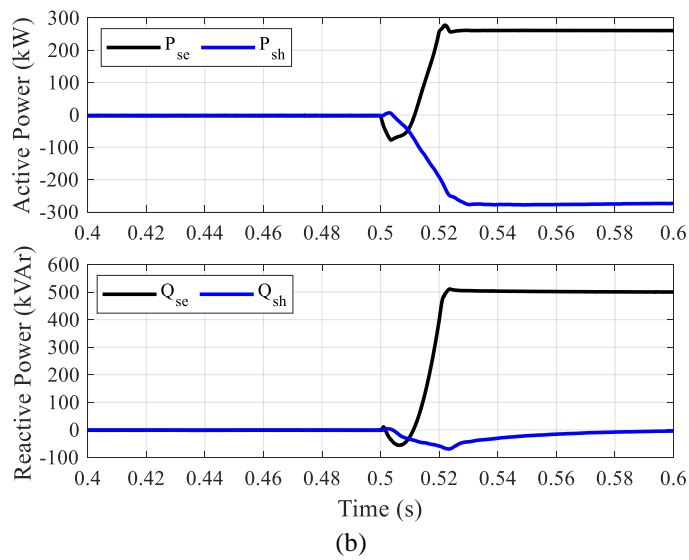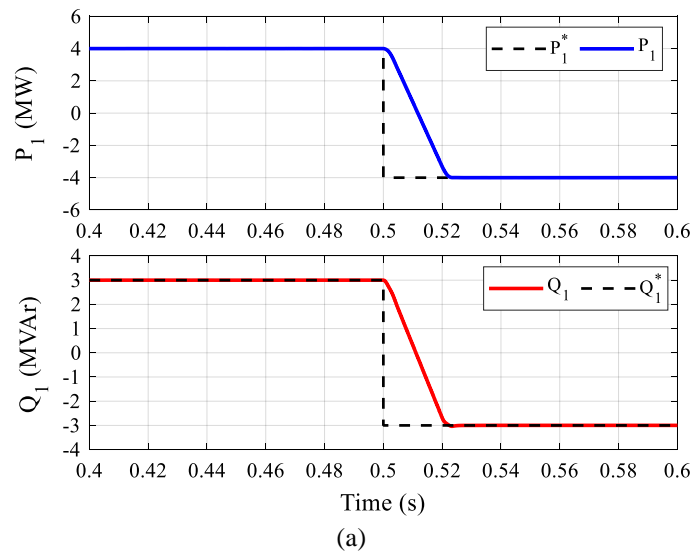
Figure 6-9 Response of the Improved UPFC to a power flow reversal at t = 0.5 s; (a) active and reactive power of the feeder, (b) active and reactive power of the converters, (c) DC-link voltages

119

Figure 6-10 shows the output voltage of the three single-phase series converters. Before t = 0.5 s, $\left|\overline{V}_{se}\right|$ was zero. After t = 0.5 s, $\left|\overline{V}_{se}\right|$ was increased to 685 V phase-rms (i.e., $\left|\overline{V}_{se}\right|$ = 10.7 %).
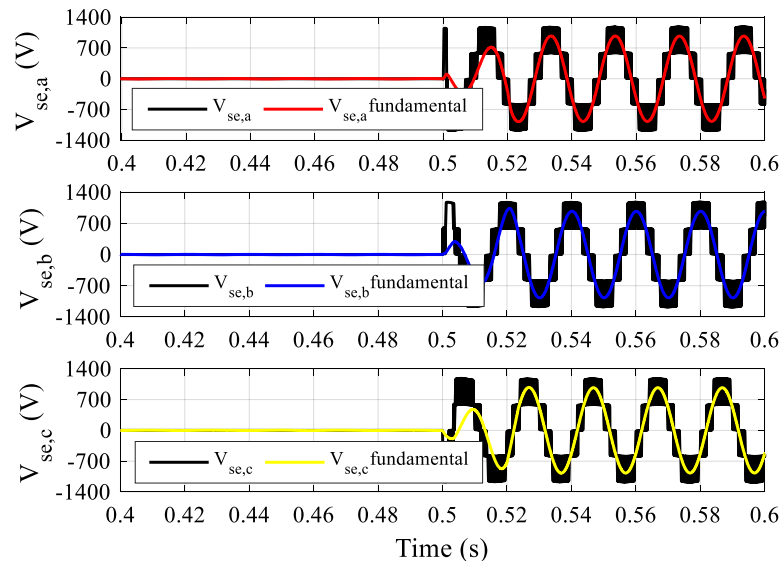
Figure 6-10 Maximum series voltage of the Improved UPFC

Figure 6-11 shows the current of Network 1 when the distribution feeder operated at full load with 262 A rms. The total harmonic distortion (THD) of current $\overline{I}_l$ was 1.35%.
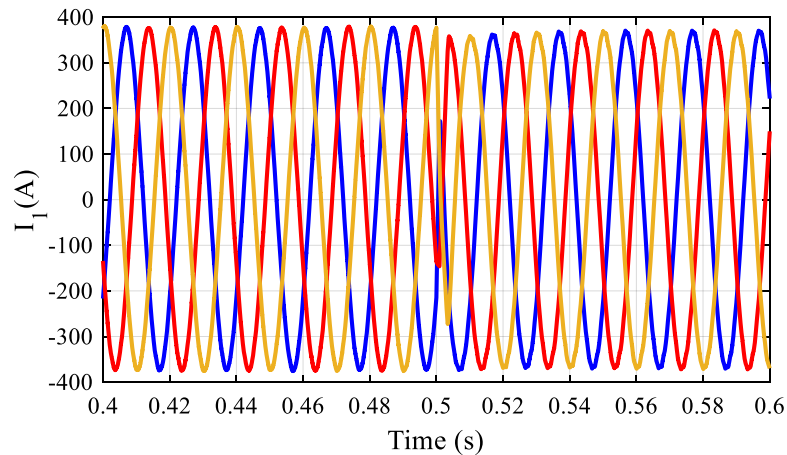
Figure 6-11 Current of Network 1 at the full load

6.5 Summary

The UPFC was improved for use in MV distribution networks by eliminating its interfacing series transformer. The series connection is performed using three single-phase converters with three separate DC-link buses. The shunt converters are connected B2B to the series converters and interfaced to an AC network using a three-phase shunt transformer.

A model of the Improved UPFC was built in MATLAB Simulink using the switched representation of single-phase three-level NPC converters. The single-phase series converters operated in the P-Q control scheme, and the single-phase shunt converters operated in the V_{dc}-Q control scheme. Step changes of active and reactive power and power flow reversal were performed to test the performance of the Improved UPFC connected to an 11 kV, 5 MVA two-busbar distribution network.

The Improved UPFC provided independent control of active and reactive power. The total harmonic distortion of the feeder current was low when the feeder and the series converters operated at full load.

Chapter 7 Performance of the Series Converter during Faults on the MV Distribution Network

This chapter investigates the performance of the series converter during faults on the MV distribution network and proposes a protection circuit for the series converter.

7.1 Introduction

The series converter of the Improved Unified Power Flow Controller (UPFC) provides the main function of the device. During normal operation, it controls active and reactive power of a distribution feeder by injecting a small controllable AC voltage $\overline{V}_{se} = \left|\overline{V}_{se}\right| \angle \rho$ (i.e., $0 \le \left|\overline{V}_{se}\right| \le \left|\overline{V}_{se}\right|_{max}$ and $0 \le \rho \le 360°$) in series with the distribution feeder. Figure 7-1 shows a single-line diagram of the Improved UPFC connected to a medium voltage (MV) distribution network.

Figure 7-1 Single-line diagram of the Improved UPFC connected to an MV distribution network

A large current flows through the series converter during external faults, and a large voltage is suddenly applied across its terminal. The large current and voltage can destroy the IGBTs of the series converter. Therefore, a protection circuit is required across the series converter. The protection circuit should bypass the series converter in a time scale of few milliseconds.

The objective of the protection circuit varies from radial to meshed distribution networks. In radial networks, the protection circuit should bypass the series converter and disconnect the feeders as fast as possible to avoid endangering network assets with excessive fault current. In meshed networks, the protection circuit should bypass the series converter without jeopardising the fault ride-through performance of a distribution network [153].

In this chapter: (1) the protection schemes of series converters in transmission and distribution networks during external faults were reviewed, and (2) a protection circuit

was proposed for meshed distribution networks. It has the advantage of a small number
of thyristors and a small number of switch disconnectors.

The following points were addressed:

1. the challenges facing the series converter during a three-phase fault in an
   MV distribution network were investigated. A mechanical circuit breaker
   was considered across the series converter.
2. a protection circuit suitable for MV distribution networks was proposed
   for the series converter.
3. the operation of the protection circuit and its main components (e.g.,
   thyristors, metal oxide varistors and switch disconnectors) were
   discussed.
4. a PSCAD model was used to test the performance of the proposed
   protection circuit.

A three-phase fault was applied near to the series converter. The results showed
that when a mechanical circuit breaker with a trip time of 20 ms was used to protect
the series converter, large voltage and current (e.g., 8.5 kV and 13 kA) were applied
to the IGBTs.

The proposed protection circuit managed to bypass the series converter within
1.003 ms (i.e., 1 ms time delay of the series converter protection system and 3 μs for
thyristors to turn on). The varistor clamped the voltage to 2 kV until the thyristors
turned on. The switch disconnectors completely isolated the series converter from the
network without affecting the fault path.

7.2 Literature review

7.2.1 Transmission networks

The protection schemes of UPFCs in transmission networks were reviewed. In
[154], [155], the protection scheme of the series converter of a UPFC relies on a fast
bypass system [156]. Figure 7-2 shows the fast bypass system used to protect the series
converter against faults in transmission networks [157], [158].
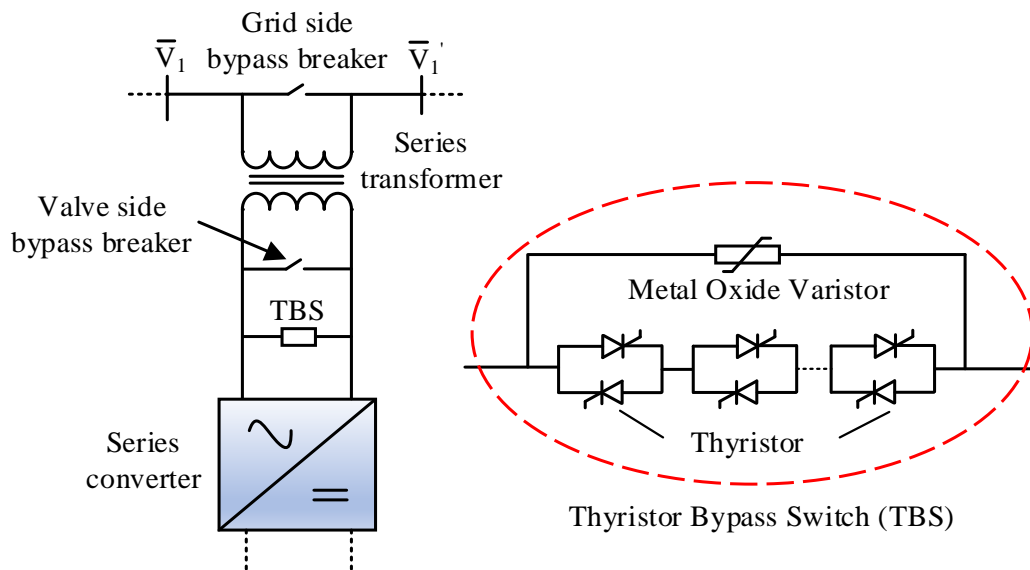
Figure 7-2 Fast bypass system for protecting the series converter [159]

The fast bypass system consists of thyristor bypass switches (TBS) and mechanical bypass breakers. The TBS comprises antiparallel connected thyristors and auxiliary components such as metal oxide varistor (MOV) [160].

During normal operation, the TBS is in a forward blocking state. When a fault is detected, the MOV protects the series converter against immediate overvoltages. The protection sends trigger signals to the TBS and both the valve side bypass breaker and the grid side bypass breaker. The TBS conducts in less than 1 ms, and the series converter is bypassed [161]. Once the bypass breakers are closed, the firing pulses of the TBS are removed, and the TBS turns off at the current zero-crossing point.

The valve-side bypass breaker provides a path for the fault current instead of the TBS. Its operation is essential to switch off the TBS. Therefore, the TBS does not need cooling equipment [162]. The grid-side bypass breaker ensures a safe and reliable operation of the UPFC [160].

The grid side bypass breaker carries the fault current until either the fault disappears (i.e., temporary fault) or the grid protection is activated (i.e., permanent fault).

125

7.2.2 Distribution networks

The performance of the series converter during faults in distribution networks is still under investigation. In 2018, a power electronic device with a series converter was proposed by the UK Power Networks project [163]. The project proposes a device called "Soft Power Bridge" to control the power flow in an 11 kV, 5 MVA distribution feeder using partially rated converters. No details have been published yet about the protection arrangements of the series converter.

In [164], a thyristor crowbar circuit was proposed to protect the series converter of a Static Series Synchronous Compensator (SSSC) against external faults and to ensure that the fault level of the network is unaffected. Figure 7-3 shows the thyristor crowbar circuit proposed for radial distribution networks.
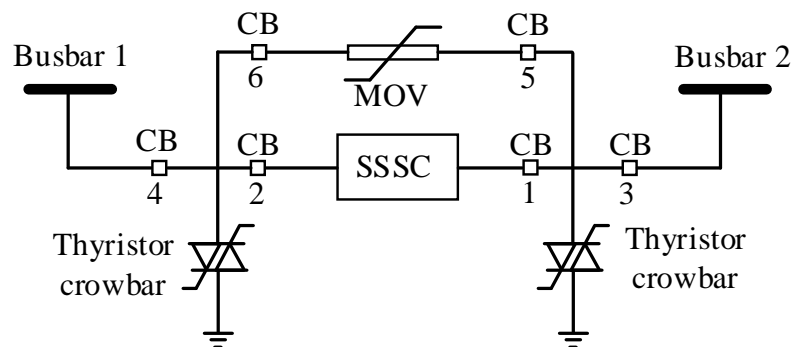
Figure 7-3 Protection scheme using thyristors crowbar [164]

The thyristor crowbar circuit comprises several thyristors installed at each side of the series converter to the ground.

When a fault occurs, the MOV clamps the voltage for a short time. This time includes the protection time and the thyristors turn-on time [164]. The thyristors are turned on to route the fault current away from the series converter. The series converter is isolated once circuit breakers 1, 2, 5, 6 are opened. Then, the thyristor crowbars are turned off. Circuit breakers 3 and 4 are back-up for 1 and 2.

The protection scheme offered fast isolation of the series converter during faults in distribution networks. However, the arrangement requires a string of thyristors to withstand the full network voltage, and it uses many circuit breakers. In additions, the operation of the thyristor crowbars imposes a momentarily fault on a healthy feeder. For an instant, when an AC fault occurs at Busbar 1, the operation of the crowbar circuit connects both Busbar 1 and Busbar 2 to the ground.

7.2.3 Components of a Thyristor Bypass Switch

- **Thyristor**

A thyristor's datasheet provides a non-repetitive surge current representing the thyristor's destruction limits and is defined using half-cycle conduction of a sinusoidal wave. In addition, some datasheets provide a repetitive surge current for multiple half cycles of sine wave [165].

During the operation of a TBS, the maximum fault current of the thyristor should not exceed its overcurrent capability described in the datasheet.

- **Varistor**

A Varistor is a nonlinear resistor used to clamp the voltage to a safe level when exposed to high-voltage surges. During normal operation, a varistor has high resistance and resemble an open circuit. A varistor becomes highly conductive during abnormal conditions such as faults, presenting a low impedance path to high-voltage surges [166], [167].

Varistors conduct rapidly, with no apparent time lag [168]. The ratings of varistors are typically described based on 8/20 µs impulse current waveform of the maximum peak current and at the rated voltage (i.e., 8 µs rise and 20 µs to 50% decay of peak value) [169], [170].

The energy of a varistor (E_{MOV}) developed during conduction time (T) must be within the datasheet limits to avoid varistor destruction. E_{MOV} is calculated as in (7-1), where V_{MOV} and I_{MOV} are the voltage and current of the varistor.

$$E_{MOV} = \int_{0}^{T} V_{MOV}(t)\, I_{MOV}(t)\, dt \qquad\qquad (7\text{-}1)$$

7.2.4 Summary of the literature review

To sum up, a series converter is prone to large current and voltage during faults in distribution networks. A protection circuit is required to bypass the series converter as fast as possible when faults occur.

The concept of the protection circuit to be used in distribution networks is similar to transmission networks. The operation of the protection circuit relies on a fast bypass

system that consists of an MOV, thyristors and mechanical bypass breakers. The MOV
protects the IGBTs against immediate overvoltages. The thyristors provide the
required fast response, and their firing signals should be removed after the bypass
breakers are closed.

Investigations are required to examine the performance of the series converter
during faults in MV distribution networks. A protection circuit suitable for MV
distribution networks is required for the series converter.

7.3 Performance of the series converter during an AC fault

During a network fault, an overvoltage or overcurrent is detected and the operation
of the series converter is blocked [141]. Figure 7-4 shows the equivalent circuit of a
blocked two-level VSC converter with a three-phase external fault.
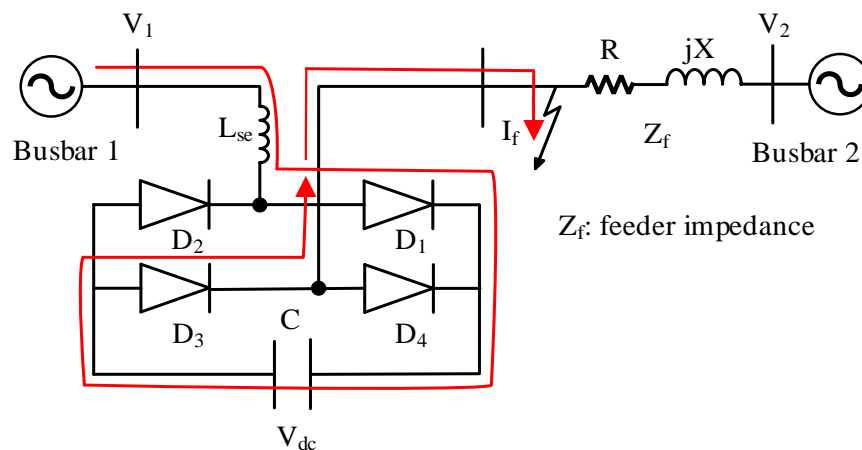
Figure 7-4 Equivalent circuit of the blocked two-level VSC

The path of the fault current I_f is shown in one pair of diodes (D_1 and D_3) over a
half cycle. The fault current depends on the MVA short-circuit level of a distribution
network. For example, an 11 kV, 250 MVA_{sc} distribution network has a prospective
fault current of 13 kA (symmetrical short circuit current); this does not include the
effect of the DC component of the short circuit current. The actual short circuit current
comprises a DC component that increases the peak short circuit current.

The fault current charges the DC-link capacitor(s) through the anti-parallel diodes
of the blocked IGBTs. This imposes a large voltage across the IGBTs and the DC-link
capacitor(s).

The DC voltage can reach almost the peak voltage of the network (i.e., $V_{dc} = V_{1,peak} - I_f X_{se}$), where $X_{se} = 2\pi f\, L_{se}$, and L_{se} is the filter inductance.

7.4 The proposed protection circuit

Figure 7-5 shows the proposed protection circuit of the series converter in an MV distribution network. The main objective of the proposed protection circuit is to bypass and isolate the series converter from the distribution network as fast as possible without affecting the fault path.

The protection circuit consists of antiparallel thyristors T1 and T2, an MOV and switch disconnectors SD1, SD2 and SD3.
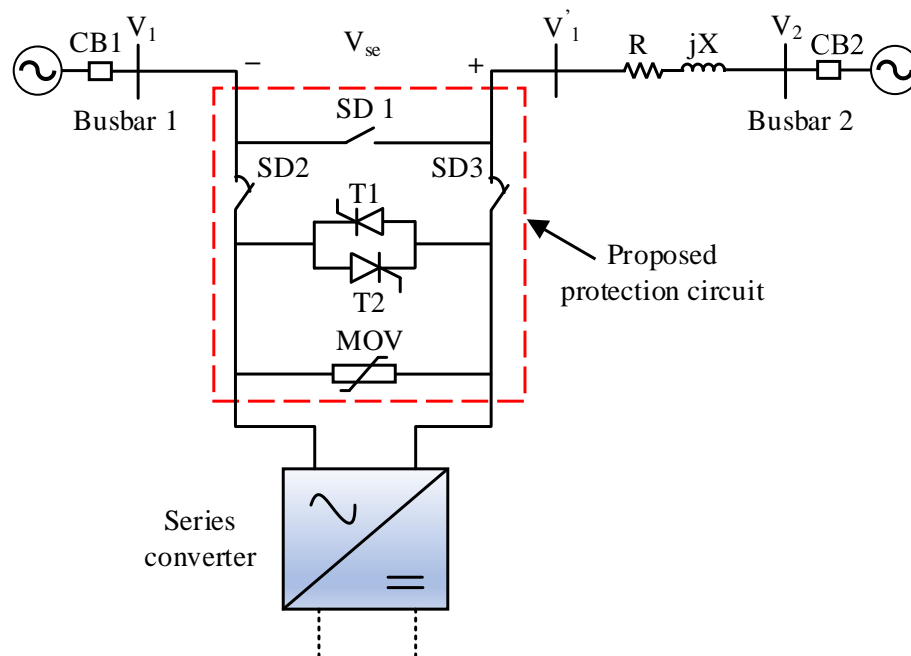
Figure 7-5 The proposed protection circuit for the series converter

Figure 7-6 shows a timing diagram describing the operation of the proposed protection circuit when an external fault occurs on the distribution network in Figure 7-5.
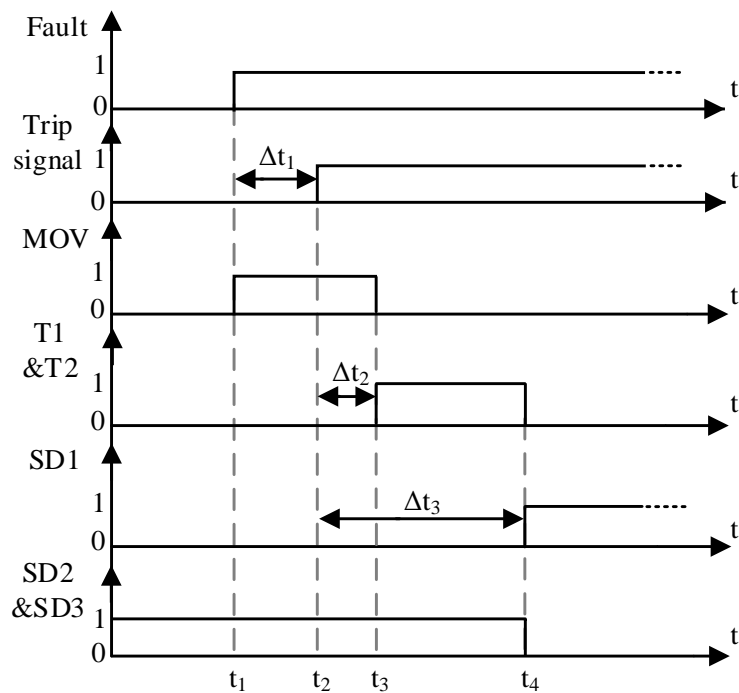
Figure 7-6 Timing diagram of the proposed protection circuit

When a fault occurs on the distribution network (i.e., $t = t_1$), the MOV immediately conducts and limits the voltage across the series converter to a safe limit. The protection of the series converter trips and sends control signals to the thyristors and switch disconnectors at $t = t_2$ following a protection time delay of Δt_1.

At $t = t_3$, thyristors T1 and T2 turn on and bypass the series converter. The fault current passes through T1 and T2, and the MOV comes off. Note that Δt_2 represents the turn-on time of the thyristors.

At $t = t_4$, disconnector SD1 is closed, and disconnectors SD2 and SD3 are open. Δt_3 is the time required for the switch disconnectors to operate. The series converter is now isolated from the network. The firing pulses of the thyristors are removed, and they turn off at the current zero-crossing point.

The operation of SD1, SD2, and SD3 are essential. SD1 provides a path for the fault current and ensures that thyristors T1 and T2 conduct over a short time. SD2 and SD3 ensure complete isolation of the series converter from the network.

Disconnectors SD1, SD2 and SD3, can carry and make current under normal and abnormal conditions. They can break the current under normal conditions only [171].

Note that the proposed protection circuit protects the series converter from the impacts of external faults on the distribution network within few milliseconds (i.e., Δt_1 + Δt_2). However, clearing faults on the distribution network is undertaken by the distribution network protection, which takes approximately 120-150 ms after fault inception [172], [173].

7.5 Selection of metal oxide varistor and thyristor

The series converter of the Improved UPFC was connected to control the power flow of an 11 kV, 5 MVA two-busbar distribution network. The short-circuit level of the network is 250 MVA_{sc}. The maximum output voltage of the series converter $\left|\overline{V}_{se}\right|_{max}$ is 10% (V_{base} = 11 kV).

7.5.1 Metal oxide varistor (MOV)

The Littelfuse MOV (V751BA60) of 750 V continuous rms voltage, 70 kA peak current and 2600 J energy capability was selected and modelled in PSCAD using its datasheet IV characteristics [174].

Figure 7-7 shows the maximum clamping voltage of the Littelfuse MOV (V751BA60). The maximum clamping voltage of the MOV can be obtained corresponding to its peak fault current. For example, the maximum peak clamping voltage of the MOV is 2.76 kV when its peak current is 15 kA.
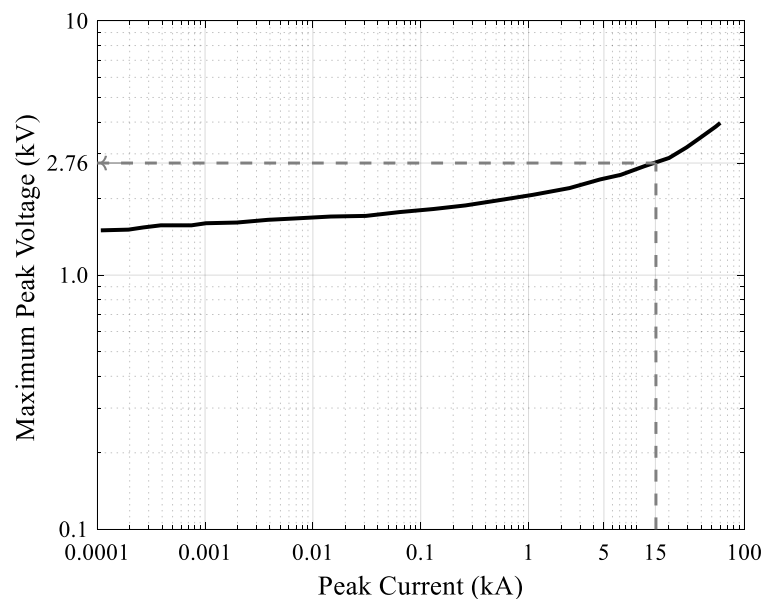
Figure 7-7 Maximum peak clamping voltage of Littelfuse MOV V751BA60 [174]

7.5.2 Thyristor

The thyristors were selected to withstand the prospective fault current during conduction. Thyristors are in conduction until the switch disconnectors operate and the thyristors' current passes the zero-crossing point.

In this application, the switch disconnectors (SD1, SD2 and SD3) were assumed to operate in 20 ms (i.e., $\Delta t_3 = 20$ ms, see Figure 7-6). The ABB (5STP 45N2800) thyristor was selected. Its peak non-repetitive surge current is 75 kA at a junction temperature of 125 °C, and its maximum repetitive peak blocking voltage of 2800 V.

Figure 7-8 shows the surge current versus the number of pulses of the ABB 5STP 45N2800 [175]. The maximum allowable surge current is 49 kA for two half-sine wave pulses (i.e., 20 ms) and 43.5 kA for three half-sine wave pulses with a maximum reapplied reverse voltage of 60% of the rated repetitive peak blocking voltage of the device. Note that a typical fault current has a different waveshape than the half-sine wave. The ABB 5STP 45N2800 switch was selected with a fault current capability margin to account for the different waveshape of the fault current than half-sine (i.e., asymmetrical).
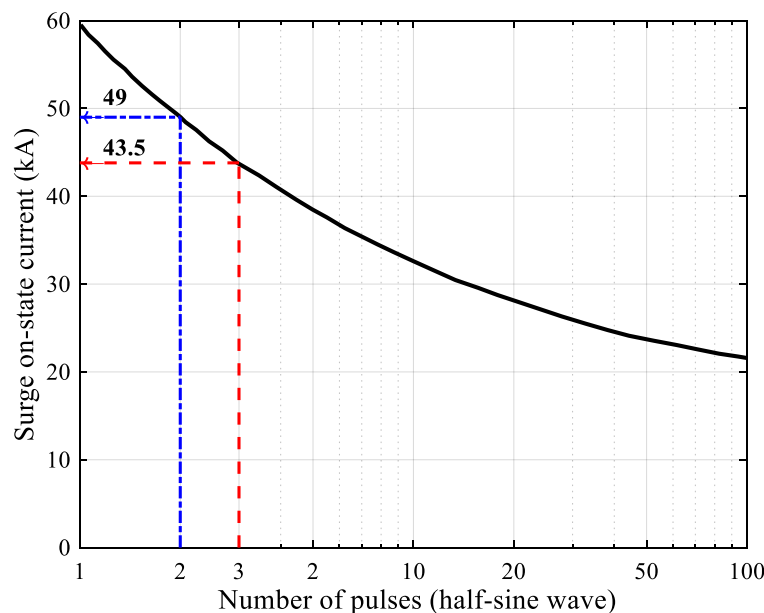
Figure 7-8 Surge on-state current of thyristor vs the number of half-sine wave pulses

Thyristors conduct very quickly [176]. The turn-on time of a thyristor strongly depends on the thyristor gate-current pulse [177]. Assuming a suitable initial gate-current pulse (e.g., the recommended gate-pulse for ABB thyristors [177]), the turn-

on time of a thyristor can have a value of 1 μs to 5 μs [178]. The turn-on time of the
ABB (5STP 45N2800) thyristor was considered 3 μs (i.e., $\Delta t_2 = 3$ μs, see Figure 7-6)
[179].

The detailed design analyses of the thyristors and their auxiliary components (e.g.,
RC-snubber circuit) are out of the scope of this work.

7.6 Simulation results

Figure 7-9 shows a schematic diagram of the Improved UPFC connected to an 11
kV two-busbar distribution network. The converters were modelled in PSCAD using
the switched representation of single-phase three-level NPC VSCs.
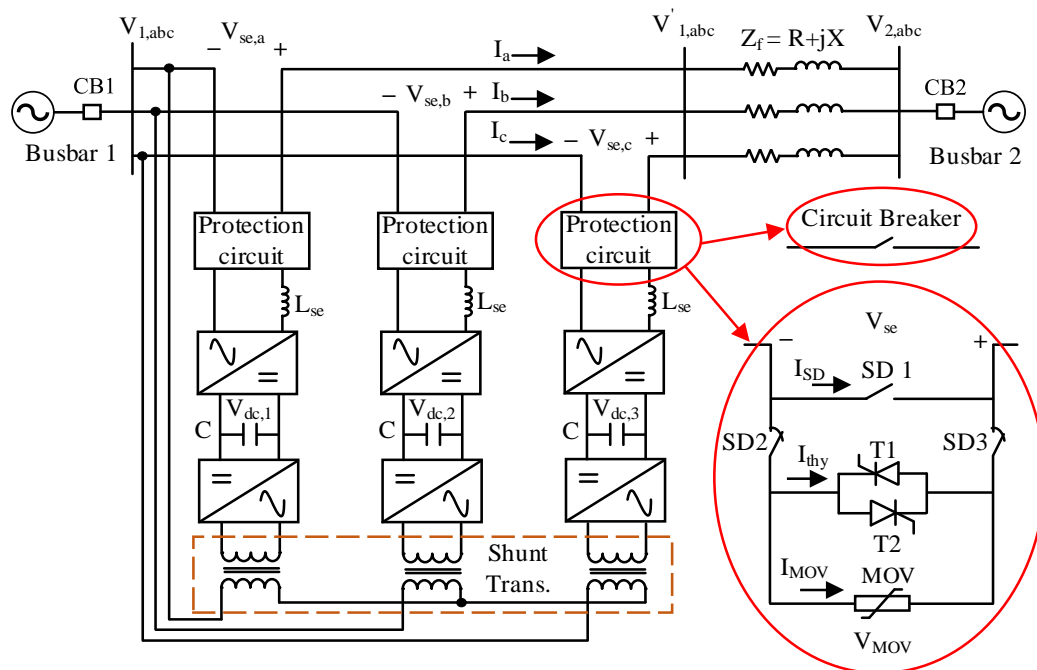
Figure 7-9 Schematic diagram of the simulation test system

133

The parameters of the test system are given in Table 7-1.

Table 7-1 Parameters of the test system

Parameters	Value
System voltage	11 kV, 50 Hz
Short circuit level	250 MVA
Feeder's impedance	R = 0.57 Ω, X = 1.14Ω
Filter inductance, L_{se}	150 μH
DC capacitance, C	12 mF
DC voltage, V_{dc}	1200 V
Shunt transformer	11/1.4 kV, 630 kVA, $Z_{tr,sh}$=6%

The performance of the series converters was examined in the worst-case scenario of a three-phase fault applied at busbar $V_1^{'}$. The resistance between branches (i.e., fault on resistance) equals 0.001 Ω.

The results were obtained considering mechanical circuit breakers across the series converters, then the proposed protection circuit.

7.6.1 Performance of the series converters with mechanical circuit breakers

The performance of the series converters was assessed when mechanical circuit breakers of a 20 ms trip time were connected across their terminals. This aims to examine the voltage, and current immediately applied to the series converters when external faults occur, and it provides the basis for the fast protection circuit.

At t = 0.305 s (i.e., the instant of phase-a peak voltage), a three-phase fault occurred at busbar $V_{1,abc}^{'}$. Figure 7-10 shows the performance of the series converters during the three-phase fault.

Figure 7-10(a) shows the current through the IGBTs of the series converters. After t = 0.305 s, the current increased up to 13 kA, and then it decreased as the DC-link capacitors were charged through the anti-parallel diodes. At t = 0.325 s, the mechanical

circuit breakers isolated the series converters from the AC network. After t = 0.325, the fault current passes through the distribution feeder until either the fault disappears or in case of a permanent fault, the protection of the distribution network will trip the feeder using CB1 and CB2.

Figure 7-10(b) shows the voltages across the DC-link capacitors. The DC-link voltage increased up to 8.5 kV, almost the peak phase-voltage of the connected AC network. Figure 7-10(c) shows the series voltage $V_{se,abc}$.
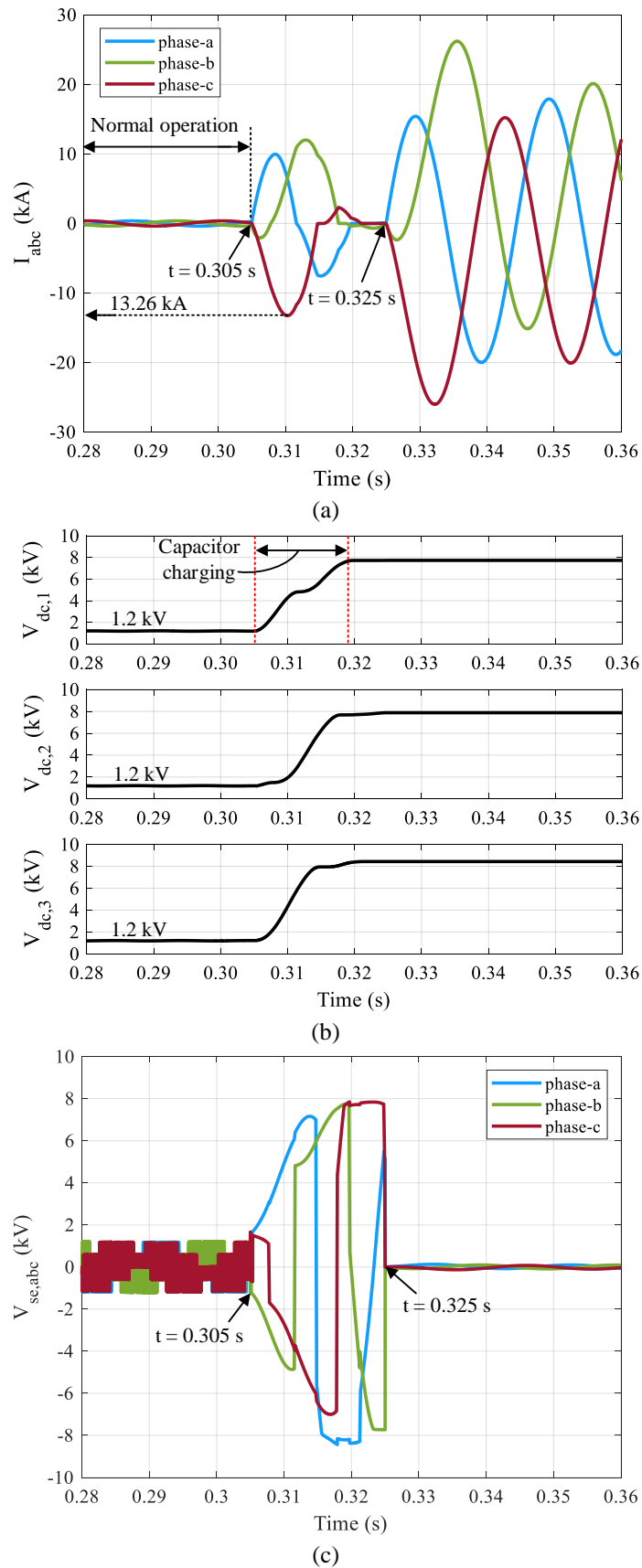
Figure 7-10 Performance of the series converters during external three-phase fault;(a) feeder current, (b) DC-link voltage, and (c) series voltage.

7.6.2 Performance of the series converters with the proposed protection circuit

The performance of the proposed protection circuit was examined when the same three-phase fault was applied at busbar $V'_{1,abc}$ at t = 0.305 s. The protection system of the series converter was assumed to trip after 1 ms (i.e., Δt_1 = 1 ms, see Figure 7-6) [164].

Figures 7-11 shows the voltage at busbar $V'_{1,abc}$. After t = 0.305 s, Voltage $V'_{1,abc}$ dropped close to zero.
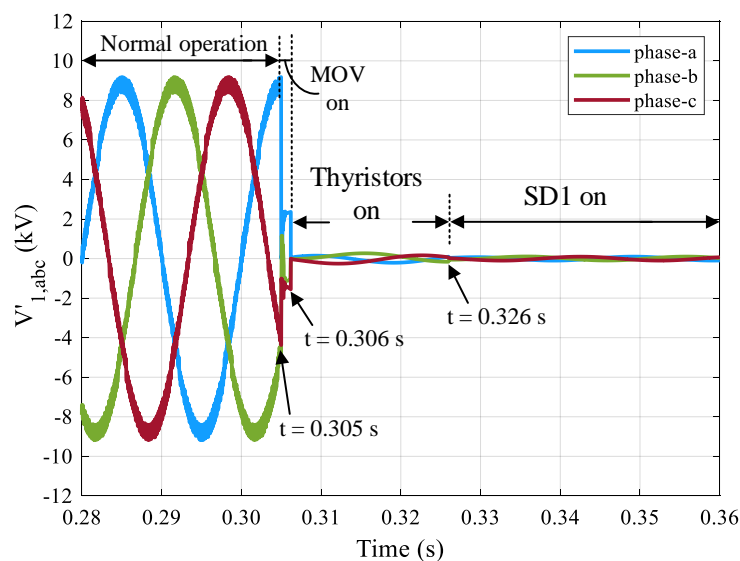
Figure 7-11 Voltage waveform at the faulted busbar

Figure 7-12 shows the voltage across the series converters. When the faults occurred at t = 0.305 s, the voltage across the series converters increased immediately, and the MOVs clamped the voltage to 2.0 kV until the thyristors operated and bypassed the series converters.
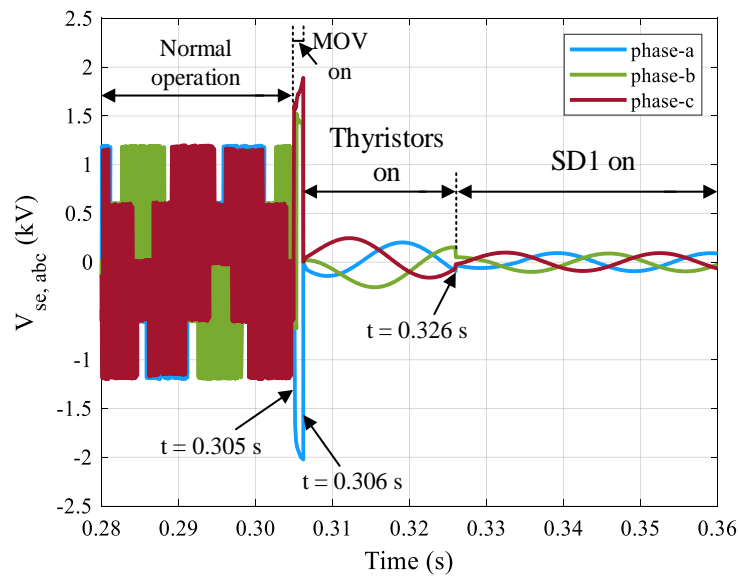
Figure 7-12 Series voltage during external three-phase fault

Figure 7-13 shows the current through the MOVs during conduction. The peak current of the MOVs was up to 0.9 kA.
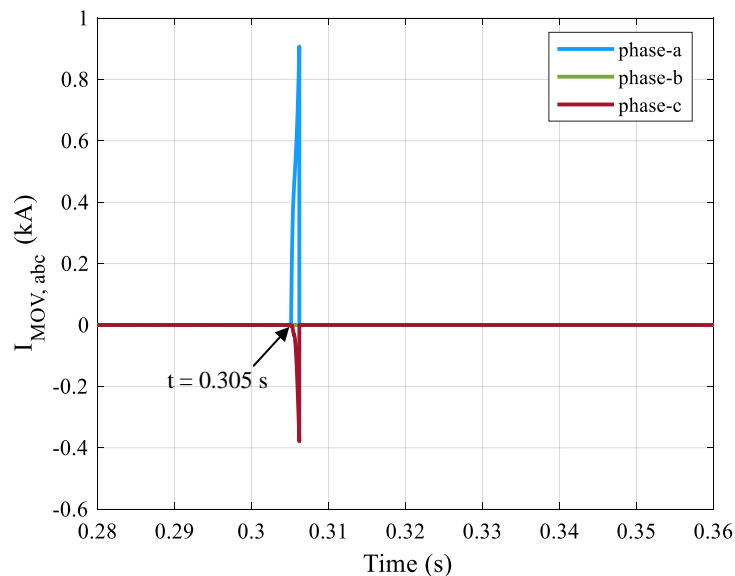
Figure 7-13 Current through MOVs during conduction

Figure 7-14 shows the power dissipated by the MOV during conduction. Phase-a has the highest power dissipation of 1.8 MW. The energy absorbed by the MOV across phase-a was calculated using equation (7-1) and was found to be 1057 J which is less than the datasheet energy dissipation of 2600 J.
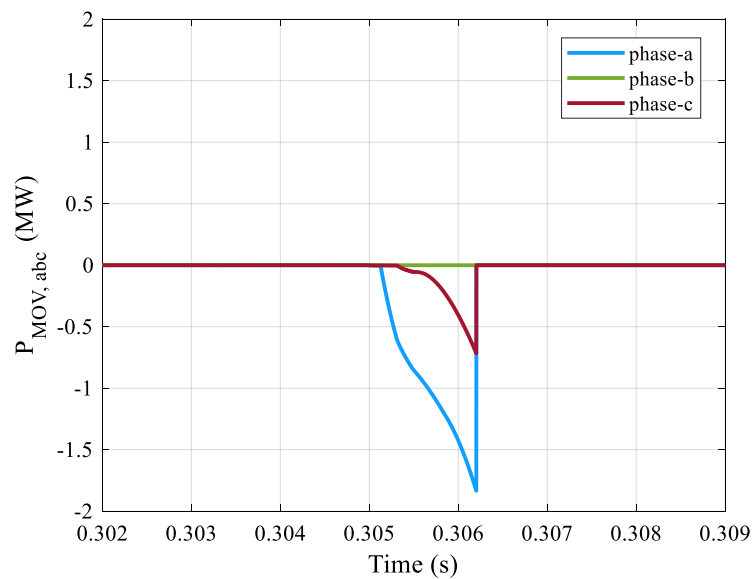
Figure 7-14 MOVs power dissipation during conduction

Figure 7-15 shows the current of the thyristors. At $t \approx 0.306$ s, the thyristors turned on, and the series converters were bypassed. At $t = 0.326$ s, the firing pulses of the thyristors were removed, and they turned off at the current zero-crossing point.

The conduction times of the thyristors on phases a, b, and c are 28 ms, 24 ms and 21 ms. The currents of the thyristors were asymmetrical. The peak currents on phases a, b, and c were 25.6 kA, 24.6 kA, and 20.2 kA. Note that the thyristors can withstand 43.5 kA for three half-sine wave pulses (i.e., 30 ms).
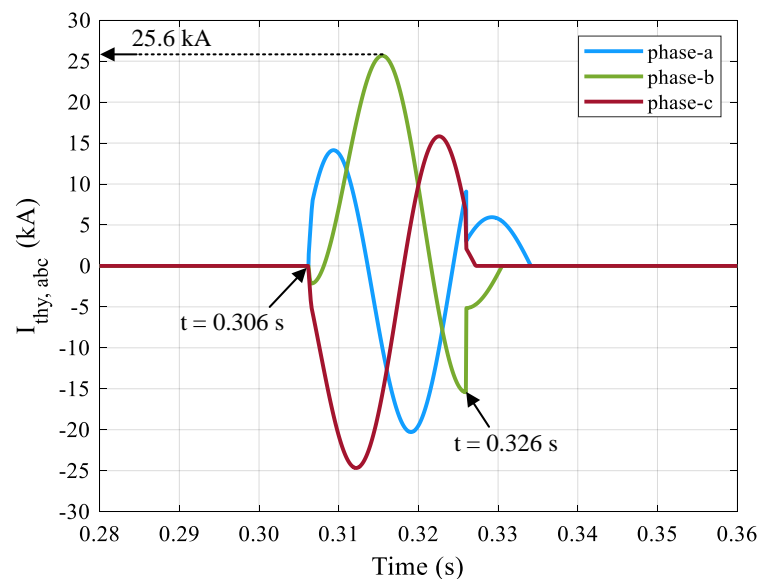
Figure 7-15 Current of the thyristors

At t = 0.326, the switch disconnectors operated (i.e., SD1 closed, SD2 and SD3 opened). Figure 7-16 shows the current through SD1. The current was divided between the thyristors and SD1 until the thyristors turned off at the current zero-crossing points.
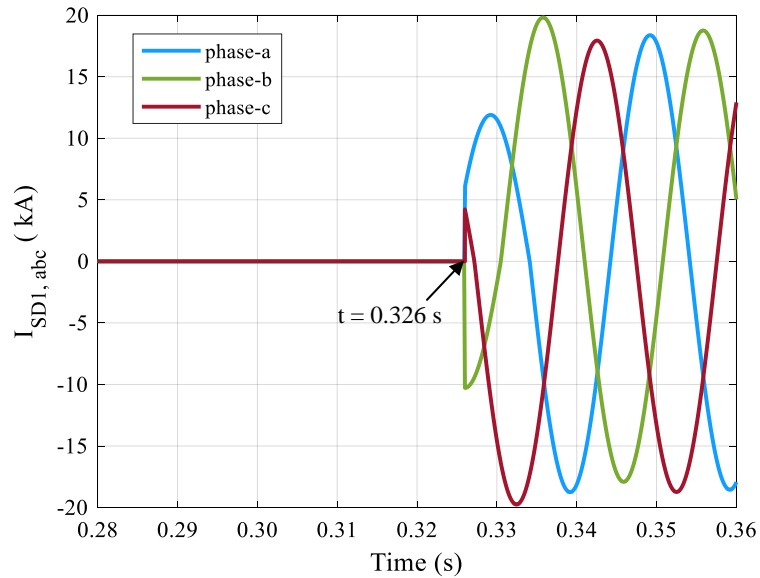
Figure 7-16 Fault current through the switch disconnector SD1

Figure 7-17 shows the current of the distribution feeder. The operation of the protection circuit did not affect the path of the fault current.
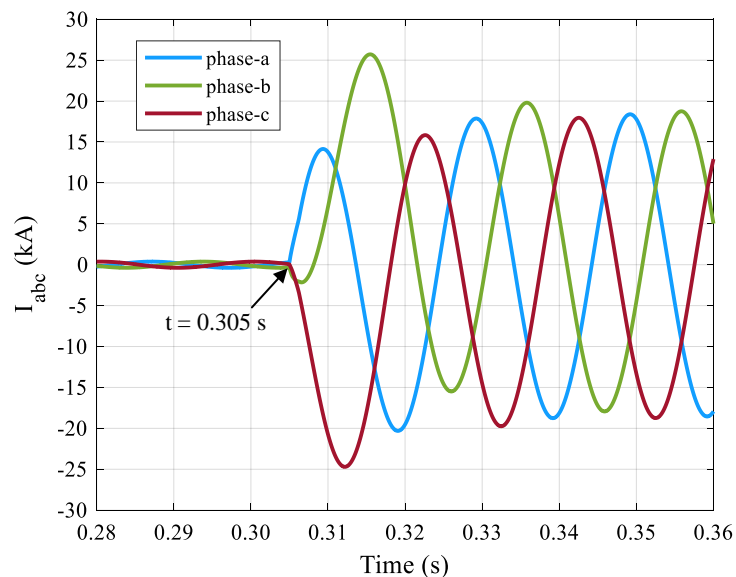
Figure 7-17 Current of the distribution feeder

7.7 Summary

The Improved UPFC is a power electronic device that can control the power flow in MV distribution networks using partially rated converters and with no need for an interfacing series transformer. During external faults, the series converters are prone to overvoltage and overcurrent.

A protection circuit is required across the series converters. The protection circuit must isolate the converters from the connected AC network in order of few milliseconds.

A protection circuit was proposed to protect the series converter. The protection circuit consists of antiparallel thyristors, MOVs and switch disconnectors.

The results showed the effectiveness of the proposed protection circuit to protect the series converter from the impacts of faults on the distribution network without affecting the fault path.

Chapter 8 Conclusions and Suggestions for Future Work

This chapter outlines the main findings and conclusions of the thesis. It also presents suggestions for future work.

8.1 Conclusions

The connection of multiple Distributed Generators (DGs) to distribution networks may cause operational challenges, such as voltage rise and network congestion.

Soft Open Points (SOPs) are power electronic devices installed in distribution networks to control the power flow, maintain the voltages and currents within limits, improve the utilisation of existing assets, and support the growth of Low Carbon Technologies (LCTs).

There are two types of SOPs; 1) fully-rated back-to-back (B2B) SOPs and 2) partially rated SOPs.

Fully rated B2B SOPs can be implemented using two or multiple Voltage Source Converters (VSCs) that share a common DC-link (i.e., a two-terminal SOP and a multi-terminal SOP). A multi-terminal SOP offers more benefits than a two-terminal SOP by realising mutual power exchange among multiple circuits.

The benefits of using a multi-terminal fully-rated B2B SOP in a medium voltage (MV) distribution network were investigated. The results showed that the multi-terminal SOP enabled the distribution network to host additional levels of DGs more than a two-terminal SOP and reduced the energy losses. Despite the benefits of using the multi-terminal fully-rated B2B SOPs, they are expensive and have not yet been widely deployed in MV distribution networks.

Partially rated SOPs (i.e., SOPs with a series connection) is an alternative solution to control power flow. Several topologies of SOPs with a series connection of VSCs were investigated. This includes the conventional Unified Power Flow Controller (UPFC), the Transformer-less UPFC, and the Improved UPFC. The results showed that SOPs with a series connection could provide power flow control and voltage regulation similar to that of B2B fully-rated SOPs with lower rating converters and size.

The main conclusions of the thesis are summarised in the following sections:

8.1.1 Benefits of multi-terminal fully-rated back-to-back Soft Open Points

Multi-terminal fully-rated B2B SOPSs are able to control active and reactive power in the four-quadrant of operation by controlling the magnitude and phase angle of the terminal voltages.

A 34-bus distribution network was used to quantify the benefits of the multi-terminal SOP. Then a comparison of the distribution network with a three-terminal SOP, a two-terminal SOP and no SOPs was undertaken. The results showed the benefits of the three-terminal SOP over the two-terminal SOP in terms of the penetration levels of Distributed Generators and the energy losses.

Without an SOP, the distribution network managed to host a 50% penetration level of DGs without violating the voltage constraints. However, a further increase of DGs beyond the 50% penetration level resulted in overvoltages.

A three-terminal SOP of 6 MVA total capacity enabled the distribution network to host a DG penetration level of 90%, increasing 20% more than the two-terminal SOP of 4 MVA and reduced the energy losses. The three-terminal SOP also achieved a higher DG penetration level and lower energy losses than the two-terminal SOP when both have the same total capacity of 6 MVA (e.g., the three-terminal SOP achieved a DG penetration level of 90% and the two-terminal SOP 80%).

Despite the benefits of using fully-rated B2B SOPs, they have not been widely deployed in MV distribution networks as they are expensive. The cost and size of the fully-rated converters and the interfacing transformers account for the lack of applications of fully-rated B2B VSCs in MV distribution networks.

The series connection of VSCs is an alternative solution to provide power flow control in MV distribution networks similar to the well-established UPFC. The main advantage of the series connection of VSCs is partially rated converters.

8.1.2 Performance of a Transformer-less UPFC in medium voltage distribution networks

A Transformer-less UPFC can provide independent control of active and reactive power using series and shunt converters that are not connected to a common DC-link. The main advantage of the Transformer-less UPFC over a conventional UPFC is the

complete removal of the interfacing transformers, significantly reducing its size and cost.

The operation of a Transformer-less UPFC relies on controlling the series and shunt converters together such that both converters exchange only reactive power with the AC network. The series converter injects controllable voltage that is responsible for achieving the target power flow. The shunt converter ensures zero active power exchange between each of the series and shunt converters and the connected AC network.

The power rating of the series converter depends on the magnitude of the series voltage. The series voltage is advantageously small in an MV distribution network compared to a transmission network due to the smaller impedance of distribution networks.

The shunt converter has full network voltage applied across its terminals. The power rating of the shunt converter depends on the magnitude of the shunt current.

The analysis showed that a Transformer-less UPFC could provide active power control using a partially rated converter. However, it has limited reactive power control as this requires a large shunt current.

The control scheme of a Transformer-less UPFC is quite complex. The series and shunt converters of the Transformer-less UPFC regulate the floating DC bus voltages of the series and shunt converters. In addition, the series converter controls the series voltage phasor, and the shunt converter controls the shunt current phasor. The control scheme requires information on the receiving-end voltage and the feeder's impedance.

The limitation of a Transformer-less UPFC to control reactive power makes it an unattractive power flow controller in MV distribution networks.

8.1.3 An Improved topology of a UPFC for a distribution circuit

An Improved UPFC was proposed to control power flow using partially rated converters and without an interfacing series transformer that reduces the size and cost of the device.

The Improved UPFC consists of series and shunt VSCs converters. The series connection of the Improved UPFC is performed using three separate single-phase converters directly connected in series to an MV distribution network. The Improved

UPFC has three separate DC-link buses. The shunt converters are connected B2B to the series converters, and they are interfaced to an AC network using a three-phase interfacing shunt transformer.

The single-phase converters of the Improved UPFC were built using a three-level neutral-point-clamped (NPC) topology. The three-level topology reduces the blocking voltage of the IGBTs and provides AC voltage with lower harmonic distortion compared to a two-level topology. It has also been used for MV motor drive applications.

The removal of the series transformer is also adopted in the Soft Power Bridge (SPB) device being trialled by the UK Power Networks project entitled "Active Response to Distribution Network Constraints", indicating business benefits of removing this part.

The Improved UPFC was controlled in the power flow control mode using the well-established current control loops. The series converters operated in the P-Q control scheme and regulated the active and reactive power flow of a distribution feeder. The shunt converters operated in the V_{dc}-Q control scheme and maintained constant DC voltages.

The Improved UPFC model demonstrated the capability of the series converters to control the power flow of a 5 MVA distribution feeder using partially rated series converters of 630 kVA. Further analysis is required to perform a cost-benefit analysis of using single-phase and three-phase shunt converters.

8.1.4 Performance of the series converter during faults on the medium voltage distribution network

SOPs with a series connection are vulnerable to immediate overvoltages and overcurrents when faults occur on the distribution network. The overvoltages and overcurrents can destroy the IGBTs of the series converter and overcharge the DC-link capacitor. Therefore, a protection circuit across the series converter is essential.

A protection circuit was proposed to protect the series converter during external faults. The protection circuit consists of thyristors (i.e., provide fast-bypass action), metal oxide varistors (MOVs) (i.e., suppress overvoltages) and switch disconnectors (i.e., isolate the series converter from the AC network).

146

The main elements of the proposed protection circuit were selected to ensure that the protection circuit operates properly during external faults. The Littelfuse MOV was selected to suppress the overvoltages. The thyristors were chosen to provide fast-bypass action until the switch disconnectors operate. Fast switch disconnectors were used so that the thyristors operate over a short period. Thus, the thyristors do not need cooling equipment.

The performance of the series converters was examined in the worst-case scenario of a three-phase fault applied near to the series converter. The results were obtained considering mechanical circuit breakers across the series converters, then the proposed protection circuit.

The results showed that when a mechanical circuit breaker with a trip time of 20 ms was used to protect the series converter, large voltage and current (e.g., 8.5 kV and 13 kA) were applied to the IGBTs.

The proposed protection circuit managed to bypass the series converter within 1.003 ms (i.e., 1 ms time delay of the series converter protection system and 3 μs for thyristors to turn on). The varistor clamped the voltage to 2.0 kV until the thyristors turned on. The switch disconnectors completely isolated the series converter from the network without affecting the fault path.

8.2 Suggestions for future work

The work in this thesis has focused on managing power flow in distribution networks with multiple Distributed Generators and considering the balanced operation of the distribution network. It also examined the performance of SOPs at the system level. Suggestions for future work are summarised as follows.

8.2.1 Optimal operation of partially rated Soft Open Points

Further analysis is required to develop a generic power injection model that considers the power injections of partially rated SOPs. Hence, partially rated SOPs can be incorporated into existing power flow platforms. The model should consider the internal power losses of the SOPs.

An optimisation problem can be formulated to achieve control objective(s) (e.g., Energy Loss Minimisation). By solving this optimisation problem, the optimal active and reactive power setpoints of partially rated Soft Open Points can be determined, which ensure optimal operation of distribution networks.

8.2.2 Performance of the Improved Unified Power Flow Controller during faults on a medium voltage distribution network

The Improved Unified Power Flow Controller consists of series and shunt Voltage Source Converters. During faults, the series converter's protection circuit operates and bypasses the series converter in a few milliseconds.

Further analysis is required to investigate the performance of the shunt converter during external faults. For example, the control strategy of the shunt converter should have a fault-ride-through capability. This enables the shunt converter to provide reactive power support unless there is a material disturbance on the distribution network. This should be conducted using benchmark distribution networks.

8.2.3 Regulating the DC-link voltage of the Improved Unified Power Flow Controller during faults on a medium voltage distribution network

The Improved Unified Power Flow Controller (UPFC) consists of series and shunt Voltage Source Converters connected back-to-back through three separate common DC-link buses. When faults occur on the distribution network, overvoltages occur across the DC-link buses. These overvoltages affect the power ratings of the IGBTs, and they need to be kept as low as possible.

Further analysis is required to investigate the use of DC voltage regulators to suppress the overvoltages that arises during faults on the distribution networks.

8.2.4 Comparison between conventional UPFC, Improved UPFC and Transformer-less UPFC in MV distribution networks

Power electronic devices are required to control power flow in MV distribution networks. The performance of the conventional UPFC, the Improved UPFC and the Transformer-less UPFC was investigated when connected to a distribution feeder of a low X/R ratio. Each topology has its pros and cons.

Further analysis is required to compare the cost-benefit of these topologies and provide recommendations to the DNOs. The comparison might rely on finding the design parameters of the three topologies when connected to a distribution network— for example, calculating the number of IGBTs, the required DC voltage, the current and voltage ratings of IGBTs, the DC capacitance and the AC inductors, size and weight.

References

[1] "Causes of climate change", https://ec.europa.eu/clima/climate-change/causes-climate-change_en, accessed Oct. 22, 2021.

[2] "Global Warming vs. Climate Change | Resources – Climate Change: Vital Signs of the Planet", https://climate.nasa.gov/resources/global-warming-vs-climate-change, accessed Oct. 22, 2021.

[3] "The Effects of Climate Change", https://climate.nasa.gov/effects, accessed Oct. 22, 2021.

[4] "Global Greenhouse Gas Emissions Data", https://www.epa.gov/ghgemissions/global-greenhouse-gas-emissions-data , accessed Oct. 22, 2021.

[5] "Paris Agreement| Climate Action", https://ec.europa.eu/clima/policies/ international/negotiations/paris_en, accessed Sep. 10, 2021.

[6] Stewart, H., " Review of GB energy system operation", Ofgem, Jan. 2021.

[7] Mackres, E., "6 Lessons on Energy Decarbonization from Countries Leading the Way", https://www.wri.org/insights/6-lessons-energy-decarbonization-countries-leading-way, accessed Oct. 23, 2021.

[8] "What is decarbonisation?", https://www.drax.com/carbon-capture/what-is-decarbonisation, accessed Oct. 24, 2021.

[9] "Ofgem decarbonisation programme action plan", Ofgem, Feb. 2020.

[10] B. Kroposki *et al.*, "Autonomous Energy Grids: Controlling the Future Grid with Large Amounts of Distributed Energy Resources," IEEE Power Energy Mag., vol. 18, no. 6, pp. 37–46, Nov. 2020, doi: 10.1109/MPE.2020.3014540.

[11] "Renewable capacity highlights", IRENA, Mar. 2021.

[12] P. Johansson, M. Vendel, and C. Nuur, "Integrating distributed energy resources in electricity distribution systems: An explorative study of challenges facing DSOs in Sweden," Utilities Policy, vol. 67, Dec. 2020, doi: 10.1016/J.JUP.2020.101117.

[13] "Operability of Highly Renewable Electricity Systems", National Infrastrucutre Commission, Feb. 2021.

[14] I. Talavera *et al.*, "Flexible Reactive Power Exchange Between Medium and High Voltage Networks: Case study, " 23rd International Conference on Electricity Distribution, CIRED, Lyon 2015.

[15] P. Schäfer, H. Vennegeerts, S. Krahl, and A. Moser, "Derivation of Recommendations for the Future Reactive Power Exchange at the Interface between Distribution and Transmission Grid," 23rd International Conference on Electricity Distribution, CIRED, Lyon 2015.

[16] "Carbon Plan", HM Government, Nov. 2021.

[17] "UK becomes first major economy to pass net zero emissions law", https://www.gov.uk/government/news/uk-becomes-first-major-economy-to-pass-net-zero-emissions-law, accessed Sep. 10, 2021.

[18] "Net Zero Strategy: Build Back Greener", HM Government, October 2021.

[19] "UK energy in brief 2020", www.gov.uk/government/statistics/uk-energy-in-brief-2020, accessed Oct. 19, 2021.

[20] "Operability Strategy Report 2021", National Grid ESO, Dec. 2020.

[21] "Summer Outlook Report 2018", National Grid ESO, April 2018.

[22] "Ofgem Innovation Vision 2021 – 2025", Ofgem, May 2021.

[23] "The network innovation review: our consultation proposals", Ofgem, Dec. 2016

[24] "Future medium voltage distribution applications of power electronics- CIGRE-UK", https://cigre.org.uk/uk-news/future-medium-voltage-distribution-applications-of-power-electronics, accessed Aug. 13, 2020.

[25] "Electricity NIC Initial Screening Submission 2019 - 'DC Share' (WPD) | Ofgem", https://www.ofgem.gov.uk/publications/electricity-nic-initial-screening-submission-2019-dc-share-wpd, accessed Oct. 24, 2021.

[26] "Network Innovation Competition 2017- 'LV Engine' ", https://www.ofgem.gov.uk/system/files/docs/2017/11/lv_engine_2017_nic_full_resubmission_-_clean_redacted.pdf, accessed Nov. 28, 2019.

[27] "UK Power Networks Innovation - Active Response",

https://innovation.ukpowernetworks.co.uk/projects/active-response, accessed Oct. 24, 2021.

[28]   "Grid intertie Converter with extended STATCOM functionality", ABB Advanced Power Electronics.

[29]   G. Bathurst, G. Hwang, and L. Tejwani, "MVDC-the new technology for distribution networks," 11th IET International Conference on AC and DC Power Transmission, vol. Feb. 2015, doi: 10.1049/CP.2015.0037.

[30]   Y. Liu, X. Cao, and M. Fu, "The Upgrading Renovation of an Existing XLPE Cable Circuit by Conversion of AC Line to DC Operation," IEEE Trans. Power Deliv., vol. 32, no. 3, pp. 1321–1328, Jun. 2017, doi: 10.1109/TPWRD.2015.2496178.

[31]   B. Ruben, A. Cross, D. Strickland, M. Aten, and R. Ferris, "Meshing radial networks at 11kV," IEEE PES Innov. Smart Grid Technol. Conf. Eur., 2011, doi: 10.1109/ISGTEUROPE.2011.6162691.

[32]   C. L. Masters, "Voltage rise: the big issue when connecting embedded generation to long 11 kV overhead lines," Power Eng. J., vol. 16, no. 1, pp. 5–12, 2002, doi: 10.1049/pe:20020101.

[33]   A. N. M. M. Haque, M. Nijhuis, G. Ye, P. H. Nguyen, F. W. Bliek, and J. G. Slootweg, "Integrating Direct and Indirect Load Control for Congestion Management in LV Networks," IEEE Trans. Smart Grid, vol. 10, no. 1, pp. 741–751, Jan. 2019, doi: 10.1109/TSG.2017.2751743.

[34]   M. E. Baran and F. F. Wu, "Network reconfiguration in distribution systems for loss reduction and load balancing," Power Deliv. IEEE Trans., vol. 4, no. 2, pp. 1401–1407, 1989, doi: 10.1109/61.25627.

[35]   V. Levi, M. Kay, and I. Povey, "Reverse power flow capability of tap-changers," 18th International Conference and Exhibition on Electricity Distribution, CIRED, vol. 4, no. 2005–11034, pp. 213–217, 2005, doi: 10.1049/CP:20051241.

[36]   S. Georgiopoulos, C. Marantes, and D. Openshaw, "Flexible plug and play low carbon networks enabling the integration of renewable energy," CIRED Workshop, Integration of Renewables into Distribution Grid, no. 86, pp. 1–4, 2012, doi: 10.1049/cp.2012.0746.

[37] Q. Wang, N. Zhou, and L. Ye, "Fault analysis for distribution networks with current-controlled three-phase inverter-interfaced distributed generators," IEEE Trans. Power Deliv., vol. 30, no. 3, pp. 1532–1542, Jun. 2015, doi: 10.1109/TPWRD.2015.2407883.

[38] D. S. Kumar, D. Srinivasan, and T. Reindl, "A Fast and Scalable Protection Scheme for Distribution Networks with Distributed Generation," IEEE Trans. Power Deliv., vol. 31, no. 1, pp. 67–75, Feb. 2016, doi: 10.1109/TPWRD.2015.2464107.

[39] E. J. Coster, J. M. A. Myrzik, B. Kruimer, and W. L. Kling, "Integration Issues of Distributed Generation in Distribution Grids," Proceedings of the IEEE, vol. 99, no. 1, pp. 28–39, Jan. 2011, doi: 10.1109/JPROC.2010.2052776.

[40] C. Deckmyn, T. L. Vandoorn, B. Meersman, L. Gevaert, and J. Desmet, "A coordinated voltage control strategy for on-load tap changing transformers with the utilisation of distributed generators", IEEE International Energy Conference (ENERGYCON), Leuven, Belgium, July 2016, doi:10.1109/ENERGYCON.2016.7514093.

[41] L. Chin Koon, Abdul Aziz Abdul Majid, Tenaga Nasional Berhad, "Technical Issues on Distributed Generation (DG) Connection and Guidlines," 19th International Conference on Electricity Distribution, CIRED, Vienna, May 2007.

[42] S. K. Salman and I. M. Rida, "ANN-based AVC relay for voltage control of distribution network with and without embedded generation," DRPT 2000 - Int. Conf. Electr. Util. Deregul. Restruct. Power Technol. Proc., pp. 263–267, 2000, doi: 10.1109/DRPT.2000.855674.

[43] Z. Tang, D. J. Hill, and T. Liu, "Distributed Coordinated Reactive Power Control for Voltage Regulation in Distribution Networks," IEEE Trans. Smart Grid, vol. 12, no. 1, pp. 312–323, Jan. 2021, doi: 10.1109/TSG.2020.3018633.

[44] N. Mahmud and A. Zahedi, "Review of control strategies for voltage regulation of the smart distribution network with high penetration of renewable distributed generation," Renew. Sustain. Energy Rev., vol. 64, pp. 582–595, Oct. 2016, doi: 10.1016/J.RSER.2016.06.030.

[45] J. Kondoh, H. Aki, H. Yamaguchi, A. Murata, and I. Ishii, "Study on voltage regulation methods for distribution systems with dispersed generators," Electr. Eng. Japan, vol. 154, no. 4, pp. 16–23, Mar. 2006, doi: 10.1002/EEJ.20246.

[46] A. Edris, A. S. Mehraban, M. Rahman, L. Gyugyi, S. Arabi, and T. Reitman, "Controlling the flow of real and reactive power," IEEE Comput. Appl. Power, vol. 11, no. 1, pp. 20–25, Jan. 1998, doi: 10.1109/67.648493.

[47] J. Barr and R. Majumder, "Integration of distributed generation in the Volt/VAR management system for active distribution networks," IEEE Trans. Smart Grid, vol. 6, no. 2, pp. 576–586, Mar. 2015, doi: 10.1109/TSG.2014.2363051.

[48] L. Gyugyi, R. A. Otto, and T. H. Putman, "Principles and applications of static, thyristor-controlled shunt compensators," IEEE Trans. Power Appar. Syst., vol. PAS-97, no. 5, pp. 1935–1945, 1978, doi: 10.1109/TPAS.1978.354690.

[49] L. Gyugyi, C. D. Schauder, and K. K. Sen, "Static synchronous series compensator: a solid-state approach to the series compensation of transmission lines," IEEE Trans. Power Deliv., vol. 12, no. 1, pp. 406–417, 1997, doi: 10.1109/61.568265.

[50] P. Kou, D. Liang, R. Gao, C. Yang, and L. Gao, "Optimal Placement and Sizing of Reactive Power Sources in Active Distribution Networks: A Model Predictive Control Approach," IEEE Trans. Sustain. Energy, vol. 12, no. 2, pp. 966–977, Apr. 2021, doi: 10.1109/TSTE.2020.3028118.

[51] A. Noori, Y. Zhang, N. Nouri, and M. Hajivand, "Multi-Objective Optimal Placement and Sizing of Distribution Static Compensator in Radial Distribution Networks with Variable Residential, Commercial and Industrial Demands Considering Reliability," IEEE Access, vol. 9, pp. 46911–46926, 2021, doi: 10.1109/ACCESS.2021.3065883.

[52] O. F. B. Angarita, R. C. Leborgne, D. D. S. Gazzana, and C. Bortolosso, "Power loss and voltage variation in distribution systems with optimal allocation of distributed generation," IEEE PES Innov. Smart Grid Technol. Lat. Am. ISGT LATAM, pp. 214–218, Oct. 2015, doi: 10.1109/ISGT-LA.2015.7381156.

[53] "DER Technical Requirements v2.5.1.", National Grid ESO, UK Power

Networks,https://www.nationalgrid.com/sites/default/files/documents/DER_T echnical_Requirements_v2.5.1.pdf, accessed Jul. 19, 2021.

[54]   A. Ellis *et al.*, "Reactive Power Performance Requirements for Wind and Solar Plants," IEEE Power and Energy Society General Meeting, San Diego, CA, USA, July 2012, doi: 10.1109/PESGM.2012.6345568.

[55]   R. K. Varma, V. Khadkikar, and R. Seethapathy, "Nighttime application of PV solar farm as STATCOM to regulate grid voltage," IEEE Trans. Energy Convers., vol. 24, no. 4, pp. 983–985, Dec. 2009, doi: 10.1109/TEC.2009.2031814.

[56]   C. J. Zhan *et al.*, "Two electrical models of the lead-acid battery used in a dynamic voltage restorer," IEE Proc. Commun., vol. 150, no. 2, pp. 175–182, Mar. 2003, doi: 10.1049/IP-GTD:20030124.

[57]   A. Pashaie, B. Zahawi, and D. Giaouris, "Distributed Static Series Compensation for distribution network line voltage profile improvement," IEEE PES Innov. Smart Grid Technol. Conf. Eur., 2011, doi: 10.1109/ISGTEUROPE.2011.6162823.

[58]   H. Akagi, S. Inoue, and T. Yoshii, "Control and performance of a transformerless cascade PWM STATCOM with star configuration," IEEE Trans. Ind. Appl., vol. 43, no. 4, pp. 1041–1049, Jul. 2007, doi: 10.1109/TIA.2007.900487.

[59]   Y. Koyama, Y. Nakazawa, H. Mochikawa, A. Kuzumaki, K. Sano, and N. Okada, "A Transformerless 6.6-kV STATCOM Based on a Hybrid Cascade Multilevel Converter Using SiC Devices," IEEE Transactions on Power Electronics, Sep. 2018, vol. 33, no. 9, pp. 7411–7423, doi: 10.1109/TPEL.2017.2770143.

[60]   L. Bird, J. Cochran, and X. Wang, "Wind and Solar Energy Curtailment: Experience and Practices in the United States," NREL, Mar.2014.

[61]   K. Jacobsen, H. ; Schröder, S. Thorsten, H. Klinge Jacobsen, and S. T. Schröder, "Curtailment of renewable generation: Economic optimality and incentives," Energy Policy, 2012, vol. 49, issue C, 663-675, doi: 10.1016/j.enpol.2012.07.004.

[62] C. Marantes, S. Georgiopoulos, and G. Manhangwe, "Flexible plug and play low carbon networks: quadrature booster trial at 33 KV," 22nd International Conference and Exhibition on Electricity Distribution, CIRED, 2013, pp. 0789–0789, doi: 10.1049/cp.2013.0929.

[63] David Neilson, "Flexible Connections and Principles Of Access Policy," SP Energy Networks, Oct. 2020.

[64] ENA, "Distributed Generation Connection Guides," G98 for multiple premises, November, 2011.

[65] Q. Zhou, "Generation curtailment to manage voltage constraints in distribution networks," IET Gener. Transm. Distrib., vol. 1, no. 2, pp. 492–498, 2007, doi: 10.1049/iet-gtd.

[66] S. Georgiopoulos, C. Marantes, and D. Openshaw, "Flexible plug and play low carbon networks enabling the integration of renewable energy," Workshop: Integration of Renewables into the Distribution Grid, CIRED, 2012, pp. 86–86, doi: 10.1049/cp.2012.0746.

[67] M. H. Shariatkhah and M. R. Haghifam, "Using feeder reconfiguration for congestion management of smart distribution network with high DG penetration," *C*IRED Workshop: Integration of Renewables into the Distribution Grid, pp. 316–316, Sep. 2012, doi: 10.1049/CP.2012.0863.

[68] Q. Zhou, D. Shirmohammadi, and W. H. E. Liu, "Distribution feeder reconfiguration for service restoration and load balancing," IEEE Trans. Power Syst., vol. 12, no. 2, pp. 724–729, 1997, doi: 10.1109/59.589664.

[69] R. S. Rao, K. Ravindra, K. Satish, and S. V. L. Narasimham, "Power Loss Minimization in Distribution System Using Network Reconfiguration in the Presence of Distributed Generation," IEEE Trans. Power Syst., vol. 28, no. 1, pp. 1–9, 2012, doi: 10.1109/TPWRS.2012.2197227.

[70] N. C. Koutsoukis, Di. O. Siagkas, P. S. Georgilakis, and N. D. Hatziargyriou, "Online Reconfiguration of Active Distribution Networks for Maximum Integration of Distributed Generation," IEEE Trans. Autom. Sci. Eng., vol. 14, no. 2, pp. 437–448, 2017, doi: 10.1109/TASE.2016.2628091.

[71] M. R. Dorostkar-Ghamsari, M. Fotuhi-Firuzabad, M. Lehtonen, and A.

Safdarian, "Value of Distribution Network Reconfiguration in Presence of Renewable Energy Resources," IEEE Trans. Power Syst., vol. 31, no. 3, pp. 1879–1888, 2016, doi: 10.1109/TPWRS.2015.2457954.

[72]   E. López, H. Opazo, L. García, and P. Bastard, "Online Reconfiguration Considering Variability Demand: Applications to Real Networks," *IEEE Transactions on Power Systems,* vol. 19, issue: 1, pp. 549–553, 2004.

[73]   A. Zidan, "Network Reconfiguration in Balanced Distribution Renewable Resources Generation," IEEE Power Energy Soc. Gen. Meet., pp. 1–8, 2012, doi: 10.1109/PESGM.2012.6345160.

[74]   K. S. Fuad, H. Hafezi, K. Kauhaniemi, and H. Laaksonen, "Soft Open Point in Distribution Networks," IEEE Access, vol. 8, pp. 210550–210565, 2020, doi: 10.1109/ACCESS.2020.3039552.

[75]   P. Favre-Perrod, "Soft-open points for medium voltage networks-A Case study," 25th International Conference on Electricity Distribution, CIRED, June 2019.

[76]   H. Hafezi and H. Laaksonen, "Autonomous soft open point control for active distribution network voltage level management," IEEE Milan PowerTech, PowerTech 2019, Jun. 2019, doi: 10.1109/PTC.2019.8810735.

[77]   Q. Qi, J. Wu, and C. Long, "Multi-objective operation optimization of an electrical distribution network with soft open point," Appl. Energy, vol. 208, pp. 734–744, Dec. 2017, doi: 10.1016/J.APENERGY.2017.09.075.

[78]   C. Lou, J. Yang, T. Li, and E. Vega-Fuentes, "New phase-changing soft open point and impacts on optimising unbalanced power distribution networks," IET Generation, Transmission & Distribution, Sep. 2020 doi: 10.1049/iet-gtd.2019.1660.

[79]   F. Sun, J. Ma, M. Yu, and W. Wei, "Optimized Two-Time Scale Robust Dispatching Method for the Multi-Terminal Soft Open Point in Unbalanced Active Distribution Networks," IEEE Trans. Sustain. Energy, vol. 12, no. 1, pp. 587–598, Jan. 2021, doi: 10.1109/TSTE.2020.3013386.

[80]   H. Ji, C. Wang, S. Ma, P. Li, G. Song, and H. Yu, "Operation and Optimization Technologies of Active Distribution Network with Multi-terminal Soft Open

Points," 25th International Conference on Electricity Distribution, CIRED, June 2019.

[81]   F. Attanasio, S. Wasterlain, T. Pidancier, M. Marchesoni, P. Favre-Perrod, and M. Carpita, "Low Voltage Soft Open Point with Energy Storage: System Simulation and Prototype Preliminary Test Results," Proc. Int. Symp. Power Electron. Electr. Drives, Autom. Motion, pp. 254–261, Aug. 2018, doi: 10.1109/SPEEDAM.2018.8445244.

[82]   J. Xiao *et al.*, "Flexible distribution network: Definition, configuration, operation, and pilot project," IET Gener. Transm. Distrib., vol. 12, no. 20, pp. 4492–4498, Nov. 2018, doi: 10.1049/IET-GTD.2018.5641.

[83]   A. Aithal, C. Long, W. Cao, J. Wu, and C. E. Ugalde-Loo, "Impact of soft open point on feeder automation," IEEE Int. Energy Conf. ENERGYCON, Jul. 2016, doi: 10.1109/ENERGYCON.2016.7514101.

[84]   A. Aithal, G. Li, J. Wu, and J. Yu, "Performance of an electrical distribution network with Soft Open Point during a grid side AC fault," Appl. Energy, vol. 227, pp. 262–272, Oct. 2018, doi: 10.1016/j.apenergy.2017.08.152.

[85]   W. Cao, "Soft Open Points for the Operation of Medium Voltage Distribution Networks,"PhD thesis, Cardiff University, 2015.

[86]   W. Kramer, S. Chakraborty, B. Kroposki, and H. Thomas, "Advanced Power Electronic Interfaces for Distributed Energy Systems; Part 1: Systems and Topologies," NREL, Mar. 2008.

[87]   J. Alcala, V. Cardenas, a Ramírez, and J. Gudino, "Study of the bidirectional power flow in Back - to - Back converters by using linear and nonlinear control strategies," IEEE Energy Convers. Congr. Expo., pp. 806–813, 2011, doi: 10.1109/ECCE.2011.6063853.

[88]   Tatjana Kalitjuka, "Control of Voltage Source Converters for Power System Applications," M.Sc. thesis, Norwegian University of Science and Technology, 2011.

[89]   A. Tyagi and K. . Padiyar, "Dynamic analysis and simulation of a VSC based Back-to-Back HVDC link," India International Conference on Power Electronics, Dec. 2006, pp. 232–238, doi: 10.1109/IICPE.2006.4685374.

[90]   Y. Gan-gui, J. Gui-qiang, Mu Gang, Li Jun-hui, Chen Tao, H. Ya-feng, W. Jian, "Dynamic modeling and nonlinear decoupled control of back-to-back voltage source converter," International Conference on Electrical Machines and Systems,Wuhan, Oct. 2008.

[91]   L. Wang, "Modeling and control of sustainable power systems : towards smarter and greener electric grids," Springer, 2012.

[92]   Z. Yuan, S. W. H. De Haan, J. B. Ferreira, and D. Cvoric, "A FACTS device: Distributed power-flow controller (DPFC)," IEEE Trans. Power Electron., vol. 25, no. 10, pp. 2564–2572, 2010, doi: 10.1109/TPEL.2010.2050494.

[93]   H. Fujita, Y. Watanabe, and H. Akagi, "Control and analysis of a unified power flow controller," IEEE Trans. Power Electron., vol. 14, no. 6, pp. 1021–1027, 1999, doi: 10.1109/63.803395.

[94]   I. Papic, P. Zunko, D. Povh, and M. Weinhold, "Basic Control of Unifie Power Flow Controller," IEEE Trans. Power Syst., vol. 12, no. 4, pp. 1734–1739, 1997.

[95]   "Low Carbon London- Project Closedown Report," UK Power Networks, Apr. 2015.

[96]   Peter Lang, "FUN-LV Dual terminal power electronics device," UK Power Networks, Apr. 2015.

[97]   J. Berry, N. Murdoch, and D. Hardman, "Design and integration of an MVDC system on a GB 33kV network," 15th IET International Conference on AC and DC Power Transmission (ACDC), Feb. 2019, doi: 10.1049/cp.2019.0018.

[98]   S. C. E. Jupe, S. Hoda, J. E. King, D. A. Dale, and J. Berry, "Controlling a 33 kV Flexible Power Link in Gb's distribution network," *15*[th] IET International Conference on AC and DC Power Transmission (ACDC), Feb. 2019,, doi: 10.1049/cp.2019.0021.

[99]   J. Yu, K. Smith, M. Urizarbarrena, N. MacLeod, R. Bryans, and A. Moon, "Initial designs for the ANGLE DC project; converting existing AC cable and overhead line into DC operation," 13th IET International Conference on AC and DC Power Transmission (ACDC), Feb. 2017, doi: 10.1049/cp.2017.0002.

[100] C. Long, J. Wu, K. Smith, A. Moon, R. Bryans, and J. Yu, "MVDC link in a 33

kV distribution network," 24th International Conference & Exhibition on Electricity Distribution (CIRED), June 2017, doi: 10.1049/oap-cired.2017.0168.

[101] A. Aithal and J. Wu, "Operation and performance of a medium-voltage DC link," 24th International Conference & Exhibition on Electricity Distribution (CIRED), June 2017, doi: 10.1049/oap-cired.2017.0946.

[102] T. Joseph, J. Liang, G. Li, A. Moon, K. Smith, and J. Yu, "Dynamic control of MVDC link embedded in distribution network: - Case study on ANGLE-DC," IEEE Conference on Energy Internet and Energy System Integration, Jun. 2018, doi: 10.1109/EI2.2017.8245752.

[103] G. Abeynayake and J. Liang, "Analysis and Control of MVDC Demonstration Project in the UK : ANGLE-DC," DC collection systems for offshore wind power plants, October 2020, doi: 10.19421/j.cnki.1006-6357.2020.10.007.

[104] "Electricity NIC submission: UK Power Networks– Active Response to Distribution Network Constraints," Ofgem, https://www.ofgem.gov.uk/publications-and-updates/electricity-nic-submission-uk-power-networks-active-response-distribution-network-constraints, accessed Jul. 2018.

[105] J. M. Bloemink and T. C. Green, "Increasing distributed generation penetration using soft normally-open points," IEEE PES Gen. Meet., 2010, doi: 10.1109/PES.2010.5589629.

[106] W. Cao, J. Wu, N. Jenkins, C. Wang, and T. Green, "Benefits analysis of Soft Open Points for electrical distribution network operation," Appl. Energy, vol. 165, pp. 36–47, 2016, doi: 10.1016/j.apenergy.2015.12.022.

[107] C. Long, J. Wu, L. Thomas, and N. Jenkins, "Optimal operation of soft open points in medium voltage electrical distribution networks with distributed generation," Appl. Energy, vol. 184, pp. 427–437, Dec. 2016, doi: 10.1016/j.apenergy.2016.10.031.

[108] J. M. Bloemink and T. C. Green, "Increasing photovoltaic penetration with local energy storage and soft normally-open points," IEEE Power Energy Soc. Gen. Meet., 2011, doi: 10.1109/PES.2011.6039561.

[109] H. Ji, C. Wang, P. Li, J. Zhao, G. Song, and J. Wu, "Quantified flexibility evaluation of soft open points to improve distributed generator penetration in

160

active distribution networks based on difference-of-convex programming," Appl. Energy, vol. 218, no. December 2017, pp. 338–348, 2018, doi: 10.1016/j.apenergy.2018.02.170.

[110] "Flexible Urban Networks-Low Voltage/project progress report," https://innovation.ukpowernetworks.co.uk/wpcontent/uploads/2019/06/FUNL V_PMD_027_PMO_FUN-LV-Bi-annual-report-Jan-to-June-2016-v1.0-PXM-2016-06-15-signed.pdf, accessed Oct. 29, 2021.

[111] S. Carter and C. Walton, "Secondary substation load profiling - identification visualisation of changes," 22nd International Conference and Exhibition on Electricity Distribution (CIRED), June 2013, doi: 10.1049/cp.2013.1143.

[112] C. Newton, C. Walton, and J. Gooding, "Selecting Sites for Fun-Lv Field Trials," 23rd Int. Conf. Electr. Distrib., Cired, July 2015.

[113] N. Bottrell, P. Lang, and T. Green, "Algorithm for soft open points to solve thermal and voltage constraints in low-voltage distribution networks," 24th International Conference & Exhibition on Electricity Distribution (CIRED), June 2017, doi: 10.1049/oap-cired.2017.0648.

[114] P. Li, H. Ji, S. Member, C. Wang, and S. Member, "Coordinated Control Method of Voltage and Reactive Power for Active Distribution Networks Based on Soft Open Point," IEEE Transactions Sustain. Energy, vol. 8, no. 4, pp. 1430–1442, 2017.

[115] P. Li et al., "Optimal Operation of Soft Open Points in Active Distribution Networks Under Three-Phase Unbalanced Conditions," IEEE Trans. Smart Grid, vol. 3053, no. c, 2017, doi: 10.1109/TSG.2017.2739999.

[116] P. Li et al., "Combined decentralized and local voltage control strategy of soft open points in active distribution networks," Appl. Energy, vol. 241, pp. 613–624, May 2019, doi: 10.1016/J.APENERGY.2019.03.031.

[117] W. Cao, J. Wu, N. Jenkins, C. Wang, and T. Green, "Operating principle of Soft Open Points for electrical distribution network operation," Appl. Energy, vol. 164, pp. 245–257, 2016, doi: 10.1016/j.apenergy.2015.12.005.

[118] P. Li, G. Song, H. Ji, J. Zhao, C. Wang, and J. Wu, "A supply restoration method of distribution system based on Soft Open Point," IEEE PES Innov.

Smart Grid Technol. Conf. Eur., pp. 535–539, Dec. 2016, doi: 10.1109/ISGT-ASIA.2016.7796441.

[119] "Find minimum of constrained nonlinear multivariable function-MATLAB fmincon," https://www.mathworks.com/help/optim/ug/fmincon.html#d123e87139, accessed Aug. 20, 2021.

[120] G. K. V. Raju and P. R. Bijwe, "An efficient algorithm for minimum loss reconfiguration of distribution system based on sensitivity and heuristics," IEEE Trans. Power Syst., vol. 23, no. 3, pp. 1280–1287, 2008, doi: 10.1109/TPWRS.2008.926084.

[121] W. Cao, J. Wu, and N. Jenkins, "Feeder load balancing in MV distribution networks using soft normally-open points," IEEE PES Innovative Smart Grid Technologies Conference Europe, Jan. 2015, doi: 10.1109/ISGTEurope.2014.7028874.

[122] L. Clotea and A. Forcos, "Power losses evaluation of two and three-level NPC inverters considering drive applications," 13th International Conference on Optimization of Electrical and Electronic Equipment (OPTIM), Brasov, Romania, pp. 929–934, 2012, doi: 10.1109/OPTIM.2012.6231984.

[123] L. Gyugyi, C. D. Schauder, S. L. Williams, T. R. Rietman, D. R. Torgerson, and A. Edris, "The unified power flow controller: A new approach to power transmission control," IEEE Trans. Power Deliv., vol. 10, no. 2, pp. 1085–1097, 1995, doi: 10.1109/61.400878.

[124] F. Z. Peng, "Flexible AC Transmission Systems (FACTS) and Resilient AC Distribution Systems (RACDS) in Smart Grid," Proc. IEEE, vol. 105, no. 11, pp. 2099–2115, Nov. 2017, doi: 10.1109/JPROC.2017.2714022.

[125] S. Kannan, S. Jayaram, and M. M. A. Salama, "Real and Reactive Power Coordination for a Unified Power Flow Controller," IEEE Trans. Power Syst., vol. 19, no. 3, pp. 1454–1461, Aug. 2004, doi: 10.1109/TPWRS.2004.831690.

[126] L. Harnefors and H. P. Nee, "Model-based current control of ac machines using the internal model control method," IEEE Trans. Ind. Appl., vol. 34, no. 1, pp. 133–141, 1998, doi: 10.1109/28.658735.

[127] F. Zheng, S. Zhang, S. Yang, D. Gunasekaran, and U. Karki, "Transformer-less unified power flow controller using the cascade multilevel inverter,"

International Power Electronics Conference, IPEC-Hiroshima - ECCE Asia, 2014, pp. 1342–1349, doi: 10.1109/IPEC.2014.6869760.

[128] F. Z. Peng, J. S. Lai, J. McKeever, and J. VanCoevering, "Multilevel voltage-source inverter with separate DC sources for static var generation," IAS Annual Meeting (IEEE Industry Applications Society), 1995, vol. 3, pp. 2541–2548, doi: 10.1109/ias.1995.530626.

[129] J. Wang and F. Z. Peng, "Unified Power Flow Controller Using the Cascade Multilevel Inverter," IEEE Trans. Power Electron., vol. 19, no. 4, pp. 1077–1084, Jul. 2004, doi: 10.1109/TPEL.2004.830073.

[130] Z. Pu *et al.*, "Fault characteristics analysis and protection design for MMC-UPFC with high reliability," IEEE International Conference on Industrial Technology, Apr. 2018, doi: 10.1109/ICIT.2018.8352353.

[131] B. Gultekin and M. Ermis, "Cascaded multilevel converter-based transmission STATCOM: System design methodology and development of a 12 kV ±12 MVAr power stage," IEEE Trans. Power Electron., vol. 28, no. 11, pp. 4930–4950, 2013, doi: 10.1109/TPEL.2013.2238642.

[132] Y. Liu, S. Yang, X. Wang, D. Gunasekaran, U. Karki, and F. Z. Peng, "Application of Transformer-Less UPFC for Interconnecting Two Synchronous AC Grids with Large Phase Difference," IEEE Trans. Power Electron., vol. 31, no. 9, pp. 6092–6103, Sep. 2016, doi: 10.1109/TPEL.2015.2500033.

[133] F. Z. Peng, Y. Liu, S. Yang, S. Zhang, D. Gunasekaran, and U. Karki, "Transformer-Less Unified Power-Flow Controller Using the Cascade Multilevel Inverter," IEEE Trans. Power Electron., vol. 31, no. 8, pp. 5461–5472, Aug. 2016, doi: 10.1109/TPEL.2015.2497078.

[134] S. Yang, D. Gunasekaran, Y. Liu, U. Karki, and F. Z. Peng, "Application of transformer-less UPFC for interconnecting synchronous AC grids," IEEE Energy Conversion Congress and Exposition, *ECCE 2015*, Oct. 2015, pp. 4993–4999, doi: 10.1109/ECCE.2015.7310364.

[135] D. Gunasekaran, S. Yang, and F. Z. Peng, "Fractionally rated transformer-less unified power flow controllers for interconnecting synchronous AC grids," IEEE Applied Power Electronics Conference and Exposition - *APEC*, May

2015, doi: 10.1109/APEC.2015.7104590.

[136] S. Yang, Y. Liu, X. Wang, D. Gunasekaran, U. Karki, and F. Z. Peng, "Modulation and Control of Transformerless UPFC," IEEE Trans. Power Electron., vol. 31, no. 2, pp. 1050–1063, Feb. 2016, doi: 10.1109/TPEL.2015.2416331.

[137] S. Yang, S. Zhang, X. Wang, D. Gunasekaran, and F. Z. Peng, "Optimization of fundamental frequency modulation for cascaded multilevel inverter based transformer-less UPFC," IEEE Energy Conversion Congress and Exposition, ECCE, Nov. 2014, pp. 4647–4652, doi: 10.1109/ECCE.2014.6954037.

[138] C. Bajracharya, M. Molinas, J. A. Suul, and T. M. Undeland, "Understanding of tuning techniques of converter controllers for VSC-HVDC" Nordic workshop on power and industrial electronics, June 2008.

[139] M. Alharbi and S. Bhattacharya, "Scale-Up Methodology of a Modular Multilevel Converter for HVdc Applications," IEEE Trans. Ind. Appl., vol. 55, Sep. 2019, doi: 10.1109/TIA.2019.2925055.

[140] J. Zhu, "Tuning Method for VSC Current Controller Gains Aimed at Optimized Settling Time and Damping Ratio," 53rd Int. Univ. Power Eng. Conf. UPEC, Nov. 2018, doi: 10.1109/UPEC.2018.8541890.

[141] "Power inverter modules - Building blocks for power converters," imperix, https://imperix.com/products/power-inverter-modules/, accessed Jun. 23, 2021.

[142] "Puissance power amplifier (PA-3000-AB/260v/2G)," puissance, https://www.puissanceplus.com/products.html, accessed Jun. 23, 2021.

[143] "OP4500 RT-LAB- System user guide," OPAL-RT Technologies, www.opal-rt.com, accessed Jun. 23, 2021.

[144] "MV7000 | Medium Voltage Drives," GE Power Conversion, https://www.gepowerconversion.com/product-solutions/medium-voltage-drives/mv7000, accessed Nov. 16, 2020.

[145] "Active Response to Distribution Network Constraints- Network Innovation Competition,"https://www.ofgem.gov.uk/system/files/docs/2017/11/active_re sponse_fsp_v3.1_public.pdf, accessed: May 02, 2019.

References

[146] "Power Semiconductors-Medium-Voltage Inverters," Fuji Electric , https://www.fujielectric.com/products/semiconductor/usage/mv_inverter.html , accessed May 26, 2021.

[147] A. Kuperman, "Proportional-Resonant Current Controllers Design Based on Desired Transient Performance," IEEE Trans. Power Electron., vol. 30, no. 10, pp. 5341–5345, Oct. 2015, doi: 10.1109/TPEL.2015.2408053.

[148] B. P. McGrath, D. G. Holmes, and L. McNabb, "A Signal Conditioning Antiwindup Approach for Digital Stationary Frame Current Regulators," IEEE Trans. Ind. Appl., vol. 55, no. 6, pp. 6036–6046, Nov. 2019, doi: 10.1109/TIA.2019.2929144.

[149] D. G. Holmes, T. A. Lipo, B. P. McGrath, and W. Y. Kong, "Optimized design of stationary frame three phase AC Current regulators," IEEE Trans. Power Electron., vol. 24, no. 11, pp. 2417–2426, 2009, doi: 10.1109/TPEL.2009.2029548.

[150] A. Marzoughi, R. Burgos, D. Boroyevich, and Y. Xue, "Design and Comparison of Cascaded H-Bridge, Modular Multilevel Converter, and 5-L Active Neutral Point Clamped Topologies for Motor Drive Applications," IEEE Transactions on Industry Applications, Mar. 2018, vol. 54, no. 2, pp. 1404–1413, doi: 10.1109/TIA.2017.2767538.

[151] "IGBT Module, Dual, 300 A, 1.2 kV, 1.595 kW, Module," https://uk.farnell.com/fuji-electric/2mbi300vn-120-50/igbt-2-pk-v-ser-300a-1200v-m254/dp/2060200, accessed Jun. 25, 2021.

[152] D. Neumayr, "The Essence of the Little Box Challenge-Part A: Key Design Challenges & Solutions," CPSS Trans. Power Electron. Appl., vol. 5, no. 2, pp. 158–179, Jun. 2020, doi: 10.24295/CPSSTPEA.2020.00014.

[153] "Engineering Recommendation G99," www.energynetworks.org, accessed: Mar. 01, 2021.

[154] Y. Morioka and M. Kato, "Implementation of unified power flow controller and verification for transmission capability improvement," IEEE Trans. Power Syst., vol. 14, no. 2, pp. 575–581, 1999, doi: 10.1109/59.761883.

[155] C. D. Schauder et al., "Operation of the unified power flow controller (UPFC)

under practical constraints," IEEE Trans. Power Deliv., vol. 13, no. 2, pp. 630–639, Apr. 1998, doi: 10.1109/61.660949.

[156] "2745.1-2019 - IEEE Guide for Technology of Unified Power Flow Controller Using Modular Multilevel Converter - Part 1 : Functions," IEEE, Nov. 2019, doi: 10.1109/IEEESTD.2019.8913755.

[157] H. Cai, L. Yang, H. Wang, P. Song, and Z. Xu, "Application of Unified Power Flow Controller (UPFC) in Jiangsu power system," IEEE Power and Energy Society General Meeting, Jan. 2018, doi: 10.1109/PESGM.2017.8274211.

[158] X. Wang *et al.*, "Application of 500 kV UPFC in Suzhou southern power grid," J. Eng., Mar. 2019, doi: 10.1049/joe.2018.8556.

[159] J. Lin, M. Jiang, R. Huang, and X. Kong, "Restarting strategy of UPFC series connect unit for fault ride-through based on fault identification," International Conference on Electricity Distribution, *CICED*, Dec. 2018, pp. 362–367, doi: 10.1109/CICED.2018.8592249.

[160] "2745.3-2020 - IEEE Guide for Technology of Unified Power Flow Controller Using Modular Multilevel Converter--Part 3: Thyristor Bypass Switch," IEEE, June 2020.

[161] J. Lin, P. Li, X. Kong, H. Huang, and B. Zhang, "Coordination strategy and its realization of UPFC control protection system and power grid protection for improving fault ride-through capability," International Electrical and Energy Conference, Jun. 2018, pp. 429–435, doi: 10.1109/CIEEC.2017.8388486.

[162] Y. Jijun, "Unified Power Flow Controller Technology and Application," Science Direct, 2017.

[163] "Active Response to Distribution Network Constraints." UK Power Networks, https://www.ofgem.gov.uk/system/files/docs/2017/11/active_response_fsp_v3.1_public.pdf, accessed Oct. 02, 2018.

[164] E. Bashar *et al.*, "A New Protection Scheme for an SSSC in an MV Network by Using a Varistor and Thyristors," IEEE Trans. Power Deliv., 2020, doi: 10.1109/TPWRD.2020.2982512.

[165] "Surge currents for phase control thyristors," ABB

https://library.e.abb.com/public/4a1f7f8ebc5eb5c383257caf00430141/Surge currents for PCT_ 5SYA 2102-00.pdf, accessed Oct. 12, 2021

[166] J. G. Zola, "Simple model of metal oxide varistor for pspice simulation," IEEE Trans. Comput. Des. Integr. Circuits Syst., vol. 23, no. 10, pp. 1491–1494, Oct. 2004, doi: 10.1109/TCAD.2004.835134.

[167] M. N. Tuczek and V. Hinrichsen, "Recent experimental findings on the single and multi-impulse energy handling capability of metal-oxide varistors for use in high-voltage surge arresters," IEEE Trans. Power Deliv., vol. 29, no. 5, pp. 2197–2205, Oct. 2014, doi: 10.1109/TPWRD.2013.2283911.

[168] "Littelfuse Varistors - Basic Properties, Terminology and Theory," https://www.littelfuse.com/~/media/electronics_technical/application_notes/va ristors/littelfuse_varistors_basic_properties_terminology_and_theory_applicat ion_note.pdf, accessed Feb. 23, 2021.

[169] F. D. Martzloff, "A Standard for the 90s: IEEE C62.41 Surges Ahead," IEEE, 1991.

[170] K. E. Merrill and G. T. Heydt, "The Calculation of Energy Dissipation in Metal Oxide Varistors for Power Distribution Applications," IEEE Trans. Power Syst., vol. 34, no. 5, pp. 3967–3969, 2019, doi: 10.1109/TPWRS.2019.2918957.

[171] D. Naylor et al., "Operation of the HV AC system up to and including 33 kV," SP Energy Networks, 2019.

[172] C. B. and R. B. D E G Carson, "Calculation of System Fault Levels," SP Energy Networks, Aug. 2017.

[173] "Basic Function Vacuum Circuit Breaker 0-12kV, " Schneider Electric Global, https://www.se.com/ww/en/product/EXE123106A1B/basic-function-vacuum-circuit-breaker-0-12kv-75kvp-31.5ka-3s-630a-145-iec/, accessed Oct. 02, 2021.

[174] "Metal-OxideVaristor", https://m.littelfuse.com/~/media/electronics/datasheets/varistors/littelfuse_vari stor_ba_bb_datasheet.pdf.pdf, accessed: Jun. 15, 2021.

[175] "Phase Control Thyristor 5STP 45N2800," https://pdf.dzsc.com/autoupload/9109aee0-

167

62bc-4c9f-9430-953ed1edb765.pdf., accessed: Oct. 05, 2021.

[176] D. Jovcic and K. Ahmed, "High voltage direct current transmission : converters, systems and DC grids," WIELY, Sep. 2015.

[177] "Gate-drive recommendations for phase control and bi-directionally controlled thyristors,"https://library.e.abb.com/public/fe9dd0f01cf7be78c12573ed0036e 0b9/Gate-drive recommendations for PCT_ 5SYA 2034_02NewLay.pdf., accessed Sep. 20, 2021.

[178] J. Pollefliet, "Power Electronics, Volume 1: Switched and Converters, " ScienceDirect, 2018.

[179] "Parameter list for SCRs, TRIACs, AC switches, and DIACS." https://www.st.com/resource/en/application_note/an2703-parameter-list-for-scrs-triacs-ac-switches-and-diacs-stmicroelectronics.pdf., accessed Mar. 01, 2021.

Appendix A

Table A1 Gain parameters of the Unified Power Flow Controller

Series Converter		
k_{p1}= 0.0045, k_{i1}= 0.08	k_{p2}= 0.09, k_{i2}= 0.75	k_{p3}= 0.000001, k_{i3}= 0.004
Shunt Converter		
$k_{p,outer}$= 2.2275, $k_{i,outer}$= 2.0250	$k_{p,inner}$= 20.25, $k_{i,inner}$=20.25	

Table A2 Gain parameters of the Transformer-less Unified Power Flow Controller

Series Converter	
$k_{p,se}$= 27.5, $k_{i,se}$= 10	
Shunt Converter	
$k_{p,sh1}$= 33, $k_{i,sh1}$= 400	$k_{p,sh2}$= 800, $k_{i,sh2}$=200

Appendix B

Detailed derivation of the shunt current equation of a Transformer-less Unified Power Flow Controller.

Using equation (5-3): $\left|\bar{I}_{se}\right|\underline{|\rho - 90°} = \left|\bar{I}\right|\underline{|\phi} + \left|\bar{I}_{sh}\right|\underline{|\delta_s + 90}$ (B1)

Using equation (B1), then $\left|\bar{I}_{sh}\right| = \dfrac{\left|\bar{I}\right|\cdot\cos(\phi) - \left|\bar{I}_{se}\right|\cdot\sin(\rho)}{\sin(\delta_s)}$ (B2)

Since the active power of the shunt converter is zero (i.e., $P_{sh} = 0$), then

$$real(\overline{V}_1^{'\,*}\cdot\bar{I}_{sh}) = 0$$ (B3)

Equation (B3) can be rewritten as in B4,

$$real\,((\overline{V}_1 + \overline{V}_{se})\cdot(\bar{I}_{se} - \bar{I})) = 0$$ (B4)

From equation (B4), current $\bar{I}_{se}$ is given in (B5),

$$\left|\bar{I}_{se}\right| = \frac{\left|\overline{V}_1\right|\cdot\left|\bar{I}\right|\cdot\cos(\phi) + \left|\overline{V}_{se}\right|\cdot\left|\bar{I}\right|\cdot\cos(\rho - \phi)}{\left|\overline{V}_1\right|\cdot\sin(\rho)}$$ (B5)

Substitute from equation (B5) into (B2), current $\bar{I}_{sh}$ is expressed as in (B6),

$$\left|\bar{I}_{sh}\right| = -\frac{\left|\overline{V}_{se}\right|\cdot\left|\bar{I}\right|\cdot\cos(\rho - \phi)}{\left|\overline{V}_1\right|\cdot\sin(\delta_s)}$$ (B6)

Using KVL, voltage $\left|\overline{V}_1\right|$ can be expressed as in (B7)

$$\left|\overline{V}_1\right| = \left|\overline{V}_{se}\right|(\frac{\sin(\rho)\cdot\cos(\delta_s)}{\sin(\delta_s)} - \cos(\rho))$$ (B7)

Substitute from equation (B7) into equation (B6). Current $\bar{I}_{sh}$ is obtained as in (B8)

$$\bar{I}_{sh} = \left|\bar{I}\right|\cdot\frac{\cos(\rho - \phi)}{\sin(\rho - \delta_s)}\underline{|(\delta_s - 90)°}$$ (B8)

Appendix C

Table A 3 Specifications of Imperix power electronic rig

Power electronic building block	PEP 8032/6-10 kW
Rated DC voltage	800 V
Rated current	32 A

Appendix D

Table A 4 Specifications of Puissance power amplifier
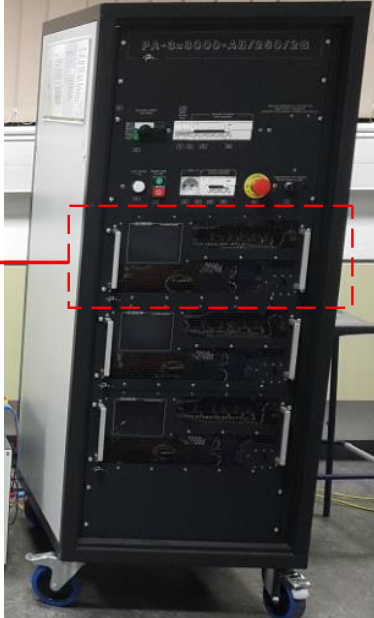
Puissance power amplifier (PA-3000-AB/260v/2G)		
AC-DC-Single-phase- 3000 VA		
Rated power	3000 VA per output	
Modes	Voltage only	
Performance in AC	PA-3000, AC-DC, 260-24 A	
Ranges	130V	260 V
Voltage Ph-N (VRMS)	0－130	0－260
Current per phase (ARMS)	0－24	0－12
Performance in DC	PA-3000, AC-DC, 260-24 A	
Ranges	130 V	260 V
Voltage (VDC)	0－±180	0－±360
Current (ADC)	0－±24	0－±12